Vibroacoustic Analysis of Plates with Viscoelastic Damping Patches:

A Layerwise Theory and the Rayleigh-Ritz Method

João Diogo Pereira Amorim

Dissertação do Mestrado Integrado em Engenharia Mecânica

Orientador:
Prof. Doutor José Fernando Dias Rodrigues

Departamento de Engenharia Mecânica
Faculdade de Engenharia da Universidade do Porto

Porto, 2013

Vibroacoustic Analysis of Plates with Viscoelastic Damping Patches:

A Layerwise Theory and the Rayleigh-Ritz Method

João Diogo Pereira Amorim

Dissertation submitted to
Faculdade de Engenharia da Universidade do Porto
for the degree of:

Mestre em Engenharia Mecânica

Advisor:
Prof. Doutor José Fernando Dias Rodrigues
(Associate Professor)

Laboratório de Vibrações de Sistemas Mecânicos
Departamento de Engenharia Mecânica
Faculdade de Engenharia da Universidade do Porto

Porto, Julho de 2013

The work presented in this dissertation was performed at the
Laboratory of Vibrations of Mechanical Systems
Department of Mechanical Engineering
Faculty of Engineering
University of Porto
Porto, Portugal.

João Diogo Pereira Amorim
E-mail: em08145@fe.up.pt

Faculdade de Engenharia da Universidade do Porto
Departamento de Engenharia Mecânica
Laboratório de Vibrações de Sistemas Mecânicos
Rua Dr. Roberto Frias s/n, Sala M206
4200-465 Porto
Portugal

Resumo

Nos dias de hoje, as propriedades de vibração e acústicas de estruturas de elevada performance são, cada vez mais, consideradas parâmetros chave durante a fase de projecto em indústrias como a automóvel, ferroviária ou aeroespacial. Para além da integridade estrutural dos equipamentos, a consciencialização pública da importância do ruído como fonte de poluição e incómodo tem crescido, assim como a qualidade sonora como critério de escolha. Contudo, com a procura cada vez mais elevada de estruturas seguras e eficientes, os engenheiros necessitam de desenvolver modelos complexos cada vez mais refinados e precisos de estruturas multicamada com tecnologias de amortecimento para satisfazer as necessidades referidas anteriormente.

Nesta perspectiva, são abordados nesta dissertação temas como o controlo passivo de vibração e ruído sendo estudado um modelo eficiente para simular o comportamento dinâmico e acústico de placas com tratamentos parciais com camada de restrição. Neste modelo, é usado o método de Rayleigh-Ritz que surge como uma sólida alternativa ao muito utilizado método dos elementos finitos e oferece uma solução interessante e muito eficiente no que diz respeito à manipulação dos tratamentos parciais. Tirando partido das soluções engenhosas que este modelo oferece, a eficiência de tratamentos de amortecimento em termos de localização, espessura das camadas e configurações geométricas é analisada e discutida. As vantagens mas também os inconvenientes deste modelo são estudados comparando-o com o método dos elementos finitos.

Palavras-Chave: placa, multicamada, vibração, ruído, controlo, amortecimento, viscoelástico, tratamento parcial, Rayleigh-Ritz.

Abstract

Nowadays, the vibrational and acoustic properties of high performance structures are increasingly considered as key constraints in automotive, railway or aerospace industries during the design process. Beyond the structural integrity of these structures, the public realisation of the importance of noise as a major pollution and annoyance source has grown as well as the sound quality notion among the choice criteria. However, with the ever increasing strong demands of more efficient and reliable structures, engineers need to develop refined and more accurate multiphysics models of complex multilayer structures with damping technologies.

In this perspective, this dissertation work addresses issues on vibration and noise control studying an efficient model to simulate the dynamic and acoustic behaviour of plates with constraining-layer damping patches. In this model, the Rayleigh-Ritz method arises as a reliable alternative to the widely used finite element method and offers a very efficient solution regarding patches handling. Taking advantage of the resourceful solutions that this model offers the efficiency of the damping treatments in terms of location, thicknesses of the layers and geometric configuration is analyzed and discussed. The advantages but also the drawbacks of this model are studied and comparisons with the finite element method are made.

Keywords: plate, multilayer, vibration, noise, control, damping, viscoelastic, patch, Rayleigh-Ritz.

To João Paulo Carvalho Garcia Pereira

Acknowledgments

This dissertation is a very personal work but would not have been possible without the invaluable help of many people. First of all, I am deeply grateful to Dr. José Dias Rodrigues, my advisor in this work, for his supervision but also for his unconditional support during this laborious semester. I also owe a special acknowledgment to Luís Cardoso for his prompt help to my many requests during the entire work. I'm, of course, thankful to FEUP for all the conditions and opportunities that gave me, providing all that was necessary.

However, this dissertation is also the result of a long cycle of 5 years in which I spent good times and bad times and I'm bound to express my sincere gratitude to the people who accompanied me during this stage. I would like to thank to my aunt Maria do Carmo for welcoming me in her home during this years and I'm indebted to my cousins for all the funny moments that we spent. A hug for my comrades César Ferreira and Vitor Canedo for their friendship and support which have been unconditional since I meet them.

Last but not least, I would like to express a very warm thank to my closest family, in which I include my grandparents, but special to my parents that always supported me and I'm proud of the education and values they gave me. They and my brother are the most important people in my life and I appreciate everything they have done and continue to do for me.

"You are always a student,
never a master.
You have to keep moving forward."

Conrad Hall

Contents

List of Figures

List of Tables

List of Symbols

Indices

i	general counter
j	general counter or degree of freedom
ℓ	material layer index
m	general counter
p	general counter
q	general counter
r	modal index

Identifiers

$()^B$	relative to bending component
$()^M$	relative to membrane component
$()^S$	relative to transverse shear component
$()^{B/M}$	relative to bending/membrane component
$()^{B/S}$	relative to bending/shear component
$()^{M/M}$	relative to membrane/membrane component
$()^{M/S}$	relative to membrane/shear component
$()^{S/S}$	relative to shear/shear component
$()^j$	relative to multilayered material j
$()_{\mathrm{c}}$	relative to covered area
$()_{\mathrm{p}}$	relative to base plate
$()_{\mathrm{cl}}$	relative to constraining layer
$()_{\mathrm{vl}}$	relative to viscoelastic layer

Acronyms

CLD	Constrained Layer Damping
FLD	Free Layer Damping
GHM	*Golla-Hughes-McTavish*
ADF	*Anelastic Displacement Fields*
CLT	Classical Laminate Theory
ESL	Equivalent Single Layer
3M ISD112	Viscoelastic material

Operators

$[\,]^{\mathrm{T}}$	transposed matrix
$[\,]^*$	complex conjugated matrix
$\tilde{[\,]}$	complex matrix
$(\tilde{\bullet})$	complex variable
$\mathcal{L}(\bullet)$	Lagragian operator
$(\dot{\bullet})$	time derivative
$(\ddot{\bullet})$	second time derivative
$\Re(\bullet)$	real component
$\Im(\bullet)$	imaginary component
d	differential operator
j	complex operator $\mathrm{j} = \sqrt{-1}$

Scalar Variables $(\bullet)$

a	length [m]	$\in \mathbb{R}$
a	weighting factor	$\in \mathbb{R}$
$\mathcal{A}(\omega)$	accelerance function [m.s^2/N]	$\in \mathbb{C}$
b	width [m]	$\in \mathbb{R}$
b	weighting factor	$\in \mathbb{R}$
e_t	surface density of kinetic energy [J/m]	$\in \mathbb{R}$
e_v	surface density of deformation energy [J/m]	$\in \mathbb{C}$
E	Young modulus or extensional modulus [Pa]	$\in \mathbb{R}$

$\tilde{E}$	complex modulus [Pa]	$\in \mathbb{C}$
E'	storage modulus [Pa]	$\in \mathbb{R}$
E''	loss modulus [Pa]	$\in \mathbb{R}$
F	force [N]	$\in \mathbb{R}$
$\tilde{G}$	complex shear modulus [Pa]	$\in \mathbb{C}$
G'	storage shear modulus [Pa]	$\in \mathbb{R}$
G''	loss shear modulus [Pa]	$\in \mathbb{R}$
h	thickness [m]	$\in \mathbb{R}$
h_{cld}	thicknesses ratio	$\in \mathbb{R}$
$J_{\bar{S}}$	objective function for the covered area	$\in \mathbb{R}$
J_t	objective function for the treatment's thickness	$\in \mathbb{R}$
k	wave number [m^{-1}]	$\in \mathbb{R}$
m	maximum order for in x-direction	$\in \mathbb{N}$
$\overline{m}$	added mass function of the base plate mass	$\in \mathbb{R}$
n	maximum order for in y-direction	$\in \mathbb{N}$
N	number of layers	$\in \mathbb{N}$
$\tilde{p}_{\mathrm{inc}}$	incident plane wave [Pa]	$\in \mathbb{C}$
$\tilde{P}_{\mathrm{inc}}$	incident pressure field [Pa]	$\in \mathbb{C}$
q	generalized displacements	$\in \mathbb{C}$
Q^{ext}	generalized external forces	$\in \mathbb{C}$
t	time variable [s]	$\in \mathbb{R}$
T	temperature [°C]	$\in \mathbb{R}$
T	kinetic energy [J]	$\in \mathbb{R}$
TL	transmission loss	$\in \mathbb{R}$
S	surface area [m^2]	$\in \mathbb{R}^2$
$\bar{S}$	non-dimensional covered area	$\in \mathbb{R}$
u	translation along x axis	$\in \mathbb{R}$
u_0	membrane displacement along x axis	$\in \mathbb{R}$
v	translation along y axis	$\in \mathbb{R}$
v_0	membrane displacement along y axis	$\in \mathbb{R}$
V	deformation energy [J]	$\in \mathbb{C}$
$\langle V^2 \rangle$	mean square velocity [m^2/s^2]	$\in \mathbb{R}$
w	transverse displacement	$\in \mathbb{R}$
W_{inc}	incident pressure [Pa]	$\in \mathbb{R}$
W_{t}	radiated acoustic pressure [Pa]	$\in \mathbb{R}$
x	coordinate of the cartesian referential	$\in \mathbb{R}$
y	coordinate of the cartesian referential	$\in \mathbb{R}$
$Y(\omega)$	mobility function [ms^{-1}/N]	$\in \mathbb{C}$
z	coordinate of the cartesian referential	$\in \mathbb{R}$
$\alpha(\omega)$	receptance function [m/N]	$\in \mathbb{C}$

α_{xx}, α_{yy}	link variables	$\in \mathbb{C}$
β	link variable	$\in \mathbb{R}$
δ	lag or variation	$\in \mathbb{R}$
δ_i	mass coefficient	$\in \mathbb{R}$
δ_{xx}, δ_{yy}	link variables	$\in \mathbb{C}$
η	loss factor	$\in \mathbb{R}$
λ_i	stiffness coefficient	$\in \mathbb{C}$
ν	Poisson's ratio	$\in \mathbb{R}$
ω	frequency [rad/s]	$\in \mathbb{R}$
ω_r	natural frequency of order r [rad/s]	$\in \mathbb{R}$
ω_s	iterated natural frequency [rad/s]	$\in \mathbb{R}$
ρ	density [Kg/m^3]	$\in \mathbb{R}$
σ	radiation efficiency	$\in \mathbb{R}$
$\tau(\theta, \varphi)$	incidence transmission coefficient	$\in \mathbb{R}$
φ_x	rotation around x axis due to the shear stress	$\in \mathbb{R}$
φ_y	rotation around y axis due to the shear stress	$\in \mathbb{R}$

Vector Variables {}

$\{\mathbf{A}(t)\}$	unknowns vector	$\in \mathbb{C}$
$\{\mathbf{B}(t)\}$	unknowns vector	$\in \mathbb{C}$
$\{\mathbf{C}(t)\}$	unknowns vector	$\in \mathbb{C}$
$\{\mathbf{D}(t)\}$	unknowns vector	$\in \mathbb{C}$
$\{\mathbf{E}(t)\}$	unknowns vector	$\in \mathbb{C}$
$\{\mathbf{F}(t)\}$	external force vector	$\in \mathbb{C}$
$\{q\}$	generalized displacements vector	$\in \mathbb{C}$
$\{\mathbf{X}(t)\}$	unknowns vector or system response vector	$\in \mathbb{C}$
$\{\phi\}$	eigenvector	$\in \mathbb{C}$
$\{\boldsymbol{\phi}(x, y)\}$	basis functions vector	$\in \mathbb{R}$
$\varepsilon/\{\varepsilon\}$	deformation field/vector	$\in \mathbb{C}$
$\gamma/\{\gamma\}$	shear deformation field/vector	$\in \mathbb{C}$
$\sigma/\{\sigma\}$	stress field/vector	$\in \mathbb{C}$
$\tau/\{\tau\}$	shear stress field/vector	$\in \mathbb{C}$
$\{\boldsymbol{\Upsilon}\}$	displacements vector	$\in \mathbb{C}$

Matrix Variables [ ]

$[\boldsymbol{\mathcal{A}}]$	shear stiffness relation matrix	$\in \mathbb{C}$
$[\boldsymbol{\mathcal{B}}]$	layer height matrix	$\in \mathbb{C}$
$[\mathbf{C}]$	constitutive matrix	$\in \mathbb{C}$
$[\mathbf{C}_s]$	shear stiffness matrix	$\in \mathbb{C}$
$[\boldsymbol{\mathcal{D}}]$	auxiliary shear stiffness matrix	$\in \mathbb{C}$
$[\mathbf{I}]$	identity matrix	$\in \mathbb{R}$
$[\tilde{\mathbf{K}}]$	stiffness matrix	$\in \mathbb{C}$
$[\mathbf{M}]$	mass matrix	$\in \mathbb{R}$
$[\boldsymbol{\mathcal{M}}]$	shear stiffness relation matrix	$\in \mathbb{C}$
$[\boldsymbol{\Omega}]$	link matrix	$\in \mathbb{C}$

Referential

x, y, z	cartesian coordinate system
x', y', z'	auxiliary cartesian coordinate system

Chapter 1

Introduction

1.1 Historical Perspective and Future Demands

In a world that increasingly claims by technological innovation, structural engineering needs, now more then even, tools that are able to satisfy the complex requirements of the 21st century. These requirements are nowadays different from those of the last decades and are beyond the purely structural ones. Issues like comfort and welfare are now a competitive factor that need be remembered by all the companies that want to remain in the global market.

For everything that was sad, noise reduction is now of great importance in many industries. The noise level in a car cabin caused by the rotation of the motor, for example, is no longer tolerated like was in the past. Vibration and noise in a dynamic system can be reduced by a number of means but a common one is the called passive damping. In this technology (as opposed to active damping[1]) a dissipative material, usually viscoelastic, is added to the base material to complete the properties of the designed product with noise and vibration performance. This process, as a technology, has been dominant in the non-commercial aerospace industry since the early 1960s[2]. However advances in the material technology along with newer and more efficient analytical and experimental tools for modeling the dynamical behaviour of materials and structures have led these materials to many applications in current days like automotive, railway and aircraft applications. In these industries the weight is also a crucial requirement for obvious reasons. The use of viscoelastic materials in partial treatments and his optimal design, plays an important role in the project of structures like the ones that are mentioned and brings a much better cost/benefit ratio that is essential for the competitiveness.

1.1.1 The Importance of Vibroacoustics

The study of sound and vibration are closely related. Sound is a mechanical wave that is an oscillation of pressure transmitted through some medium, like air or water. The vocal cords, for example, are vibrating structures that generate pressure waves which in turn induce the vibration in ear drums. The vocal cords or other structures like pianos, radio loudspeakers or church bells, are generally desirable sources of sound but others like internal combustion engines, train wheels or magnetic resonance imaging machines are not. The subject of sound radiation from vibrating structures is of great practical importance[3]. It is absolutely necessary that designers of loudspeakers understand the mechanism of sound radiation to improve the product quality. On the other hand, the designers of industrial machinery must taken into account the noise limitations regulation and the comfort and welfare of the people. The commercial competitiveness of many structures is strongly affected by the noise levels that they generate and in this work this topic is a matter of interest. Once that the study of sound and vibration are closely related, when trying to reduce noise it is often a problem in trying to reduce vibration which is the main objective of this work with the use of viscoelastic treatments.

1.2 Viscoelastic Damping Treatments

Viscoelastic materials are know by their damping capabilities. Due to their particular molecular structure, these materials are able to dissipate deformation energy. This is achieved because the deformation energy of the host structure increase internal molecular friction of the viscoelastic layer and yields energy dissipation due to the heating effect[1].

The viscoelastic treatments can be done in different arrangements. The primary methods of increasing the passive damping in a structure are the passive free (or unconstrained) layer damping (FLD) and passive constrained layer damping (CLD) (see Figure 1.1).

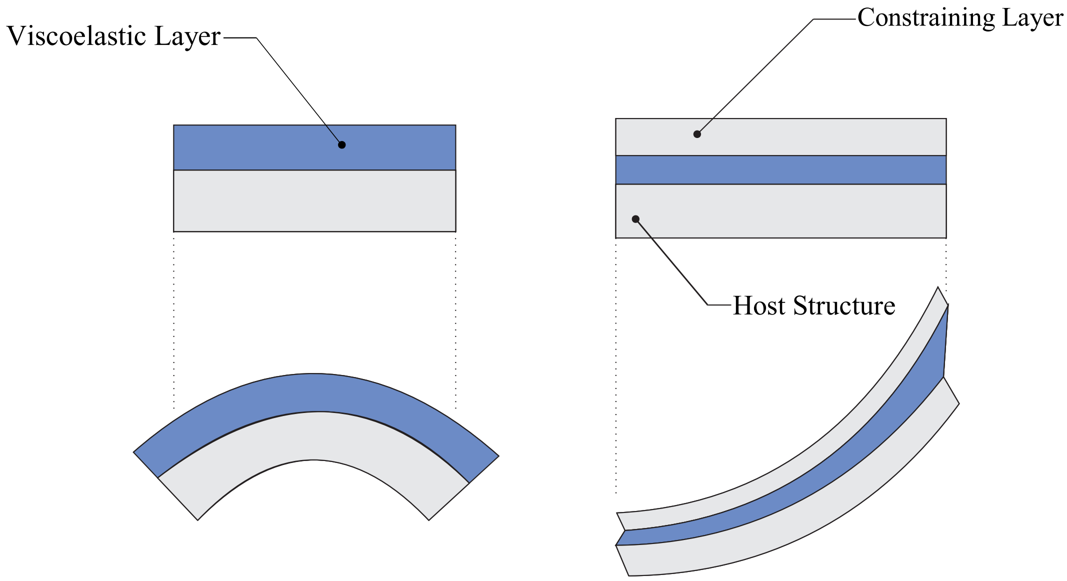

(a) Free-Layer Damping **(b)** Constrained-Layer Damping

Figure 1.1: Basic configurations for viscoelastic damping

In the FLD treatment, the energy is dissipated in the viscoelastic layer mainly due to the cyclic extensional deformation. In fact, an increase in the thickness and length of the treatment would increase the energy dissipation, however in competitive industries where the weight and cost/benefit ratio are of crucial importance, like the ones that are mentioned in the earlier section, this approach is out of interest. In opposition, has been demonstrated that the CLD is a much more efficient treatment due to their superior damping performance with low weight increase. In this treatment, an upper layer made of high elastic modulus material can be superimposed to the low modulus viscoelastic material in order to force shear deformation in the viscoelastic layer, what increases the energy dissipation. The passive constrained-layer damping treatments, are being increasingly used in automotive, railway and aircraft applications.

1.2.1 Partial Treatments: Viscoelastic Patches

The viscoelastic materials show high efficiency at a low cost but their major advantage is the fact that is a self-sufficient treatment[4]. Although the use of viscoelastic treatments could be very efficient, their performance can be improved, namely by the use of partial treatments, that decrease the structural modification in the host structure, decrease the added mass and enables a selective damping. The concept could not be more simple, add the viscoelastic material only in strategic areas - this is know as viscoelastic patches (see Figure 1.2).

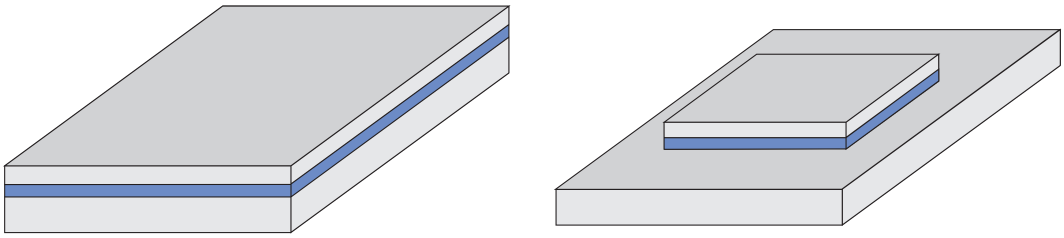

(a) Classical CLD (b) CLD Patch

Figure 1.2: Total and partial viscoelastic treatment

1.3 Models of Viscoelastic Structural Systems

The major objective in the design of viscoelastic structural systems, as well as so many others engineering systems, is their optimal performance. For this purpose, is absolutely necessary test different configurations of the structure and tune all the key parameters. In this case, questions like the thickness of the viscoelastic layers, how many viscoelastic layers are needed or what is the minimum mass added that fulfill the dynamic requirements of the structure, need to be answered. According Hazard [5], the design of a viscoelastic damping treatment involves five main design options:

- The thickness of the viscoelastic layer;
- The modulus of the viscoelastic layer (which is both temperature and frequency dependent);
- The location of the viscoelastic damping treatment;
- The thickness of the constraining layer;
- The modulus of the constraining layer;

The design process requires finding the right combination of all these variables and the models used to answer to the earlier questions have to encompass all the important physical phenomena that occur during the damping mechanism. An accurate representation of the shear strain and stress fields is absolutely critical for the success of the physical representation and the dynamic simulation of the structural system. In the case of the constrained layer damping treatment, a special and dedicated deformation theory able to capture the high shear deformation pattern developed in the viscoelastic layer during the structure vibration is needful. The *Classical Laminate Theory* (CLT) that is typically applied to structural laminates, for example, is unable to represent the shear strain deformation within the layers and cannot be used here. The *Equivalent Single-Layer* (ESL) do not take into account the interlaminar and intralaminar effects and cannot be used to, by lack of accuracy and generalization[1].

1.3.1 "Composite" Models

The first and easiest way that researchers used to simulate structures with viscoelastic treatments applied was using the modeling capabilities of existing finite element codes. Once that the structure is made with different material properties the model can be done by the assemblage of different finite elements for each layer, creating a "composite" model. In the "composite" models, layered schemes of beam, plate and solid finite elements, are used to model the host structure, viscoelastic and constraining layer[1].

Benefiting from the usual standard discretization procedures of the commercial finite element codes, an easiest way to build a "composite" model is use solid brick elements for all the layers (see Figure 1.3) . With this model, a full 3-D stress-strain state is considered and a good physical representation is obtained, however, this model requires a high computational cost due to the many degrees of freedom considered[1].

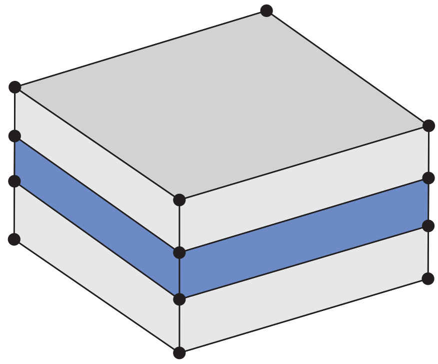

Figure 1.3: "Composite " Model - solid/solid/solid

An alternative to this model is consider solid brick elements to model the viscoelastic layer too but the host structure and constraining layer are simulated using plate elements. In this model, the translational degrees of freedom of the plate are connected to the brick ones by rigid links (see Figure 1.4). Although this model is complicated, is possible simulate the bonding failure between the viscoelastic layer and the elastic layers removing the rigid links in the desired nodes. Like in the first mentioned model, from the computational cost point of view this model is heavy too.

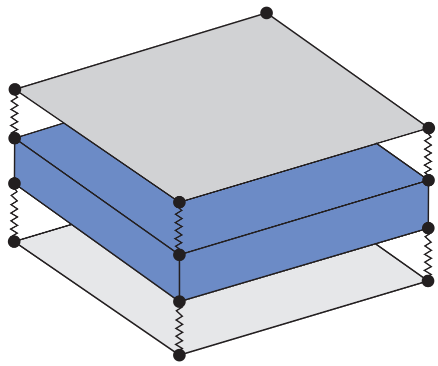

Figure 1.4: "Composite " Model - plate/rigid link/solid/rigid link/plate

Another model, similar to the previous one, consists in attach the plate elements (host structure and constraining layer) to the solid elements (viscoelastic layer) without the rigid links (see Figure 1.5). Albeit this model brings some difficulties, namely in the offsetting the nodes from the plate mid-plane to the plate surface and in establish the continuity between the different elements, it allows a degrees of freedom reduction due to the common nodes between solid and plate elements.

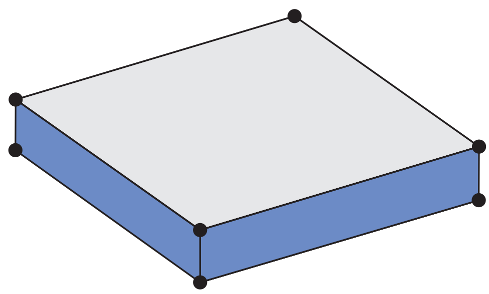

Figure 1.5: "Composite " Model - plate/solid/plate

The mentioned models share the solid brick element to simulate the viscoelastic layer. This approach provides accurate results but requires a great computational time. To overcome this issue, the viscoelastic core can be modeled using beam elements connecting the base plate to the constrained layer (plate elements) - see Figure 1.6. This simple approximation allows the reduction of the total nodal points and provides accurate predictions for linear vibratory systems.

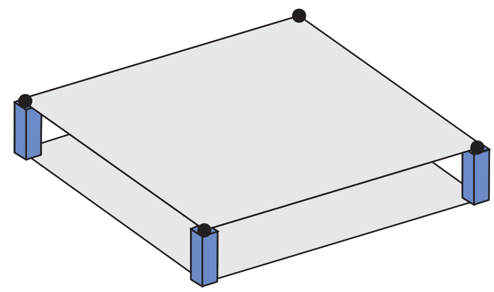

Figure 1.6: "Composite " Model - plate/beam/plate

1.3.2 Discrete-Layer (Layerwise) Models

The major advantage of the "composite" models is take the finite elements available in the commercial programs to model the sandwich structure however, this task requires a high intervention of the designer during the spatial modeling. This is an endeavor task when is necessary change the geometric parameters of the structure such as the thickness of the viscoelastic layer for an optimal design. To overcome this drawback the layerwise models (see Figure 1.7) can be used which inherently yields an higher degree of automation. Different deformation theories of different orders might be postulated for each layer and this model had been implemented with a great success in beam, plate and shell structures. These models have the great advantage of simplify the spatial model generation because the out-of-plane description such as the layers thicknesses are defined in the formulation due to the coupled-layer kinematics.

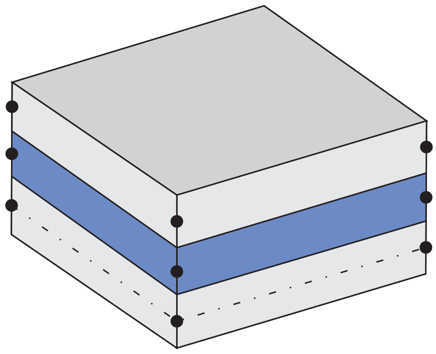

Figure 1.7: Layerwise Model

1.4 Motivations

As was said in the first section of this chapter, the use of viscoelastic structural systems has grown in the automotive, railway and aircraft industries. With the increasing use of these structures, grows the need of models which are able to represent the physical phenomena involved in such systems. The great purpose of such models, is the optimal design at a low cost and in feasible period of time. With these tight requirements in mind, the major objective of this work is study and implement a theory, firstly developed by Guyader and Lesueur [6], to model laminate structures and adapt it to model viscoelastic structural systems. The proposed model, besides the fact that shares the advantages of the discrete-layer (layerwise) models mentioned in the earlier section, have a particular advantage, the number of degrees of freedom is independent of the number of layers. The total number of degrees of freedom is equal to the number of degrees of freedom of the first layer. This is the result of writing continuities of both displacements and shear stresses at each interface. It can be said that the proposed model gathers the advantages of the layerwise models with the number of degrees of freedom of a single-layer theory. A model that is accurate with a little number of degrees of freedom brings many advantages. Firstly, the computational cost is much less when compared with models using a purely discrete-layer theory and furthermore, this is a major advantage when the viscoelastic constitutive model is obtained using an internal variables model like *Golla-Hughes-McTavish (GHM)* or *Anelastic Displacement Fields (ADF)* because the sum used in each of these models depends on the number of degrees of freedom[1, 4]. For systems with a high number of degrees of freedom, these constitutive models may not even provide results due to memory shortage and the proposed structural model, leading to systems with a much less degrees of freedom, may prove to be a powerful tool in these cases.

It is well known that a general approach able to represent structural systems, like the ones that are in study here, is the finite element method. The finite element method is the most used tool to modeling complex structures and can be used as a reliable and useful tool to characterize the structure response and analysing the effects of any damping treatment. However, in this work it will be used a Rayleigh-Ritz method, which is a direct variational method in which the minimum of a functional defined on a normed linear space is approximated by a linear combination of elements from that space. The use of this method is due to the much more easier viscoelastic patches handling, once that it works at an energetic level. The importance of the partial treatments was previously referred and this is a point of interest in this work. Furthermore, like was said before, the requirements of the 21st century are different from those of the past decades and issues like noise reduction is now of great importance. In order to understand the phenomena and provide the necessary tools to design products with the required performance, a numerical vibroacoustic analysis is done in this work.

1.5 Objectives

The main objectives aimed by the present work are the following:

- Analyse the widespread models used for the modeling of viscoelastic damping treatments and study its capability in dealing with viscoelastic damping patches;
- Understand the basic phenomena of the viscoelastic materials and study their dependencies with the view to its implementation on the mechanical model;
- Development and implementation of a Rayleigh-Ritz model for the study of orthotropic plates with viscoelastic damping treatments, specially designed for the handling of viscoelastic patches;
- Implementation of a vibroacoustic model which is capable to provide efficient and reliable results for the vibroacoustic design of plates with viscoelastic damping treatments;
- To contribute, through the development of optimisation tools and parametric analysis to the mechanical and vibroacoustic project of plates with viscoelastic damping treatments;

1.6 Organization of the Dissertation

Considering the aforementioned motivations, this dissertation work is organized in seven chapters that describe its time evolution:

- In Chapter 1 is presented the *Introduction* where the historical perspective of the theme is addressed and the new demands on this research area are mentioned focusing the strongly related study of vibration and sound. The technology of viscoelastic damping treatments is also described in this first chapter where their damping capabilities and possible arrangements are considered as well as the advantages of partial viscoelastic damping treatments using viscoelastic patches. Lastly, the structural models that have been used by the researchers to simulate these complex structures are itemized and the motivations to this work are also specified.
- The *Viscoelastic Materials* are presented in Chapter 2. In this chapter the viscoelastic materials are treated from a user viewpoint and with that in mind the material characterization by its complex modulus is explained. The constitutive behaviour of these materials is also studied in order to achieve the best properties for a given application. The mechanical properties of the viscoelastic material used in this work (3M-ISD112) are also presented in this chapter.
- In Chapter 3 is presented the *Structural Mathematical Model*, where the analytical modeling of viscoelastic damping treatments applied to multilayered plates proposed in this work is detailed. The mechanical modeling of the multilayered plates is extensively studied and the stiffness and mass matrices are obtained using a Rayleigh-Ritz method. Besides that, the major advantages of the model studied and implemented in this work are highlighted as well as its drawbacks.

- The mathematical formulation of *Mechanical and Vibroacoustic Indicators* that are used in the analysis of constrained-layer damping patches is presented in Chapter 4. As mechanical indicators the frequency response function is exposed and the IMSE (Iterative Modal Strain Energy) algorithm is explained in order to quantify the capability of the system to dissipate energy. The vibroacoustic indicators used in this work are also presented in this chapter in order to provide an efficient tool to understand the modifications introduced by the viscoelastic patches at a vibroacoustic level.

- In Chapter 5 the *Model Validation and Evaluation* is performed. The main characteristics of the mechanical and vibroacoustic model are appraised and comparisons with other models and results are made.

- The *Analysis of Constrained-Layer Damping Patches* is performed in Chapter 6. The influence of these treatments are made in a mechanical and vibroacoustic perspective in this chapter where the main objective is the optimization of key parameters in viscoelastic damping treatments such as the location of viscoelastic patches, thicknesses of the layers and geometric configuration.

- Lastly, this dissertation work is concluded in Chapter 7 – *Conclusion.* A summary of the contributions and the results obtained with this work is made, discussing the advantages and disadvantages, and giving suggestions for further work in this area.

Chapter 2

Viscoelastic Materials

2.1 Introduction

In most cases, vibrations are an undesirable consequence of a structure or machine operation and the engineers try to reduce them dampening the structure. Dampen the structure consists in remove some part of the vibration energy converting it into other forms of energy like heat, for instance. The damping characterization has been an area of active research once that the term covers a large number of physical mechanisms. This subject has been studied for a long time and a vast body of literature can be found. However, in this work, the main interest is the use of viscoelastic materials in damping treatments where the energy loss comes from the shear deformation energy of the viscoelastic material layer which is partially dissipated in the form of heat. Viscoelastic treatments are very efficient solutions as damping mechanisms for light structures but its design and analysis are quite difficult[1]. One of these difficulties is the frequency and temperature dependence and in this chapter the constitutive properties of general viscoelastic materials is studied in order to understand the behaviour of these complex materials and achieve the optimal viscoelastic damping treatment.

2.2 Viscoelastic Material Characterization

Materials for which the relationship between stress and strain depends on time are called viscoelastic[5]. These materials are rubber-like polymers composed by intertwined and cross-linked molecular chains and during the deformation the internal molecular interactions that occur give rise to macroscopic properties such as energy dissipation. This mechanism is the basis of the viscoelastic damping treatments.

2.2.1 Dynamic Loading and Complex Modulus

If linear viscoelasticity is assumed and considering an one-dimensional harmonic load applied, the following stress field is created:

$$\sigma(t) = \sigma_0 \sin(\omega t) \tag{2.2.1}$$

Due to their damping capability, when a viscoelastic material is under load, the strain is not in phase with the stress but lags behind δ, and takes the form:

$$\varepsilon(t) = \varepsilon_0 \sin(\omega t - \delta) \tag{2.2.2}$$

The lag δ is an indicator of the damping capability of the viscoelastic material, the greater the lag the greater the damping. A common way to represent the damping capability of the material is the loss factor η, that is equal to $\tan(\delta)$.

The relation between stress and strain can be defined by the complex modulus. For isotropic and homogeneous materials, the complex modulus is described by a complex Young modulus E^* and a complex Poisson's ratio ν^*[5]. However, the experimental measurement of these two quantities is not easy and generally, the Poisson's ratio is considered constant (not frequency-dependent). Mathematically, the relation between stress and strain in the frequency domain can be written as:

$$\begin{aligned} \sigma(\omega) &= \tilde{E}(\omega)\varepsilon(\omega) \\ &= [E'(\omega) + \mathrm{j}E''(\omega)]\varepsilon(\omega) \\ &= E'(\omega)\ [1 + \mathrm{j}\eta(\omega)]\varepsilon(\omega) \end{aligned} \tag{2.2.3}$$

where $\tilde{E}(\omega)$ is the complex extensional modulus, $E'(\omega)$ is the storage modulus and represents the real part of the complex modulus, $E''(\omega)$ is the loss modulus and represents the imaginary part of the complex modulus and $\eta(\omega)$ is the loss factor that was mentioned before and can be written as:

$$\eta(\omega) = \frac{E''(\omega)}{E'(\omega)} \tag{2.2.4}$$

The loss factor is a relation between imaginary and real parts of the complex modulus and can be viewed as a relation between the dissipated energy (imaginary part) and the stored one (real part). In an analogous way, if we consider shear deformation a complex shear modulus can be defined:

$$\begin{aligned} \tau(\omega) &= \tilde{G}(\omega)\gamma(\omega) \\ &= [G'(\omega) + \mathrm{j}G''(\omega)]\gamma(\omega) \\ &= G'(\omega)\ [1 + \mathrm{j}\eta(\omega)]\gamma(\omega) \end{aligned} \tag{2.2.5}$$

The complex modulus describes an elliptical trajectory in the stress/strain plane, as can be seen in Figure 2.1.

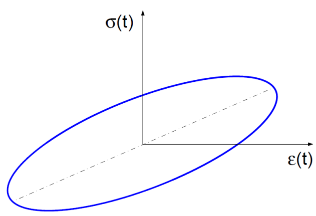

Figure 2.1: Hysteretic cycle of a viscoelastic material [4]

The shape of the ellipse in Figure 2.1 varies with the loss factor η and it describes an hysteresis trajectory where the internal area is proportional to the dissipated energy.

2.3 Selection of the Material

In general, the constitutive behaviour of the viscoelastic materials depend upon the frequency, working temperature, amplitude and type of excitation[1]. For simplicity, the amplitude and type of excitation are often overlooked since these effects are of reduced importance. However, the frequency and temperature dependence are of great importance. The temperature is an important environmental factor that affecting the dynamic properties of damping materials. This effect is shown in Figure 2.2 and four different areas can be seen. The first region is the glassy state where the material has very large storage modulus but very low damping once that the loss modulus is small. In the transition region, the material changes from a glassy state to a rubbery state and the material modulus decreases with increasing temperature. In this region, usually, the loss factor achieve his maximum. In the rubbery state the storage modulus and loss factor take low values and vary very slow with the temperature. Lastly, in the flow region the loss factor reaches very high values while material storage modulus decreases[2]. Apart from temperature, also the vibration frequency has a significant effect on the damping and dynamic modulus of viscoelastic materials. The variation of the modulus and loss factor of a typical high damping material with frequency over a range of three to five decades shows that for a material without the flow region, the effect of increasing temperature on the storage modulus is similar to the effect of reducing frequency.

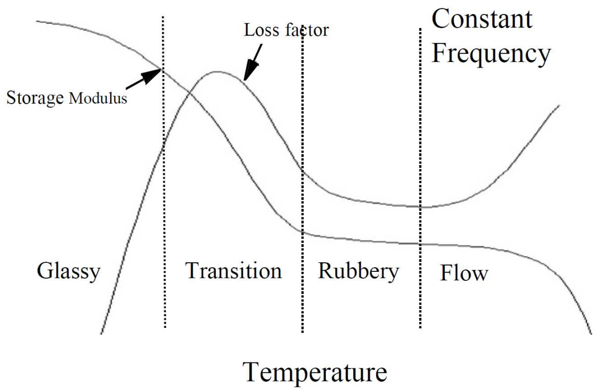

Figure 2.2: Temperature dependence of storage modulus and loss factor [2]

The knowledge of the constitutive behaviour of viscoelastic materials is extremely important in the choice of a viscoelastic material for a given application. Therefore, the loss factor peak should ideally corresponds to the standard temperature for the system in function. Ideally, the material should also have a broad loss factor peek, in order to exhibit good damping properties for a wide range of temperatures. The properties of viscoelastic materials are also affected by environmental factors such as humidity and this limits the efficiency of these materials.

These dependencies introduce serious difficulties in the definition of an accurate model able to simulate the dynamic behaviour of the damped structure. For this reason, isothermal conditions are usually assumed and only the frequency dependence is taken into account. The temperature-frequency superposition principle forms the basis of reduction of the three dimensional relation between the modulus (or loss factor), frequency and temperature to a two dimensional one. This involves the use of the reduced frequency or the reduced temperature, which combines the effects of frequency and temperature by the use of shift factors. This subject is not treated here but some references are suggested [1, 4, 5].

2.3.1 Viscoelastic Material - 3M ISD112

The viscoelastic material considered in this work is the 3M ISD112 which was chosen because it is a widely used material due to its commercial availability. In Ref.[7] the mechanical properties of this viscoelastic material, for a temperature of 25°C, are given. The properties can be seen in Table 2.1.

Table 2.1: Frequency dependence of the mechanical properties of the viscoelastic material ISD112 (T=25°C)

Frequency (Hz)	Storage Modulus (Pa)	Loss Factor	Poisson's Ratio	Density (Kg.m^{-3})
10	7.28×10^5	0.90	0.45	1140
100	2.34×10^6	1.00		
500	5.20×10^6	1.00		
1000	7.28×10^6	0.90		
2000	9.88×10^6	0.80		
3000	1.17×10^7	0.75		
4000	1.38×10^7	0.70		

In order to provide an easy computation of the mechanical properties of the viscoelastic material Castel et al. [7] gives formulas for the frequency dependence of storage modulus and loss factor:

$$E'(\omega) = 10^{(0.4884\log(\omega)+5.3848)} \tag{2.3.1}$$

$$\eta(\omega) = 10^{(-0.0175\log(\omega)^3+0.0571\log(\omega)^2+0.0015\log(\omega)-0.0874)} \tag{2.3.2}$$

where the storage modulus $E'(\omega)$ is in Pascal and the frequency ω is in Hertz. These properties can be seen in Figure 2.3.

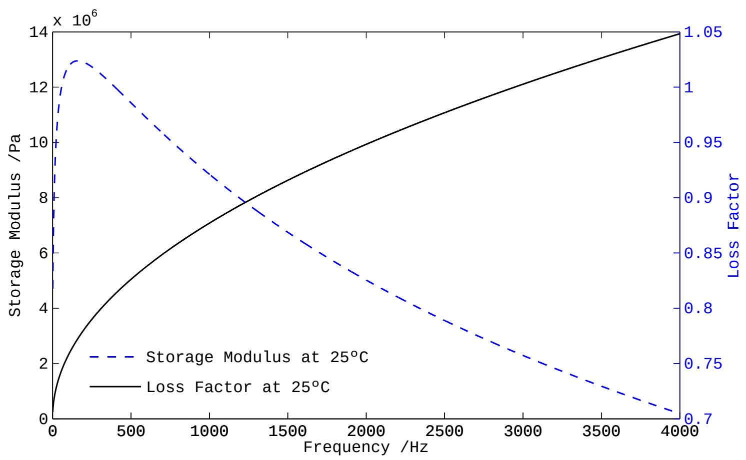

Figure 2.3: Frequency dependence of storage modulus and loss factor of selected material at 25°C

As can be seen in Figure 2.3 the storage modulus of the selected material increases with frequency while the loss factor reaches its peak at thereabout 160 Hz and then decreases with increasing frequency. According to what was stated before, the optimum damping is achieved at thereabout 160 Hz at 25°C. Finally, the density considered in Table 2.1 is different from that seen in [7] and for this material it is assumed the density given in References[1, 4].

Chapter 3

Structural Mathematical Model

3.1 Introduction

The increasing use of multilayered composites in automotive, railway and aircraft applications led the scientific community to the study of mechanical behaviour of such structures. Several works have been done in this area with many contributions along the years and the study of plate theories has a long history and several theories exist. These theories are based on variational approaches, and are currently solved by the finite element method or by the Rayleigh-Ritz method[8]. The early studies of this subject were performed by Kirchhoff, Rayleigh and Love, and take into account the in-plane (membrane) and flexural motion of the structure but neglects the transverse shear stress. This approximation makes this theory suitable for thin plates, where the thickness is assumed to be small compared to the wavelength. When shear deformation plays an important role compared to flexural deformation, which is the case of thick plates or composite structures, this theory doesn't represent the physical behaviour of such structure.

The first studies of this topic were followed by the works of Reissner and Mindlin. Their approaches are characterized by the account of shear stress beyond the in-plane and flexural motion which make these theories suitable for thick plates[8]. Many studies have been performed since that and first order shear deformation theories for multilayered plates are built using Reissner-Mindlin's assumptions.

From a structural point of view, the theories mentioned before can be used in different approaches when they are applied to multilayered structures as suggested by Woodcock [8]:

- **Single-Layer:** the different layers of the structure are replaced by a homogeneous single layer with equivalent mechanical properties.

- **Multi-Layer:** the multiple layers have their own behaviour and only a type of interface between consecutive layers is considered. This model has the advantage of explicitly include the mechanical behaviour in each layer. On the other hand, the number of unknowns increases with the number of layers.

- **Multi-Layer of Hybrid Type:** the major advantages of the preceding approaches are joined. The displacement field is defined in each layer but appropriate interface conditions are used between consecutive layers. With this hybrid theory, the different layers are "interconnected" and increasing the number of layers does not increase the number of unknowns. Although the mechanical behaviour of the structure is like a multi-layer approach, the number of unknowns is like a single-layer approach and all the parameters are calculated from the unknowns of the first layer.

3.2 The Present Work

The main objective of this work is to study the passive constrained-layer damping using viscoelastic materials and with this purpose, the present work is based in a multi-layer of hybrid type approach, firstly developed by Guyader and Lesueur [6] and followed by many authors in many works like [8–11]. Nevertheless, special attention is given to the model presented by Loredo et al. [10] where the constrained-layer damping patches are treated.

The particularities of viscoelastic patches for constrained layer damping were mentioned in the first chapter and the use of these treatments are taken into account in the model that is studied in this work. As can be seen in Figure 3.1, the structure is composed by two distinct regions. Each part of the structure, covered or uncovered, is composed of multilayered materials with an arbitrary number of layers.

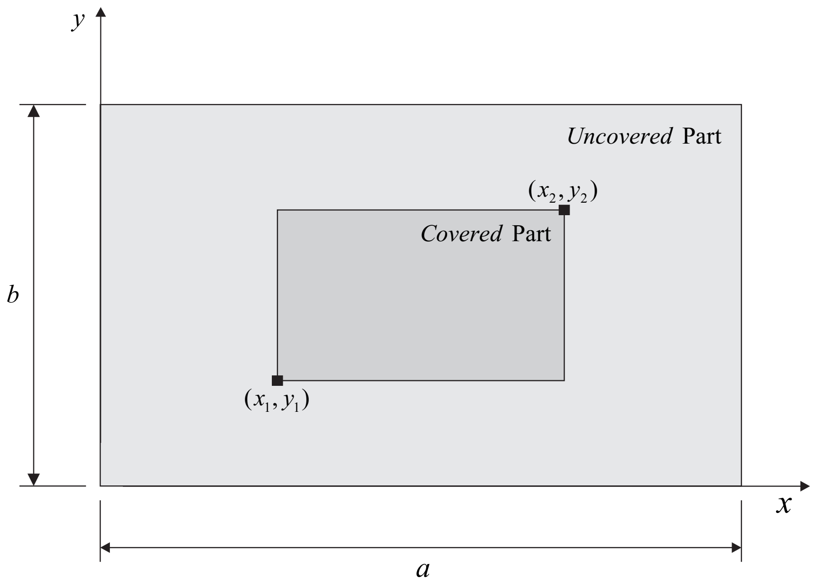

Figure 3.1: Geometrical elements of a damped plate with partial treatment

The uncovered part is the base structure and the covered part is the patch treatment applied to the base structure. The covered part (damped region) can be divided in an arbitrary number of covered parts distributed by the structure and each of these regions (uncovered and covered) can be made by an arbitrary number of layers.

The description of each layer is based on the shear deformation theory assumptions:

- the displacement gradients are small, i.e. linear hypothesis;
- the in-plane (membrane) motions are taken into account;
- the shear effect is considered, according to Mindlin's theory;

The modeling of the multi-layer system is based on the following assumptions:

- the displacement field (u, v, w) is defined for each layer;
- the transverse displacement is equal for all the layers, which means that all the layers are rigidly bonded;

- at the layers interface is assumed a continuity of displacements and shear stresses;
- a general orthotropy is included in each layer;

3.2.1 Displacement and Strain Field

This model uses a piecewise linear displacement field across the thickness where the displacement continuity is satisfied and the shear stresses continuity is enforced at each interface. The practical result is that the displacement field of each layer $\ell \in [2, ..., N]$ is linked to the displacement field of the first layer, leading to a five unknown mechanical model where all the unknowns are the unknowns of the first layer - multi-layer of hybrid type. The thicknesses and different unknowns of the displacement field for a N layer material, are shown in Figure 3.2.

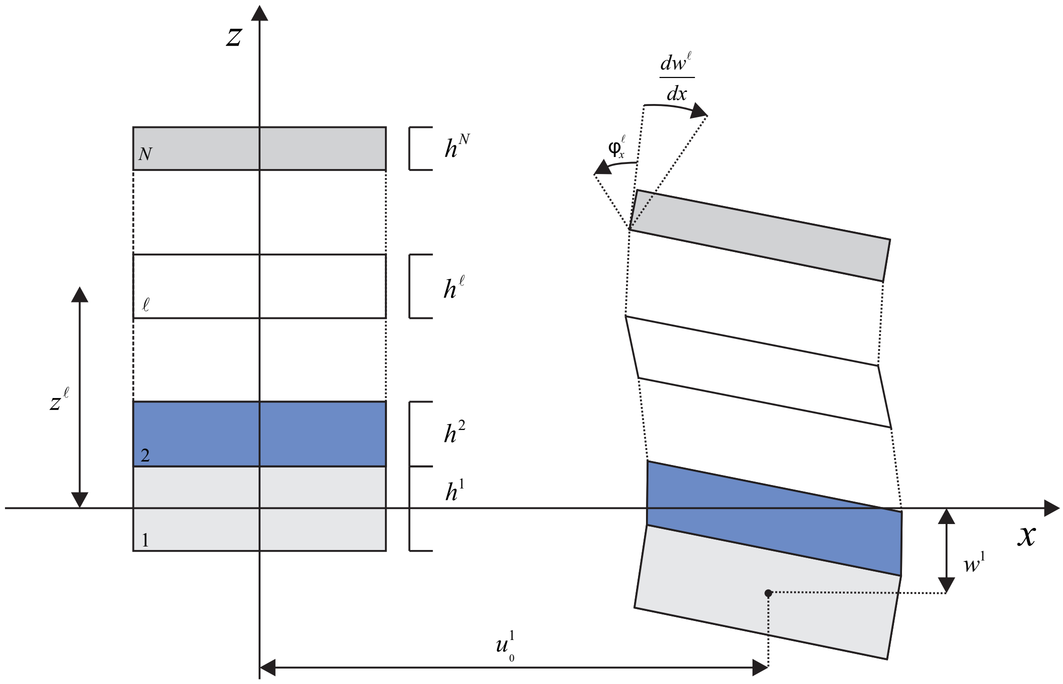

Figure 3.2: Displacement field of a multilayered material

The displacement field of each layer is written as:

$$
\begin{aligned}
u^{\ell}(x, y, z) &= u_0^{\ell}(x, y, z^{\ell}) + (z^{\ell} - z)\left(\frac{\partial w^{\ell}(x, y)}{\partial x} + \varphi_x^{\ell}(x, y)\right) \\
v^{\ell}(x, y, z) &= v_0^{\ell}(x, y, z^{\ell}) + (z^{\ell} - z)\left(\frac{\partial w^{\ell}(x, y)}{\partial y} + \varphi_y^{\ell}(x, y)\right) \\
w^{\ell}(x, y, z) &= w^{1}(x, y)
\end{aligned}
\tag{3.2.1}
$$

where $\ell \in [1, ..., N]$ is the number of the layer, w is the transverse displacement, u_0^{ℓ} and v_0^{ℓ} are the in-plane (membrane) displacements along x and y directions and φ_x^{ℓ} and φ_y^{ℓ} are the rotations caused by shear effects around x and y directions in layer ℓ, respectively. The z^{ℓ} is z-coordinate of the midplane of the layer ℓ and connects all the upper layers to the first one.

The strain field is given by:

$$\varepsilon_{ij}^{\ell} = \frac{1}{2}\left(\frac{\partial u_i^{\ell}}{\partial x_j} + \frac{\partial u_j^{\ell}}{\partial x_i}\right), \text{ for } i = j$$
$$\gamma_{ij}^{\ell} = \frac{1}{2}\left(\frac{\partial u_i^{\ell}}{\partial x_j} + \frac{\partial u_j^{\ell}}{\partial x_i}\right), \text{ for } i \neq j \tag{3.2.2}$$

where $u_{i,j}^{\ell}$ and $x_{i,j}$, respectively, denote $u^{\ell}, v^{\ell}, w^{\ell}$ and x, y, z when subscript i, j takes values x, y, z. Substituting the displacement field (3.2.1) in Equation (3.2.2):

$$\begin{aligned}
\varepsilon_{xx}^{\ell} &= \frac{\partial u_0^{\ell}}{\partial x} + (z^{\ell} - z)\left(\frac{\partial^2 w^1}{\partial^2 x} + \frac{\partial \varphi_x^{\ell}}{\partial x}\right)\\
\varepsilon_{yy}^{\ell} &= \frac{\partial v_0^{\ell}}{\partial y} + (z^{\ell} - z)\left(\frac{\partial^2 w^1}{\partial^2 y} + \frac{\partial \varphi_y^{\ell}}{\partial y}\right)\\
\gamma_{xy}^{\ell} &= \frac{1}{2}\left[\frac{\partial u_0^{\ell}}{\partial y} + (z^{\ell} - z)\left(\frac{\partial^2 w^1}{\partial x \partial y} + \frac{\partial \varphi_x^{\ell}}{\partial y}\right) + \frac{\partial v_0^{\ell}}{\partial x} + (z^{\ell} - z)\left(\frac{\partial^2 w^1}{\partial x \partial y} + \frac{\partial \varphi_y^{\ell}}{\partial x}\right)\right]\\
\gamma_{xz}^{\ell} &= \frac{1}{2}\left[\frac{\partial u_0^{\ell}}{\partial z} + (z^{\ell} - z)\left(\frac{\partial^2 w^1}{\partial x \partial z} + \frac{\partial \varphi_x^{\ell}}{\partial z}\right) + \frac{\partial w^1}{\partial x}\right]\\
\gamma_{yz}^{\ell} &= \frac{1}{2}\left[\frac{\partial v_0^{\ell}}{\partial z} + (z^{\ell} - z)\left(\frac{\partial^2 w^1}{\partial y \partial z} + \frac{\partial \varphi_y^{\ell}}{\partial z}\right) + \frac{\partial w^1}{\partial y}\right]
\end{aligned} \tag{3.2.3}$$

where dependence on x and y coordinates of the different displacements are not explicitly represented, for simplicity. As in many others plate theories, a generalized plane stress $\sigma_{zz}^{\ell} = 0$ is assumed. However, the assumed displacement field in Equation (3.2.1) leads to $\varepsilon_{zz}^{l} = 0$, which is not compatible with the generalized plane stress assumed. Nevertheless, the low values of ε_{zz}^{ℓ} compared with other strains allows this kind of displacement field. In the study of constrained viscoelastic layer damping, it should be noted that the viscoelastic material has a much lower storage modulus than the elastic layers and the preceding topic deserves a special attention. In the work performed by Loredo et al. [10] two-dimensional finite element computations over the thickness have been done and the authors say that for frequencies higher than 2 kHz this hypothesis need to be rejected.

3.2.2 Constitutive Model

In the context of a general modeling for the orthotropic properties and considering that orthotropic axes coincide with the natural axes of the plate, the stresses and the deformations are related by:

$$\begin{Bmatrix} \sigma_{xx}^{\ell} \\ \sigma_{yy}^{\ell} \\ \tau_{xy}^{\ell} \\ \tau_{xz}^{\ell} \\ \tau_{yz}^{\ell} \end{Bmatrix} = \begin{bmatrix} C_{1111}^{\ell} & C_{1122}^{\ell} & 0 & 0 & 0 \\ C_{1122}^{\ell} & C_{2222}^{\ell} & 0 & 0 & 0 \\ 0 & 0 & C_{1212}^{\ell} & 0 & 0 \\ 0 & 0 & 0 & C_{1313}^{\ell} & 0 \\ 0 & 0 & 0 & 0 & C_{2323}^{\ell} \end{bmatrix} \begin{Bmatrix} \varepsilon_{xx}^{\ell} \\ \varepsilon_{yy}^{\ell} \\ 2\gamma_{xy}^{\ell} \\ 2\gamma_{xz}^{\ell} \\ 2\gamma_{yz}^{\ell} \end{Bmatrix} \tag{3.2.4}$$

where the elastic components are given by:

$$
\begin{gathered}
C_{1111}^{\ell}=\frac{E_x^{\ell}}{1-\nu_{xy}^{\ell}\nu_{yx}^{\ell}};\ C_{1122}^{\ell}=\frac{E_y^{\ell}\nu_{xy}^{\ell}}{1-\nu_{xy}^{\ell}\nu_{yx}^{\ell}};\ C_{2222}^{\ell}=\frac{E_y^{\ell}}{1-\nu_{xy}^{\ell}\nu_{yx}^{\ell}}\\
C_{1212}^{\ell}=G_{xy}^{\ell};\ C_{1313}^{\ell}=G_{xz}^{\ell};\ C_{2323}^{\ell}=G_{yz}^{\ell}
\end{gathered}
\tag{3.2.5}
$$

where E_x^{ℓ} and E_y^{ℓ} are Young's modulus in x and y directions, G_{yz}^{ℓ} and G_{xz}^{ℓ} are the transverse shear modulus, G_{xy}^{ℓ} is the shear modulus in the O_{xy} plane, and ν_{xy} and ν_{yx} are the Poisson's ratios of the layer ℓ.

3.2.3 Interface Conditions and Transfer Matrix

As seen before, this model uses a piecewise linear displacement field across the thickness where the displacement continuity is satisfied and the shear stresses continuity is enforced at each interface. These conditions link the displacement fields of each layer to the base layer, regardless of the number of layers.

The conditions of displacement are written as:

$$
\begin{aligned}
&u^{\ell}(x,y,z^{\ell}+\frac{h^{\ell}}{2})=u^{\ell+1}(x,y,z^{\ell+1}-\frac{h^{\ell+1}}{2})\\
&v^{\ell}(x,y,z^{\ell}+\frac{h^{\ell}}{2})=v^{\ell+1}(x,y,z^{\ell+1}-\frac{h^{\ell+1}}{2})\\
&w^{\ell}(x,y,z)=w^{1}(x,y)
\end{aligned}
\tag{3.2.6}
$$

Relating (3.2.6) with (3.2.1) the displacement continuity can be written as:

$$
\begin{gathered}
u_0^{\ell}(x,y,z^{\ell})-\frac{h^{\ell}}{2}\left(\frac{\partial w^1(x,y)}{\partial x}+\varphi_x^{\ell}(x,y)\right)=u_0^{\ell+1}(x,y,z^{\ell+1})+\frac{h^{\ell+1}}{2}\left(\frac{\partial w^1(x,y)}{\partial x}+\varphi_x^{\ell+1}(x,y)\right)\\
v_0^{\ell}(x,y,z^{\ell})-\frac{h^{\ell}}{2}\left(\frac{\partial w^1(x,y)}{\partial y}+\varphi_y^{\ell}(x,y)\right)=v_0^{\ell+1}(x,y,z^{\ell+1})+\frac{h^{\ell+1}}{2}\left(\frac{\partial w^1(x,y)}{\partial y}+\varphi_y^{\ell+1}(x,y)\right)\\
w^{\ell}(x,y,z)=w^{1}(x,y)
\end{gathered}
\tag{3.2.7}
$$

The following equations express the shear stress continuity at each interface:

$$
\begin{aligned}
&\tau_{xz}(x,y,z^{\ell}+\frac{h^{\ell}}{2})=\tau_{xz}(x,y,z^{\ell+1}-\frac{h^{\ell+1}}{2})\\
&\tau_{yz}(x,y,z^{\ell}+\frac{h^{\ell}}{2})=\tau_{yz}(x,y,z^{\ell+1}-\frac{h^{\ell+1}}{2})
\end{aligned}
\tag{3.2.8}
$$

Relating Equation (3.2.8) with Equation (3.2.4) the transverse shear stress continuity can be written as:

$$C^{\ell}_{1313} 2\gamma^{\ell}_{xz}(x, y, z^{\ell} + \frac{h^{\ell}}{2}) = C^{\ell+1}_{1313} 2\gamma^{\ell+1}_{xz}(x, y, z^{\ell+1} - \frac{h^{\ell+1}}{2})$$
$$C^{\ell}_{2323} 2\gamma^{\ell}_{yz}(x, y, z^{\ell} + \frac{h^{\ell}}{2}) = C^{\ell+1}_{2323} 2\gamma^{\ell+1}_{yz}(x, y, z^{\ell+1} - \frac{h^{\ell+1}}{2}) \tag{3.2.9}$$

Link between the layer $\ell + 1$ and the layer ℓ:

Equations (3.2.6) and (3.2.8) allow the link between the layer $\ell + 1$ and the layer ℓ. From the constitutive model (3.2.4), and following a similar procedure to that developed by Loredo and Castel [11], we know that the relation between the transverse shear strain and transverse shear stress is defined as:

$$\begin{Bmatrix} 2\gamma^{\ell+1}_{xz} \\ 2\gamma^{\ell+1}_{yz} \end{Bmatrix} = (\mathbf{C}^{\ell+1}_s)^{-1} \begin{Bmatrix} \tau^{\ell+1}_{xz} \\ \tau^{\ell+1}_{yz} \end{Bmatrix} \tag{3.2.10}$$

where C^{ℓ}_s is the transverse shear stiffness matrix of layer ℓ, and is defined as:

$$\mathbf{C}^{\ell}_s = \begin{bmatrix} C^{\ell}_{1313} & 0 \\ 0 & C^{\ell}_{2323} \end{bmatrix} \tag{3.2.11}$$

As we know from Equation (3.2.8), at the interface between consecutive layers, the transverse shear stress continuity is assured and the Equation (3.2.10) can be written as:

$$\begin{Bmatrix} 2\gamma^{\ell+1}_{xz} \\ 2\gamma^{\ell+1}_{yz} \end{Bmatrix} = (\mathbf{C}^{\ell+1}_s)^{-1} \begin{Bmatrix} \tau^{\ell}_{xz} \\ \tau^{\ell}_{yz} \end{Bmatrix} = (\mathbf{C}^{\ell+1}_s)^{-1} \mathbf{C}^{\ell}_s \begin{Bmatrix} 2\gamma^{\ell}_{xz} \\ 2\gamma^{\ell}_{yz} \end{Bmatrix} \tag{3.2.12}$$

If we define an auxiliary variable:

$$\boldsymbol{\mathcal{A}}^{\ell+1} = (\mathbf{C}^{\ell+1}_s)^{-1} \mathbf{C}^{\ell}_s \tag{3.2.13}$$

Equation (3.2.12) can be rewritten as:

$$\begin{Bmatrix} \gamma^{\ell+1}_{xz} \\ \gamma^{\ell+1}_{yz} \end{Bmatrix} = \boldsymbol{\mathcal{A}}^{\ell+1} \begin{Bmatrix} \gamma^{\ell}_{xz} \\ \gamma^{\ell}_{yz} \end{Bmatrix} \tag{3.2.14}$$

Recovering Equation (3.2.2), the transverse shear stresses of layer ℓ can be written as:

$$\begin{Bmatrix} \gamma^{\ell}_{xz} \\ \gamma^{\ell}_{yz} \end{Bmatrix} = \begin{Bmatrix} \frac{1}{2}\left(\frac{\partial u^{\ell}}{\partial z} + \frac{\partial w^{\ell}}{\partial x}\right) \\ \frac{1}{2}\left(\frac{\partial v^{\ell}}{\partial z} + \frac{\partial w^{\ell}}{\partial y}\right) \end{Bmatrix} \tag{3.2.15}$$

Substituting the displacement field (3.2.1) in the preceding equation:

$$\begin{Bmatrix} \gamma_{xz}^{\ell} \\ \gamma_{yz}^{\ell} \end{Bmatrix} = \begin{Bmatrix} \frac{1}{2}\left(-\frac{\partial w^1}{\partial x} - \varphi_x^{\ell} + \frac{\partial w^1}{\partial x}\right) \\ \frac{1}{2}\left(-\frac{\partial w^1}{\partial y} - \varphi_y^{\ell} + \frac{\partial w^1}{\partial y}\right) \end{Bmatrix} \tag{3.2.16}$$

and the relation between transverse shear stresses and rotations due to the shear stress can be written as:

$$\begin{Bmatrix} \gamma_{xz}^{\ell} \\ \gamma_{yz}^{\ell} \end{Bmatrix} = \begin{Bmatrix} -\frac{1}{2}\varphi_x^{\ell} \\ -\frac{1}{2}\varphi_y^{\ell} \end{Bmatrix} \tag{3.2.17}$$

Taking into account the preceding relation, the relation given in Equation (3.2.14) can be written in terms of rotations:

$$\begin{Bmatrix} \varphi_x^{\ell+1}(x,y) \\ \varphi_y^{\ell+1}(x,y) \end{Bmatrix} = \boldsymbol{\mathcal{A}}^{\ell+1} \begin{Bmatrix} \varphi_x^{\ell}(x,y) \\ \varphi_y^{\ell}(x,y) \end{Bmatrix} \tag{3.2.18}$$

Rewriting the displacement continuity expressed in Equation (3.2.7), the in-plane (membrane) displacement of the layer $\ell+1$ is given by:

$$\begin{aligned} u_0^{\ell+1}(x,y,z^{\ell+1}) &= u_0^{\ell}(x,y,z^{\ell}) - \frac{h^{\ell}}{2}\left(\frac{\partial w^1(x,y)}{\partial x} + \varphi_x^{\ell}(x,y)\right) - \frac{h^{\ell+1}}{2}\left(\frac{\partial w^1(x,y)}{\partial x} + \varphi_x^{\ell+1}(x,y)\right) \\ v_0^{\ell+1}(x,y,z^{\ell+1}) &= v_0^{\ell}(x,y,z^{\ell}) - \frac{h^{\ell}}{2}\left(\frac{\partial w^1(x,y)}{\partial y} + \varphi_y^{\ell}(x,y)\right) - \frac{h^{\ell+1}}{2}\left(\frac{\partial w^1(x,y)}{\partial y} + \varphi_y^{\ell+1}(x,y)\right) \end{aligned} \tag{3.2.19}$$

which can be also written, taking into account Equation (3.2.18) and neglecting, for simplicity, the dependence of x and y coordinates of the different displacements, as:

$$\begin{Bmatrix} u_0^{\ell+1} \\ v_0^{\ell+1} \end{Bmatrix} = \mathbf{I}\begin{Bmatrix} u_0^{\ell} \\ v_0^{\ell} \end{Bmatrix} - \left(\frac{h^{\ell}}{2} + \frac{h^{\ell+1}}{2}\right)\mathbf{I}\begin{Bmatrix} \frac{\partial w^1}{\partial x} \\ \frac{\partial w^1}{\partial y} \end{Bmatrix} - \left(\frac{h^{\ell}}{2}\mathbf{I} + \frac{h^{\ell+1}}{2}\boldsymbol{\mathcal{A}}^{\ell+1}\right)\begin{Bmatrix} \varphi_x^{\ell} \\ \varphi_y^{\ell} \end{Bmatrix} \tag{3.2.20}$$

being $\mathbf{I}$ the identity matrix. For clarity, we can rewrite the preceding equation as:

$$\begin{Bmatrix} u_0^{\ell+1} \\ v_0^{\ell+1} \end{Bmatrix} = \mathbf{I}\begin{Bmatrix} u_0^{\ell} \\ v_0^{\ell} \end{Bmatrix} + \boldsymbol{\mathcal{B}}^{\ell+1}\begin{Bmatrix} \frac{\partial w^1}{\partial x} \\ \frac{\partial w^1}{\partial y} \end{Bmatrix} + \boldsymbol{\mathcal{D}}^{\ell+1}\begin{Bmatrix} \varphi_x^{\ell} \\ \varphi_y^{\ell} \end{Bmatrix} \tag{3.2.21}$$

with:

$$\boldsymbol{\mathcal{B}}^{\ell+1} = -\left(\frac{h^{\ell}}{2} + \frac{h^{\ell+1}}{2}\right)\mathbf{I} \quad \text{and} \quad \boldsymbol{\mathcal{D}}^{\ell+1} = -\left(\frac{h^{\ell}}{2}\mathbf{I} + \frac{h^{\ell+1}}{2}\boldsymbol{\mathcal{A}}^{\ell+1}\right) \tag{3.2.22}$$

We are able now to link the displacements field in the $(\ell+1)$th layer with the one of the ℓth layer:

$$\begin{Bmatrix} u_0^{\ell+1} \\ v_0^{\ell+1} \\ \frac{\partial w^{\ell+1}}{\partial x} \\ \frac{\partial w^{\ell+1}}{\partial y} \\ \varphi_x^{\ell+1} \\ \varphi_y^{\ell+1} \end{Bmatrix} = \begin{bmatrix} \mathbf{I} & \boldsymbol{\mathcal{B}}^{\ell+1} & \boldsymbol{\mathcal{D}}^{\ell+1} \\ \mathbf{0} & \mathbf{I} & \mathbf{0} \\ \mathbf{0} & \mathbf{0} & \boldsymbol{\mathcal{A}}^{\ell+1} \end{bmatrix} \begin{Bmatrix} u_0^{\ell} \\ v_0^{\ell} \\ \frac{\partial w^{\ell}}{\partial x} \\ \frac{\partial w^{\ell}}{\partial y} \\ \varphi_x^{\ell} \\ \varphi_y^{\ell} \end{Bmatrix} \tag{3.2.23}$$

This relation can also be written in a condensate way, as:

$$\boldsymbol{\Upsilon}^{\ell+1} = \boldsymbol{\Omega}^{\ell+1}\boldsymbol{\Upsilon}^{\ell} \tag{3.2.24}$$

Link between the layer ℓ and the layer 1:

With the relation given in Equation (3.2.24) the link between the layer ℓ and the layer 1 can be written as:

$$\boldsymbol{\Upsilon}^{\ell} = \boldsymbol{\Omega}^{\ell}\boldsymbol{\Omega}^{\ell-1}\ldots\,\boldsymbol{\Omega}^{2}\boldsymbol{\Upsilon}^{1} = \hat{\boldsymbol{\Omega}}^{\ell}\boldsymbol{\Upsilon}^{1} \tag{3.2.25}$$

where the block matrix $\hat{\boldsymbol{\Omega}}^{\ell}$ is the transfer matrix between the layer ℓ and layer 1, and can be written, in a condensate or expanded way, as:

$$\hat{\boldsymbol{\Omega}}^{\ell} = \begin{bmatrix} \mathbf{I} & \boldsymbol{\mathcal{B}}^{\ell} & \boldsymbol{\mathcal{D}}^{\ell} \\ \mathbf{0} & \mathbf{I} & \mathbf{0} \\ \mathbf{0} & \mathbf{0} & \boldsymbol{\mathcal{M}}^{\ell} \end{bmatrix} = \begin{bmatrix} 1 & 0 & \beta^{\ell} & 0 & \delta_{xx}^{\ell} & 0 \\ 0 & 1 & 0 & \beta^{\ell} & 0 & \delta_{yy}^{\ell} \\ 0 & 0 & 1 & 0 & 0 & 0 \\ 0 & 0 & 0 & 1 & 0 & 0 \\ 0 & 0 & 0 & 0 & \alpha_{xx}^{\ell} & 0 \\ 0 & 0 & 0 & 0 & 0 & \alpha_{yy}^{\ell} \end{bmatrix} \tag{3.2.26}$$

where

$$\boldsymbol{\mathcal{M}}^{\ell} = (\mathbf{C}_s^{\ell})^{-1}\mathbf{C}_s^{1} \tag{3.2.27}$$

$$\boldsymbol{\mathcal{D}}^{\ell} = -\left(\frac{h^1}{2}\mathbf{I} + \sum_{m=2}^{\ell-1} h^m \boldsymbol{\mathcal{M}}^m + \frac{h^{\ell}}{2}\boldsymbol{\mathcal{M}}^{\ell}\right) \tag{3.2.28}$$

$$\boldsymbol{\mathcal{B}}^{\ell} = -z^{\ell}\mathbf{I} \tag{3.2.29}$$

The preceding equations can be proven by recurrence. Let us try to compute a matrix which links the layer 3 and the layer 1, for example, using Equation (3.2.25) and the relations established before for the link between an arbitrary layer $(\ell+1)$ and the layer ℓ:

$$\boldsymbol{\Upsilon}^{3} = \boldsymbol{\Omega}^{3}\boldsymbol{\Omega}^{2}\boldsymbol{\Upsilon}^{1} = \hat{\boldsymbol{\Omega}}^{3}\boldsymbol{\Upsilon}^{1} \tag{3.2.30}$$

with:

$$\boldsymbol{\Omega}^3 = \begin{bmatrix} \mathbf{I} & \boldsymbol{\mathcal{B}}^{2+1} & \boldsymbol{\mathcal{D}}^{2+1} \\ \mathbf{0} & \mathbf{I} & \mathbf{0} \\ \mathbf{0} & \mathbf{0} & \boldsymbol{\mathcal{A}}^{2+1} \end{bmatrix}; \boldsymbol{\Omega}^2 = \begin{bmatrix} \mathbf{I} & \boldsymbol{\mathcal{B}}^{1+1} & \boldsymbol{\mathcal{D}}^{1+1} \\ \mathbf{0} & \mathbf{I} & \mathbf{0} \\ \mathbf{0} & \mathbf{0} & \boldsymbol{\mathcal{A}}^{1+1} \end{bmatrix} \tag{3.2.31}$$

The block matrix $\hat{\boldsymbol{\Omega}}^3$, that link the displacements field of the layer 3 with the one of the layer 1, can be written as:

$$\hat{\boldsymbol{\Omega}}^3 = \begin{bmatrix} \mathbf{I} & \boldsymbol{\mathcal{B}}^{2+1} & \boldsymbol{\mathcal{D}}^{2+1} \\ \mathbf{0} & \mathbf{I} & \mathbf{0} \\ \mathbf{0} & \mathbf{0} & \boldsymbol{\mathcal{A}}^{2+1} \end{bmatrix} \times \begin{bmatrix} \mathbf{I} & \boldsymbol{\mathcal{B}}^{1+1} & \boldsymbol{\mathcal{D}}^{1+1} \\ \mathbf{0} & \mathbf{I} & \mathbf{0} \\ \mathbf{0} & \mathbf{0} & \boldsymbol{\mathcal{A}}^{1+1} \end{bmatrix} = \begin{bmatrix} \mathbf{I} & \boldsymbol{\mathcal{B}}^{1+1} + \boldsymbol{\mathcal{B}}^{2+1} & \boldsymbol{\mathcal{D}}^{1+1} + \boldsymbol{\mathcal{D}}^{2+1}\boldsymbol{\mathcal{A}}^{1+1} \\ \mathbf{0} & \mathbf{I} & \mathbf{0} \\ \mathbf{0} & \mathbf{0} & \boldsymbol{\mathcal{A}}^{2+1}\boldsymbol{\mathcal{A}}^{1+1} \end{bmatrix} \tag{3.2.32}$$

and all the sub-matrices can be written as:

$$\boldsymbol{\mathcal{M}}^3 = \boldsymbol{\mathcal{A}}^{2+1}\boldsymbol{\mathcal{A}}^{1+1} = (\mathbf{C}_s^{2+1})^{-1}\mathbf{C}_s^2(\mathbf{C}_s^{1+1})^{-1}\mathbf{C}_s^1 = (\mathbf{C}_s^3)^{-1}\mathbf{C}_s^2(\mathbf{C}_s^2)^{-1}(\mathbf{C}_s^1) = (\mathbf{C}_s^3)^{-1}(\mathbf{C}_s^1) \tag{3.2.33}$$

$$\begin{aligned} \boldsymbol{\mathcal{D}}^3 &= \boldsymbol{\mathcal{D}}^{1+1} + \boldsymbol{\mathcal{D}}^{2+1}\boldsymbol{\mathcal{A}}^{1+1} \\ &= -\left(\frac{h^1}{2}\mathbf{I} + \frac{h^{1+1}}{2}\boldsymbol{\mathcal{A}}^{1+1}\right) - \left(\frac{h^2}{2}\mathbf{I} + \frac{h^{2+1}}{2}\boldsymbol{\mathcal{A}}^{2+1}\right)(\mathbf{C}_s^{1+1})^{-1}\mathbf{C}_s^1 \\ &= -\left(\frac{h^1}{2}\mathbf{I} + \frac{h^2}{2}(\mathbf{C}^2)^{-1}\mathbf{C}^1 + \frac{h^2}{2}(\mathbf{C}^2)^{-1}\mathbf{C}^1 + \frac{h^3}{2}(\mathbf{C}^3)^{-1}\mathbf{C}^2(\mathbf{C}^2)^{-1}\mathbf{C}^1\right) \\ &= -\left(\frac{h^1}{2}\mathbf{I} + h^2(\mathbf{C}^2)^{-1}\mathbf{C}^1 + \frac{h^3}{2}(\mathbf{C}^3)^{-1}\mathbf{C}^2(\mathbf{C}^2)^{-1}\mathbf{C}^1\right) \\ &= -\left(\frac{h^1}{2}\mathbf{I} + h^2(\mathbf{C}^2)^{-1}\mathbf{C}^1 + \frac{h^3}{2}(\mathbf{C}^3)^{-1}\mathbf{C}^1\right) \end{aligned} \tag{3.2.34}$$

$$\boldsymbol{\mathcal{B}}^3 = \boldsymbol{\mathcal{B}}^{1+1} + \boldsymbol{\mathcal{B}}^{2+1} = -\left(\frac{h^1}{2} + \frac{h^{1+1}}{2}\right)\mathbf{I} - \left(\frac{h^2}{2} + \frac{h^{2+1}}{2}\right)\mathbf{I} = -\left(\frac{h^1}{2} + h^2 + \frac{h^3}{2}\right)\mathbf{I} = -z^3\mathbf{I} \tag{3.2.35}$$

which proves the Equations (3.2.25) to (3.2.29). Taken into account Equations (3.2.25) and (3.2.26), the displacements of the layer ℓ can be finally written in terms of displacements of the first layer:

- The mid-plane displacements:

$$\begin{aligned} u_0^\ell(x,y,z^\ell) &= u_0^1(x,y,z^1) + \beta^\ell\left(\frac{\partial w^1(x,y)}{\partial x}\right) + \delta_{xx}^\ell\varphi_x^1(x,y) \\ v_0^\ell(x,y,z^\ell) &= v_0^1(x,y,z^1) + \beta^\ell\left(\frac{\partial w(x,y)^1}{\partial y}\right) + \delta_{yy}^\ell\varphi_y^1(x,y) \end{aligned} \tag{3.2.36}$$

- The rotations due to flexural motion:

$$\frac{\partial w^\ell(x,y)}{\partial x} = \frac{\partial w^1(x,y)}{\partial x}$$
$$\frac{\partial w^\ell(x,y)}{\partial y} = \frac{\partial w^1(x,y)}{\partial y} \tag{3.2.37}$$

- The rotations due to shear stress:

$$\varphi_x^\ell(x,y) = \alpha_{xx}^\ell \varphi_x^1(x,y)$$
$$\varphi_y^\ell(x,y) = \alpha_{yy}^\ell \varphi_y^1(x,y) \tag{3.2.38}$$

Substituting the preceding equations in the displacement field defined in (3.2.1):

$$\begin{aligned} u^\ell &= u_0^1 + \beta^\ell \left(\frac{\partial w^1}{\partial x}\right) + \delta_{xx}^\ell \varphi_x^1 + (z^\ell - z)\left(\frac{\partial w^1}{\partial x} + \alpha_{xx}^\ell \varphi_x^1\right) \\ v^\ell &= v_0^1 + \beta^\ell \left(\frac{\partial w^1}{\partial y}\right) + \delta_{yy}^\ell \varphi_y^1 + (z^\ell - z)\left(\frac{\partial w^1}{\partial y} + \alpha_{yy}^\ell \varphi_y^1\right) \\ w^\ell &= w^1 \end{aligned} \tag{3.2.39}$$

Shear Stress Continuity in Viscoelastic Layers

As can be seen in Equation (3.2.27), the shear stress continuity between layers is assured by the sub-matrix $\boldsymbol{\mathcal{M}}^\ell$. This sub-matrix is a relation between the shear modulus of the layer ℓ and the shear modulus of the layer 1, as can be seen in (3.2.27). In this work, where the use of viscoelastic damping treatments is a main interest, the transverse shear stress continuity must be made with special attention. In Chapter 2, was introduced the concept of complex modulus that is composed by a real part (which represents the stored energy) and an imaginary part (which represents the dissipated energy). Recalling the definition of complex shear modulus defined in Chapter 2:

$$\begin{aligned} \tau(\omega) &= \tilde{G}(\omega)\gamma(\omega) \\ &= [G'(\omega) + jG''(\omega)]\gamma(\omega) \end{aligned} \tag{3.2.40}$$

At this point, the shear stress continuity between layers considering a laminate with a viscoelastic layer is important once that the complex shear modulus of the viscoelastic layer has a real component and an imaginary one. Although this question is not explicitly referred in the work developed by Loredo et al. [10], for example, should be noted that for the shear stress continuity between an elastic layer and a viscoelastic layer only the real part of the complex shear modulus must be taken into account. The continuity should be imposed only considering the two real components, the shear modulus of the elastic layer and the storage modulus of the viscoelastic layer. The establishment of continuity also considering the imaginary part of the complex shear modulus does not have physical meaning.

3.2.4 Patch Contribution and Energy Formulation

In this section, an energy formulation of the structure is presented. The equations of motion are derived from the Lagrange-d'Alembert variational principle and for the present case, considering the undamped problem, it consists on solving the equation:

$$\delta \int_{t_1}^{t_2} \mathcal{L}(q^i, \dot{q}^i)\mathrm{d}t + \int_{t_1}^{t_2} Q_i^{ext} \delta q^i \mathrm{d}t = 0 \tag{3.2.41}$$

where $\mathcal{L}(q^i, \dot{q}^i)$ is the Lagragian operator and is given by:

$$\mathcal{L}(q^i, \dot{q}^i) = T - V \tag{3.2.42}$$

where T and V are, respectively, the kinetic and deformation energy of the plate, q^i and $\dot{q}^i$ are the generalized displacements and velocities, respectively, and Q_i^{ext} are the generalized external forces.

In this work, the patch handling is done solving Equation (3.2.41) for any virtual displacement δq^i and bringing all the deformation effects back to the base layer, defining a surface energy density. The Lagrangian term is divided in two parts corresponding to the covered and the uncovered parts:

$$\delta \int_{t_1}^{t_2} \left(\int_{S_u} (e_t^s - e_v^s)\mathrm{d}S + \int_{S_c} (e_t^d - e_v^d)\mathrm{d}S \right) \mathrm{d}t + \int_{t_1}^{t_2} Q_i^{ext} \delta q^i \mathrm{d}t = 0 \tag{3.2.43}$$

where S_i is the surface with $i = u$ for the uncovered part and $i = c$ for the covered part, e_t^j and e_v^j are, respectively, the surface density of kinetic energy and the surface density of deformation energy for the multilayered material j, with $j = s$ for the support (base layer) material, and $j = d$ for the damped (all the layers) material.

Between many points of interest in this model, the patch manipulation is, undoubtedly, one of the most important. As we see in Equation (3.2.43), this manipulation is done at an energetic level, which brings many advantages in comparison with other models where, usually, the patch manipulation is done with finite elements (finite element method), making the pre-processing stage an endeavor job. For the design of patch treatments, the patch manipulation of complex distributions using the finite element method can even make the pre-processing stage almost unrealizable.

To make the patch handling at an energetic level possible, the kinetic and deformation energy of the covered part must include the contribution of the base layers. Therefore, the energy of the common layers to covered and uncovered parts is retired from the energy of the entire uncovered plate. Then the total contribution of the covered part is added, as shown in Figure 3.3.

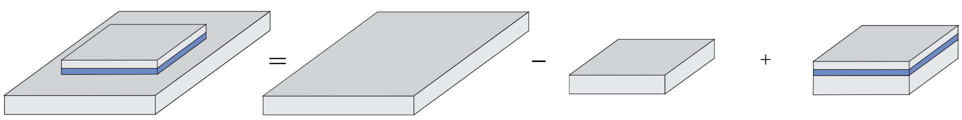

Figure 3.3: Superposition principle in the patch handling

The kinetic energy of each part, uncovered and covered, is now easily calculated from the surface density of kinetic energy of multilayered material as:

$$e_t^j = \frac{1}{2} \sum_{\ell=1}^{N^j} \int_{-\frac{h^{\ell,j}}{2}}^{\frac{h^{\ell,j}}{2}} \rho^{\ell,j} |\dot{\mathbf{u}}^{\ell,j}|^2 \mathrm{d}(z^\ell - z) \tag{3.2.44}$$

where $\rho^{\ell,j}$ is the density of the layer ℓ of the multilayered material j and $|\dot{\mathbf{u}}^{\ell,j}|^2$ is given by:

$$|\dot{\mathbf{u}}^{\ell,j}|^2 = |\dot{u}^{\ell,j}|^2 + |\dot{v}^{\ell,j}|^2 + |\dot{w}^{\ell,j}|^2 \tag{3.2.45}$$

Substituting the displacement field, given in Equation (3.2.1), in the preceding equation:

$$|\dot{\mathbf{u}}^{\ell,j}|^2 = \left(\frac{\partial u_0^\ell}{\partial t}\right)^2 + (z^\ell - z)^2 \left(\frac{\partial^2 w^1}{\partial x \partial t} + \frac{\partial \varphi_x^\ell}{\partial t}\right)^2 + \left(\frac{\partial v_0^\ell}{\partial t}\right)^2 + (z^\ell - z)^2 \left(\frac{\partial^2 w^1}{\partial y \partial t} + \frac{\partial \varphi_y^\ell}{\partial t}\right)^2 + \left(\frac{\partial w^\ell}{\partial t}\right)^2 \tag{3.2.46}$$

Taking into account that the displacements of the layer ℓ can be written in terms of displacements of the first layer, like it was demonstrated before, the preceding equation takes the form:

$$\begin{aligned}
|\dot{\mathbf{u}}^{\ell,j}|^2 &= \left(\frac{\partial u_0^1}{\partial t}\right)^2 + (\beta^\ell)^2 \left(\frac{\partial^2 w^1}{\partial x \partial t}\right)^2 + (\delta_{xx}^\ell)^2 \left(\frac{\partial \varphi_x^1}{\partial t}\right)^2 \\
&+ 2\beta^\ell \left(\frac{\partial u_0^1}{\partial t}\frac{\partial^2 w^1}{\partial x \partial t}\right) + 2\delta_{xx}^\ell \left(\frac{\partial u_0^1}{\partial t}\frac{\partial \varphi_x^1}{\partial t}\right) + 2\beta^\ell \delta_{xx}^\ell \left(\frac{\partial w^1}{\partial x}\frac{\partial \varphi_x^1}{\partial t}\right) \\
&+ (z^\ell - z)^2 \left(\frac{\partial^2 w^1}{\partial x \partial t}\right)^2 + (z^\ell - z)^2 (\alpha_{xx}^\ell)^2 \left(\frac{\partial \varphi_x^1}{\partial t}\right)^2 + 2\alpha_{xx}^\ell (z^\ell - z)^2 \left(\frac{\partial^2 w^1}{\partial x \partial t}\frac{\partial \varphi_x^1}{\partial t}\right) \\
&+ \left(\frac{\partial v_0^1}{\partial t}\right)^2 + (\beta^\ell)^2 \left(\frac{\partial^2 w^1}{\partial y \partial t}\right)^2 + (\delta_{yy}^\ell)^2 \left(\frac{\partial \varphi_y^1}{\partial t}\right)^2 \\
&+ 2\beta^\ell \left(\frac{\partial v_0^1}{\partial t}\frac{\partial^2 w^1}{\partial y \partial t}\right) + 2\delta_{yy}^\ell \left(\frac{\partial v_0^1}{\partial t}\frac{\partial \varphi_y^1}{\partial t}\right) + 2\beta^\ell \delta_{yy}^\ell \left(\frac{\partial w^1}{\partial y}\frac{\partial \varphi_y^1}{\partial t}\right) \\
&+ (z^\ell - z)^2 \left(\frac{\partial^2 w^1}{\partial y \partial t}\right)^2 + (z^\ell - z)^2 (\alpha_{yy}^\ell)^2 \left(\frac{\partial \varphi_y^1}{\partial t}\right)^2 + 2\alpha_{yy}^\ell (z^\ell - z)^2 \left(\frac{\partial^2 w^1}{\partial y \partial t}\frac{\partial \varphi_y^1}{\partial t}\right) \\
&+ \left(\frac{\partial w^1}{\partial t}\right)^2
\end{aligned} \tag{3.2.47}$$

Rearranging the preceding equation:

$$\begin{aligned}
|\dot{\mathbf{u}}^{\ell,j}|^2 &= ((\beta^\ell)^2 + (z^\ell - z)^2) \left(\frac{\partial^2 w^1}{\partial x \partial t}\right)^2 + ((\delta_{xx}^\ell)^2 + (z^\ell - z)^2 (\alpha_{xx}^\ell)^2) \left(\frac{\partial \varphi_x^1}{\partial t}\right)^2 + \left(\frac{\partial u_0^1}{\partial t}\right)^2 \\
&+ 2(\beta^\ell \delta_{xx}^\ell + \alpha_{xx}^\ell (z^\ell - z)^2) \left(\frac{\partial^2 w^1}{\partial x \partial t}\frac{\partial \varphi_x^1}{\partial t}\right) + 2\beta^\ell \left(\frac{\partial^2 w^1}{\partial x \partial t}\frac{\partial u_0^1}{\partial t}\right) + 2\delta_{xx}^\ell \left(\frac{\partial \varphi_x^1}{\partial t}\frac{\partial u_0^1}{\partial t}\right) \\
&+ ((\beta^\ell)^2 + (z^\ell - z)^2) \left(\frac{\partial^2 w^1}{\partial y \partial t}\right)^2 + ((\delta_{yy}^\ell)^2 + (z^\ell - z)^2 (\alpha_{yy}^\ell)^2) \left(\frac{\partial \varphi_y^1}{\partial t}\right)^2 + \left(\frac{\partial v_0^1}{\partial t}\right)^2
\end{aligned}$$

$$
\begin{aligned}
&+ \quad 2(\beta^\ell \delta^\ell_{yy} + \alpha^\ell_{yy}(z^\ell - z)^2) \left(\frac{\partial^2 w^1}{\partial y \partial t} \frac{\partial \varphi^1_y}{\partial t} \right) + 2\beta^\ell \left(\frac{\partial^2 w^1}{\partial y \partial t} \frac{\partial v^1_0}{\partial t} \right) + 2\delta^\ell_{yy} \left(\frac{\partial \varphi^1_y}{\partial t} \frac{\partial v^1_0}{\partial t} \right) \\
&+ \quad \left(\frac{\partial w^1}{\partial t} \right)^2
\end{aligned} \tag{3.2.48}
$$

Substituting the preceding Equation in Equation (3.2.44), the surface density of kinetic energy may be written as:

$$
\begin{aligned}
e^j_t \quad &= \quad \frac{1}{2} \Bigg[\delta^j_1 \left(\frac{\partial^2 w^1}{\partial x \partial t} \right)^2 + \delta^j_2 \left(\frac{\partial \varphi^1_x}{\partial t} \right)^2 + \delta^j_3 \left(\frac{\partial u^1_0}{\partial t} \right)^2 \\
&+ \quad \delta^j_4 \left(\frac{\partial^2 w^1}{\partial x \partial t} \frac{\partial \varphi^1_x}{\partial t} \right) + \delta^j_5 \left(\frac{\partial^2 w^1}{\partial x \partial t} \frac{\partial u^1_0}{\partial t} \right) + \delta^j_6 \left(\frac{\partial \varphi^1_x}{\partial t} \frac{\partial u^1_0}{\partial t} \right) \\
&+ \quad \delta^j_7 \left(\frac{\partial^2 w^1}{\partial y \partial t} \right)^2 + \delta^j_8 \left(\frac{\partial \varphi^1_y}{\partial t} \right)^2 + \delta^j_9 \left(\frac{\partial v^1_0}{\partial t} \right)^2 \\
&+ \quad \delta^j_{10} \left(\frac{\partial^2 w^1}{\partial y \partial t} \frac{\partial \varphi^1_y}{\partial t} \right) + \delta^j_{11} \left(\frac{\partial^2 w^1}{\partial y \partial t} \frac{\partial v^1_0}{\partial t} \right) + \delta^j_{12} \left(\frac{\partial \varphi^1_y}{\partial t} \frac{\partial v^1_0}{\partial t} \right) \\
&+ \quad \delta^j_{13} \left(\frac{\partial w^1}{\partial t} \right)^2 \Bigg]
\end{aligned} \tag{3.2.49}
$$

The coefficients δ_i are given in Appendix A. As it shown in Equation (3.2.43), the density of kinetic energy can be related with kinetic energy as:

$$
T = \int_S e^j_t \mathrm{d}S \tag{3.2.50}
$$

The surface density of deformation energy of each part, required for the calculation of the deformation energy V is given by:

$$
e^j_v = \frac{1}{2} \sum_{\ell=1}^{N^j} \int_{-\frac{h^{\ell,j}}{2}}^{\frac{h^{\ell,j}}{2}} \sigma^{\ell,j}_{ik} \varepsilon^{\ell,j}_{ik} \mathrm{d}(z^\ell - z) \tag{3.2.51}
$$

where $\sigma^{\ell,j}_{ik}$ and $\varepsilon^{\ell,j}_{ik}$ represent here, respectively, the normal and shear stresses and strains from the constitutive model defined in (3.2.4). Therefore, the surface density of deformation energy can be expressed as:

$$e_v^j = \frac{1}{2}\sum_{\ell=1}^{N^j}\int_{-\frac{h^{\ell,j}}{2}}^{\frac{h^{\ell,j}}{2}}\Big[C_{1111}^{\ell}(\varepsilon_{xx}^{\ell})^2 + C_{2222}^{\ell}(\varepsilon_{yy}^{\ell})^2 + 2C_{1122}^{\ell}\varepsilon_{xx}^{\ell}\varepsilon_{yy}^{\ell}$$
$$+4C_{1212}(\gamma_{xy}^{\ell})^2 + 4C_{1313}^{\ell}(\gamma_{xz}^{\ell})^2] + 4C_{2323}^{\ell}(\gamma_{yz}^{\ell})^2\Big]\mathrm{d}(z^{\ell}-z) \tag{3.2.52}$$

Considering the strain field defined in (3.2.3), the preceding equation can be written as:

$$\begin{aligned}
\sigma_{ik}^{\ell,j}\varepsilon_{ik}^{\ell,j} &= C_{1111}^{\ell}\Bigg[\left(\frac{\partial u_0^{\ell}}{\partial x}\right)^2 + 2(z^{\ell}-z)\left(\frac{\partial u_0^{\ell}}{\partial x}\frac{\partial^2 w^1}{\partial x^2}\right) + 2(z^{\ell}-z)\left(\frac{\partial u_0^{\ell}}{\partial x}\frac{\partial \varphi_x^{\ell}}{\partial x}\right) \\
&+ (z^{\ell}-z)^2\left(\frac{\partial^2 w^1}{\partial x^2}\right)^2 + (z^{\ell}-z)^2\left(\frac{\partial \varphi_x^{\ell}}{\partial x}\right)^2 + 2(z^{\ell}-z)^2\left(\frac{\partial^2 w^1}{\partial x^2}\frac{\partial \varphi_x^{\ell}}{\partial x}\right)\Bigg] \\
&+ C_{2222}^{\ell}\Bigg[\left(\frac{\partial v_0^{\ell}}{\partial y}\right)^2 + 2(z^{\ell}-z)\left(\frac{\partial v_0^{\ell}}{\partial y}\frac{\partial^2 w^1}{\partial y^2}\right) + 2(z^{\ell}-z)\left(\frac{\partial v_0^{\ell}}{\partial y}\frac{\partial \varphi_y^{\ell}}{\partial y}\right) \\
&+ (z^{\ell}-z)^2\left(\frac{\partial^2 w^1}{\partial y^2}\right)^2 + (z^{\ell}-z)^2\left(\frac{\partial \varphi_y^{\ell}}{\partial y}\right)^2 + 2(z^{\ell}-z)^2\left(\frac{\partial^2 w^1}{\partial y^2}\frac{\partial \varphi_y^{\ell}}{\partial y}\right)\Bigg] \\
&+ 2C_{1122}^{\ell}\Bigg[\left(\frac{\partial u_0^{\ell}}{\partial x}\frac{\partial v_0^{\ell}}{\partial y}\right) + (z^{\ell}-z)\left(\frac{\partial^2 w^1}{\partial y^2}\frac{\partial u_0^{\ell}}{\partial x}\right) + (z^{\ell}-z)\left(\frac{\partial \varphi_y^{\ell}}{\partial y}\frac{\partial u_0^{\ell}}{\partial x}\right) \\
&+ (z^{\ell}-z)\left(\frac{\partial^2 w^1}{\partial x^2}\frac{\partial v_0^{\ell}}{\partial y}\right) + (z^{\ell}-z)\left(\frac{\partial \varphi_x^{\ell}}{\partial x}\frac{\partial v_0^{\ell}}{\partial y}\right) + (z^{\ell}-z)^2\left(\frac{\partial^2 w^1}{\partial x^2}\frac{\partial^2 w^1}{\partial y^2}\right) \\
&+ (z^{\ell}-z)^2\left(\frac{\partial^2 w^1}{\partial x^2}\frac{\partial \varphi_y^{\ell}}{\partial y}\right) + (z^{\ell}-z)^2\left(\frac{\partial^2 w^1}{\partial y^2}\frac{\partial \varphi_x^{\ell}}{\partial x}\right)\Bigg] \\
&+ C_{1212}^{\ell}\Bigg[\left(\frac{\partial u_0^{\ell}}{\partial y}\right)^2 + (z^{\ell}-z)^2\left(\frac{\partial^2 w^1}{\partial x\partial y}\right)^2 + (z^{\ell}-z)^2\left(\frac{\partial \varphi_x^{\ell}}{\partial y}\right)^2 \\
&+ 2(z^{\ell}-z)^2\left(\frac{\partial^2 w^1}{\partial x\partial y}\frac{\partial \varphi_x^{\ell}}{\partial y}\right) + 2(z^{\ell}-z)\left(\frac{\partial u_0^{\ell}}{\partial y}\frac{\partial^2 w^1}{\partial x\partial y}\right) + 2(z^{\ell}-z)\left(\frac{\partial u_0^{\ell}}{\partial y}\frac{\partial \varphi_x^{\ell}}{\partial y}\right) \\
&+ \left(\frac{\partial v_0^{\ell}}{\partial x}\right)^2 + (z^{\ell}-z)^2\left(\frac{\partial^2 w^1}{\partial x\partial y}\right)^2 + (z^{\ell}-z)^2\left(\frac{\partial \varphi_y^{\ell}}{\partial x}\right)^2 + 2(z^{\ell}-z)^2\left(\frac{\partial^2 w^1}{\partial x\partial y}\frac{\partial \varphi_y^{\ell}}{\partial x}\right) \\
&+ 2(z^{\ell}-z)\left(\frac{\partial v_0^{\ell}}{\partial x}\frac{\partial^2 w^1}{\partial x\partial y}\right) + 2(z^{\ell}-z)\left(\frac{\partial v_0^{\ell}}{\partial x}\frac{\partial \varphi_y^{\ell}}{\partial x}\right)\Bigg] + C_{1313}^{\ell}(\varphi_x^{\ell})^2 + C_{2323}^{\ell}(\varphi_y^{\ell})^2
\end{aligned} \tag{3.2.53}$$

With the transfer matrix calculated in the preceding section, Equation (3.2.53) can be expressed in terms of the unknowns of the first layer as:

$$
\begin{aligned}
\sigma_{ik}^{\ell,j}\varepsilon_{ik}^{\ell,j} \;=\;& C^{\ell}_{1111}\Bigg[\left(\frac{\partial u_0^1}{\partial x}\right)^2 + 2\beta^{\ell}\left(\frac{\partial^2 w^1}{\partial x^2}\frac{\partial u_0^1}{\partial x}\right) + 2\delta^{\ell}_{xx}\left(\frac{\partial u_0^1}{\partial x}\frac{\partial \varphi_x^1}{\partial x}\right) + 2(z^{\ell}-z)\left(\frac{\partial^2 w^1}{\partial x^2}\frac{\partial u_0^1}{\partial x}\right) \\
+\;& 2\alpha^{\ell}_{xx}(z^{\ell}-z)\left(\frac{\partial u_0^1}{\partial x}\frac{\partial \varphi^1}{\partial x}\right) + (\beta^{\ell})^2\left(\frac{\partial^2 w^1}{\partial x^2}\right)^2 + 2\delta^{\ell}_{xx}\beta^{\ell}\left(\frac{\partial^2 w^1}{\partial x^2}\frac{\partial \varphi_x^1}{\partial x}\right) \\
+\;& 2\beta^{\ell}(z^{\ell}-z)\left(\frac{\partial^2 w^1}{\partial x^2}\right)^2 + 2\beta^{\ell}\alpha^{\ell}_{xx}(z^{\ell}-z)\left(\frac{\partial^2 w^1}{\partial x^2}\frac{\partial \varphi^1}{\partial x}\right) + (\delta^{\ell}_{xx})^2\left(\frac{\partial \varphi_x^1}{\partial x}\right)^2 \\
+\;& 2\delta^{\ell}_{xx}(z^{\ell}-z)\left(\frac{\partial^2 w^1}{\partial x^2}\frac{\partial \varphi_x^1}{\partial x}\right) + 2\delta^{\ell}_{xx}\alpha^{\ell}_{xx}(z^{\ell}-z)\left(\frac{\partial \varphi_x^1}{\partial x}\right)^2 + (z^{\ell}-z)^2\left(\frac{\partial^2 w^1}{\partial x^2}\right)^2 \\
+\;& (\alpha^{\ell}_{xx})^2(z^{\ell}-z)^2\left(\frac{\partial \varphi_x^1}{\partial x}\right)^2 + 2\alpha^{\ell}_{xx}(z^{\ell}-z)^2\left(\frac{\partial^2 w^1}{\partial x^2}\frac{\partial \varphi_x^1}{\partial x}\right)\Bigg] \\
+\;& C^{\ell}_{2222}\Bigg[\left(\frac{\partial v_0^1}{\partial y}\right)^2 + 2\beta^{\ell}\left(\frac{\partial^2 w^1}{\partial y^2}\frac{\partial v_0^1}{\partial y}\right) + 2\delta^{\ell}_{yy}\left(\frac{\partial v_0^1}{\partial y}\frac{\partial \varphi_y^1}{\partial y}\right) + 2(z^{\ell}-z)\left(\frac{\partial^2 w^1}{\partial y^2}\frac{\partial v_0^1}{\partial y}\right) \\
+\;& 2\alpha^{\ell}_{yy}(z^{\ell}-z)\left(\frac{\partial v_0^1}{\partial y}\frac{\partial \varphi_y^1}{\partial y}\right) + (\beta^{\ell})^2\left(\frac{\partial^2 w^1}{\partial y^2}\right)^2 + 2\delta^{\ell}_{yy}\beta^{\ell}\left(\frac{\partial^2 w^1}{\partial y^2}\frac{\partial \varphi_y^1}{\partial y}\right) \\
+\;& 2\beta^{\ell}(z^{\ell}-z)\left(\frac{\partial^2 w^1}{\partial y^2}\right)^2 + 2\beta^{\ell}\alpha^{\ell}_{yy}(z^{\ell}-z)\left(\frac{\partial^2 w^1}{\partial y^2}\frac{\partial \varphi_y^1}{\partial y}\right) + (\delta^{\ell}_{yy})^2\left(\frac{\partial \varphi_y^1}{\partial y}\right)^2 \\
+\;& 2\delta^{\ell}_{yy}(z^{\ell}-z)\left(\frac{\partial^2 w^1}{\partial y^2}\frac{\partial \varphi_y^1}{\partial y}\right) + 2\delta^{\ell}_{yy}\alpha^{\ell}_{yy}(z^{\ell}-z)\left(\frac{\partial \varphi_y^1}{\partial y}\right)^2 + (z^{\ell}-z)^2\left(\frac{\partial^2 w^1}{\partial y^2}\right)^2 \\
+\;& (\alpha^{\ell}_{yy})^2(z^{\ell}-z)^2\left(\frac{\partial \varphi_y^1}{\partial y}\right)^2 + 2\alpha^{\ell}_{yy}(z^{\ell}-z)^2\left(\frac{\partial^2 w^1}{\partial y^2}\frac{\partial \varphi_y^1}{\partial y}\right)\Bigg] \\
+\;& 2C^{\ell}_{1122}\Bigg[\left(\frac{\partial u_0^1}{\partial x}\frac{\partial v_0^1}{\partial y}\right) + \beta^{\ell}\left(\frac{\partial^2 w^1}{\partial y^2}\frac{\partial u_0^1}{\partial x}\right) + \delta^{\ell}_{yy}\left(\frac{\partial u_0^1}{\partial x}\frac{\partial \varphi_y^1}{\partial y}\right) + (\beta^{\ell})\left(\frac{\partial^2 w^1}{\partial x^2}\frac{\partial v_0^1}{\partial y}\right) \\
+\;& (\beta^{\ell})^2\left(\frac{\partial^2 w^1}{\partial x^2}\frac{\partial^2 w^1}{\partial y^2}\right) + \beta^{\ell}\delta^{\ell}_{yy}\left(\frac{\partial^2 w^1}{\partial x^2}\frac{\partial \varphi_y^1}{\partial y}\right) + \delta^{\ell}_{xx}\left(\frac{\partial \varphi_x^1}{\partial x}\frac{\partial v_0^1}{\partial y}\right) + \beta^{\ell}\delta^{\ell}_{xx}\left(\frac{\partial^2 w^1}{\partial y^2}\frac{\partial \varphi_x^1}{\partial x}\right) \\
+\;& \delta^{\ell}_{xx}\delta^{\ell}_{yy}\left(\frac{\partial \varphi_x^1}{\partial x}\frac{\partial \varphi_y^1}{\partial y}\right) + (z^{\ell}-z)\left(\frac{\partial^2 w^1}{\partial y^2}\frac{\partial u_0^1}{\partial x}\right) + \beta^{\ell}(z^{\ell}-z)\left(\frac{\partial^2 w^1}{\partial y^2}\frac{\partial^2 w^1}{\partial x^2}\right) \\
+\;& \delta^{\ell}_{xx}(z^{\ell}-z)\left(\frac{\partial^2 w^1}{\partial y^2}\frac{\partial \varphi_x^1}{\partial x}\right) + \alpha^{\ell}_{yy}(z^{\ell}-z)\left(\frac{\partial u_0^1}{\partial x}\frac{\partial \varphi_y^1}{\partial y}\right) + \beta^{\ell}\alpha^{\ell}_{yy}(z^{\ell}-z)\left(\frac{\partial^2 w^1}{\partial x^2}\frac{\partial \varphi_y^1}{\partial y}\right) \\
+\;& \delta^{\ell}_{xx}\alpha^{\ell}_{yy}(z^{\ell}-z)\left(\frac{\partial \varphi_x^1}{\partial x}\frac{\partial \varphi_y^1}{\partial y}\right) + (z^{\ell}-z)\left(\frac{\partial^2 w^1}{\partial x^2}\frac{\partial v_0^1}{\partial y}\right) + \beta^{\ell}(z^{\ell}-z)\left(\frac{\partial^2 w^1}{\partial x^2}\frac{\partial^2 w^1}{\partial y^2}\right) \\
+\;& \delta^{\ell}_{yy}(z^{\ell}-z)\left(\frac{\partial^2 w^1}{\partial x^2}\frac{\partial \varphi_y^1}{\partial y}\right)\alpha^{\ell}_{xx}(z^{\ell}-z)\left(\frac{\partial v_0^1}{\partial y}\frac{\partial \varphi_x^1}{\partial x}\right) + \beta^{\ell}\alpha^{\ell}_{xx}(z^{\ell}-z)\left(\frac{\partial^2 w^1}{\partial y^2}\frac{\partial \varphi_x^1}{\partial x}\right)
\end{aligned}
$$

$$
\begin{aligned}
&+ \quad \delta^\ell_{yy}\alpha^\ell_{xx}(z^\ell - z)\left(\frac{\partial\varphi^1_x}{\partial x}\frac{\partial\varphi^1_y}{\partial y}\right) + (z^\ell - z)^2\left(\frac{\partial^2 w^1}{\partial x^2}\frac{\partial^2 w^1}{\partial y^2}\right) + \alpha^\ell_{yy}(z^\ell - z)^2\left(\frac{\partial^2 w^1}{\partial x^2}\frac{\partial\varphi^1_y}{\partial y}\right)\\
&+ \quad \alpha^\ell_{xx}(z^\ell - z)^2\left(\frac{\partial^2 w^1}{\partial y^2}\frac{\partial\varphi^1_x}{\partial x}\right)\Bigg]\\
&+ \quad C^\ell_{1212}\Bigg[\left(\frac{\partial u^1_0}{\partial y}\right)^2 + 2\beta^\ell\left(\frac{\partial u^1_0}{\partial y}\frac{\partial^2 w^1}{\partial x\partial y}\right) + 2\delta^\ell\left(\frac{\partial u^1_0}{\partial y}\frac{\partial\varphi^1_x}{\partial y}\right) + (\beta^\ell)^2\left(\frac{\partial^2 w^1}{\partial x\partial y}\right)^2\\
&+ \quad 2\beta^\ell\delta^\ell_{xx}\left(\frac{\partial^2 w^1}{\partial x\partial y}\frac{\partial\varphi^1_x}{\partial y}\right) + (\delta^\ell_{xx})^2\left(\frac{\partial\varphi^1_x}{\partial y}\right)^2 + (z^\ell - z)^2\left(\frac{\partial^2 w^1}{\partial x\partial y}\right)^2\\
&+ \quad (\alpha^\ell_{xx})^2(z^\ell - z)^2\left(\frac{\partial\varphi^1_x}{\partial y}\right)^2 + 2\alpha^\ell_{xx}(z^\ell - z)^2\left(\frac{\partial^2 w^1}{\partial x\partial y}\frac{\partial\varphi^1_x}{\partial y}\right) + 2(z^\ell - z)\left(\frac{\partial^2 w^1}{\partial x\partial y}\frac{\partial u^1_0}{\partial y}\right)\\
&+ \quad 2\beta^\ell(z^\ell - z)\left(\frac{\partial^2 w^1}{\partial x\partial y}\right)^2 + 2\delta^\ell_{xx}(z^\ell - z)\left(\frac{\partial^2 w^1}{\partial x\partial y}\frac{\partial\varphi^1}{\partial y}\right) + 2\alpha^\ell_{xx}(z^\ell - z)\left(\frac{\partial u^1_0}{\partial y}\frac{\partial\varphi^1_x}{\partial y}\right)\\
&+ \quad 2\beta^\ell\alpha^\ell_{xx}(z^\ell - z)\left(\frac{\partial^2 w^1}{\partial x\partial y}\frac{\partial\varphi^1}{\partial y}\right) + 2\delta^\ell_{xx}\alpha^\ell_{xx}(z^\ell - z)\left(\frac{\partial\varphi^1_x}{\partial y}\right)^2\\
&+ \quad \left(\frac{\partial v^1_0}{\partial x}\right)^2 + 2\beta^\ell\left(\frac{\partial v^1_0}{\partial x}\frac{\partial^2 w^1}{\partial x\partial y}\right) + 2\delta^\ell_{yy}\left(\frac{\partial v^1_0}{\partial x}\frac{\partial\varphi^1_y}{\partial x}\right) + (\beta^\ell)^2\left(\frac{\partial^2 w^1}{\partial x\partial y}\right)^2\\
&+ \quad 2\beta^\ell\delta^\ell_{yy}\left(\frac{\partial^2 w^1}{\partial x\partial y}\frac{\partial\varphi^1_y}{\partial x}\right) + (\delta^\ell_{yy})^2\left(\frac{\partial\varphi^1_y}{\partial x}\right)^2 + (z^\ell - z)^2\left(\frac{\partial^2 w^1}{\partial x\partial y}\right)^2\\
&+ \quad (\alpha^\ell_{yy})^2(z^\ell - z)^2\left(\frac{\partial\varphi^\ell_y}{\partial x}\right)^2 + 2\alpha^\ell_{yy}(z^\ell - z)^2\left(\frac{\partial^2 w^1}{\partial x\partial y}\frac{\partial\varphi^\ell_y}{\partial x}\right)\\
&+ \quad 2(z^\ell - z)\left(\frac{\partial^2 w^1}{\partial x\partial y}\frac{\partial v^1_0}{\partial x}\right) + 2\beta^\ell(z^\ell - z)\left(\frac{\partial^2 w^1}{\partial x\partial y}\right)^2 + 2\delta^\ell_{yy}(z^\ell - z)\left(\frac{\partial^2 w^1}{\partial x\partial y}\frac{\partial\varphi^1_y}{\partial x}\right)\\
&+ \quad 2\alpha^\ell_{yy}(z^\ell - z)\left(\frac{\partial v^1_0}{\partial x}\frac{\partial\varphi^1_y}{\partial x}\right) + 2\alpha^\ell_{yy}\beta^\ell(z^\ell - z)\left(\frac{\partial^2 w^1}{\partial x\partial y}\frac{\partial\varphi^1_y}{\partial x}\right) + 2\alpha^\ell_{yy}\delta^\ell_{yy}(z^\ell - z)\left(\frac{\partial\varphi^1_y}{\partial x}\right)^2\Bigg]\\
&+ \quad C^\ell_{1313}(\alpha^\ell_{xx})^2(\varphi^1_x)^2 + C^\ell_{2323}(\alpha^\ell_{yy})^2(\varphi^1_y)^2
\end{aligned}
\tag{3.2.54}
$$

Substituting the preceding Equation in Equation (3.2.51), the surface density of deformation energy may be written as:

$$
e^j_v = \frac{1}{2}\Bigg[\lambda^j_1\left(\frac{\partial^2 w^1}{\partial x^2}\right)^2 + \lambda^j_2\left(\frac{\partial\varphi^1_x}{\partial x}\right)^2 + \lambda^j_3\left(\frac{\partial u^1_0}{\partial x}\right)^2 + \lambda^j_4\left(\frac{\partial^2 w^1}{\partial x^2}\frac{\partial\varphi^1_x}{\partial x}\right) + \lambda^j_5\left(\frac{\partial^2 w^1}{\partial x^2}\frac{\partial u^1_0}{\partial x}\right)
$$

$$
\begin{aligned}
&+ \quad \lambda_6^j\left(\frac{\partial \varphi_x^1}{\partial x}\frac{\partial u_0^1}{\partial x}\right)+\lambda_7^j\left(\frac{\partial^2 w^1}{\partial y^2}\right)^2+\lambda_8^j\left(\frac{\partial \varphi_y^1}{\partial y}\right)^2+\lambda_9^j\left(\frac{\partial v_0^1}{\partial y}\right)^2+\lambda_{10}^j\left(\frac{\partial^2 w^1}{\partial y^2}\frac{\partial \varphi_y^1}{\partial y}\right)\\
&+ \quad \lambda_{11}^j\left(\frac{\partial^2 w^1}{\partial y^2}\frac{\partial v_0^1}{\partial y}\right)+\lambda_{12}^j\left(\frac{\partial \varphi_y^1}{\partial y}\frac{\partial v_0^1}{\partial y}\right)+\lambda_{13}^j\left(\frac{\partial^2 w^1}{\partial x^2}\frac{\partial^2 w^1}{\partial y^2}\right)+\lambda_{14}^j\left(\frac{\partial^2 w^1}{\partial x^2}\frac{\partial \varphi_y^1}{\partial y}\right)\\
&+ \quad \lambda_{15}^j\left(\frac{\partial^2 w^1}{\partial x^2}\frac{\partial v_0^1}{\partial y}\right)+\lambda_{16}^j\left(\frac{\partial^2 w^1}{\partial y^2}\frac{\partial \varphi_x^1}{\partial x}\right)+\lambda_{17}^j\left(\frac{\partial \varphi_x^1}{\partial x}\frac{\partial \varphi_y^1}{\partial y}\right)+\lambda_{18}^j\left(\frac{\partial \varphi_x^1}{\partial x}\frac{\partial v_0^1}{\partial y}\right)\\
&+ \quad \lambda_{19}^j\left(\frac{\partial^2 w^1}{\partial y^2}\frac{\partial u_0^1}{\partial x}\right)+\lambda_{20}^j\left(\frac{\partial u_0^1}{\partial x}\frac{\partial \varphi_y^1}{\partial y}\right)+\lambda_{21}^j\left(\frac{\partial u_0^1}{\partial x}\frac{\partial v_y^1}{\partial y}\right)+\lambda_{22}^j\left(\frac{\partial^2 w^1}{\partial x \partial y}\right)^2+\lambda_{23}^j\left(\frac{\partial \varphi_x^1}{\partial y}\right)^2\\
&+ \quad \lambda_{24}^j\left(\frac{\partial \varphi_y^1}{\partial x}\right)^2+\lambda_{25}^j\left(\frac{\partial u_0^1}{\partial y}\right)^2+\lambda_{26}^j\left(\frac{\partial v_0^1}{\partial x}\right)^2+\lambda_{27}^j\left(\frac{\partial^2 w^1}{\partial x \partial y}\frac{\partial \varphi_x^1}{\partial y}\right)+\lambda_{28}^j\left(\frac{\partial^2 w^1}{\partial x \partial y}\frac{\partial \varphi_y^1}{\partial x}\right)\\
&+ \quad \lambda_{29}^j\left(\frac{\partial^2 w^1}{\partial x \partial y}\frac{\partial u_0^1}{\partial y}\right)+\lambda_{30}^j\left(\frac{\partial^2 w^1}{\partial x \partial y}\frac{\partial v_0^1}{\partial x}\right)+\lambda_{31}^j\left(\frac{\partial \varphi_x^1}{\partial y}\frac{\partial \varphi_y^1}{\partial x}\right)+\lambda_{32}^j\left(\frac{\partial \varphi_x^1}{\partial y}\frac{\partial u_0^1}{\partial y}\right)\\
&+ \quad \lambda_{33}^j\left(\frac{\partial \varphi_x^1}{\partial y}\frac{\partial v_0^1}{\partial x}\right)+\lambda_{34}^j\left(\frac{\partial u_0^1}{\partial y}\frac{\partial \varphi_y^1}{\partial x}\right)+\lambda_{35}^j\left(\frac{\partial v_0^1}{\partial x}\frac{\partial \varphi_y^1}{\partial x}\right)+\lambda_{36}^j\left(\frac{\partial u_0^1}{\partial y}\frac{\partial v_0^1}{\partial x}\right)\\
&+ \quad \lambda_{37}^j\left(\varphi_x^1\right)^2+\lambda_{38}^j\left(\varphi_y^1\right)^2\Big]
\end{aligned}
\tag{3.2.55}
$$

The coefficients λ_i are given in Appendix B. As we can see in Equation (3.2.43), the density of kinetic energy and deformation energy are related, respectively, with kinetic and deformation energy by:

$$
\begin{aligned}
T &= \int_S e_t^j \mathrm{d}S \\
V &= \int_S e_v^j \mathrm{d}S
\end{aligned}
\tag{3.2.56}
$$

3.2.5 Basis Functions and Equation of Motion

The equations of motion are obtained solving Equation (3.2.43) for a generalized displacement variation δq^i, which takes the form:

$$
\left\{\delta q^i\right\}=\left\{\delta w, \quad \delta u_0, \quad \delta v_0, \quad \delta \varphi_x, \quad \delta \varphi_y\right\} \tag{3.2.57}
$$

Once that Lagrange's equations can not be solved in general for any displacement variation, in this study a Rayleigh-Ritz method is used. This method requires a function basis for the expansion of the five different unknowns, where the trial functions need to satisfy the geometric boundary conditions. In this work, a trigonometric basis of functions with sine and cosine functions is considered. A polynomial basis is encountered in works like Woodcock [8], however in the study performed by Loredo et al. [10] is said that a trigonometric basis presents a better convergence rate than a polynomial basis when predicting high order natural flexural modes. This basis has a maximum order m for the x direction and a maximum order n for the y direction. For a simply supported plate the basis of functions takes the form:

$$\begin{aligned}
w(x,y,t) &= \sum_{\substack{1\le p\le m\\1\le q\le n}} A^{pq}(t)\phi_w^{pq} = \sum_{\substack{1\le p\le m\\1\le q\le n}} A^{pq}(t)\sin\left(\frac{p\pi x}{a}\right)\sin\left(\frac{q\pi y}{b}\right)\\
u_0(x,y,t) &= \sum_{\substack{1\le p\le m\\1\le q\le n}} B^{pq}(t)\phi_{u_0}^{pq} = \sum_{\substack{1\le p\le m\\1\le q\le n}} B^{pq}(t)\cos\left(\frac{p\pi x}{a}\right)\sin\left(\frac{q\pi y}{b}\right)\\
v_0(x,y,t) &= \sum_{\substack{1\le p\le m\\1\le q\le n}} C^{pq}(t)\phi_{v_0}^{pq} = \sum_{\substack{1\le p\le m\\1\le q\le n}} C^{pq}(t)\sin\left(\frac{p\pi x}{a}\right)\cos\left(\frac{q\pi y}{b}\right)\\
\varphi_x(x,y,t) &= \sum_{\substack{1\le p\le m\\1\le q\le n}} D^{pq}(t)\phi_{\varphi_x}^{pq} = \sum_{\substack{1\le p\le m\\1\le q\le n}} D^{pq}(t)\cos\left(\frac{p\pi x}{a}\right)\sin\left(\frac{q\pi y}{b}\right)\\
\varphi_y(x,y,t) &= \sum_{\substack{1\le p\le m\\1\le q\le n}} E^{pq}(t)\phi_{\varphi_y}^{pq} = \sum_{\substack{1\le p\le m\\1\le q\le n}} E^{pq}(t)\sin\left(\frac{p\pi x}{a}\right)\cos\left(\frac{q\pi y}{b}\right)
\end{aligned} \tag{3.2.58}$$

For a clamped plate the transverse displacement takes the form:

$$w(x,y,t) = \sum_{\substack{1\le p\le m\\1\le q\le n}} A^{pq}(t)\phi_w^{pq} = \sum_{\substack{1\le p\le m\\1\le q\le n}} A^{pq}(t)\left(1-\cos\left(\frac{p\pi x}{a}\right)^2\right)\left(1-\cos\left(\frac{q\pi y}{b}\right)^2\right) \tag{3.2.59}$$

while the remaining displacements are equal to the simply supported plate. Satisfying the geometric boundary conditions in the considered basis of functions any combination of boundary conditions for the plate edges can be studied with this model, including the free plate if constant terms are added to the basis in order to take into account the rigid body modes. In the preceding equations, the coefficients $A^{pq}(t), B^{pq}(t), C^{pq}(t)$, $D^{pq}(t), E^{pq}(t)$ are time-dependents and can be stacked up to build a global $5\times m\times n$ vector $\mathbf{X}(t)$ of unknowns given by:

$$\left\{\mathbf{X}(t)\right\} = \begin{Bmatrix}\mathbf{A}(t)\\ \mathbf{B}(t)\\ \mathbf{C}(t)\\ \mathbf{D}(t)\\ \mathbf{E}(t)\end{Bmatrix} = \begin{Bmatrix}A^{11}(t)\\ \vdots\\ \\ \vdots\\ E^{mn}(t)\end{Bmatrix} \tag{3.2.60}$$

while the basis of functions can be re-arranged in a vector form like:

$$\left\{\boldsymbol{\phi}(x,y)\right\} = \begin{Bmatrix}\boldsymbol{\phi_w}(x,y)\\ \boldsymbol{\phi_{u_0}}(x,y)\\ \boldsymbol{\phi_{v_0}}(x,y)\\ \boldsymbol{\phi_{\varphi_x}}(x,y)\\ \boldsymbol{\phi_{\varphi_y}}(x,y)\end{Bmatrix} = \begin{Bmatrix}\phi_w^{11}(x,y)\\ \vdots\\ \\ \vdots\\ \phi_{\varphi_y}^{mn}(x,y)\end{Bmatrix} \tag{3.2.61}$$

Equation (3.2.43) can now be solved introducing the overall coefficient vector $\mathbf{X}(t)$ and the external forces work, leading to:

$$\delta \int_{t_1}^{t_2} \mathcal{L}(\{\mathbf{X}\}, \{\dot{\mathbf{X}}\}) \mathrm{d}t + \int_{t_1}^{t_2} \{\mathbf{F}\}^{\mathrm{T}} \{\delta \mathbf{X}\}) \mathrm{d}t = 0 \tag{3.2.62}$$

where $\{\mathbf{F}\}$ is the generalized discrete external force vector. Solving Equation (3.2.62) leads to Lagrange's equation for the components of the generalized displacements X_j:

$$\frac{\mathrm{d}}{\mathrm{d}t} \frac{\partial T}{\partial \dot{X}_j} - \frac{\partial V}{\partial X_j} = F_j \tag{3.2.63}$$

Applying the Lagrange's equations for each of the unknowns, a linear system of $(5 \times m \times n)$ differential equations for the forced motion in a matrix form is obtained:

$$[\mathbf{M}]\{\ddot{\mathbf{X}}(t)\} + [\mathbf{K}]\{\mathbf{X}(t)\} = \{\mathbf{F}(t)\} \tag{3.2.64}$$

where $[\mathbf{M}]$ is the mass matrix, $[\mathbf{K}]$ the stiffness matrix and $\{\mathbf{F}(t)\}$ the external force vector. The mass matrix can be defined as:

$$[\mathbf{M}] = \begin{bmatrix} [\mathbf{M}^B] & [\mathbf{M}^{B/M_x}] & [\mathbf{M}^{B/M_y}] & [\mathbf{M}^{B/S_x}] & [\mathbf{M}^{B/S_y}] \\ & [\mathbf{M}^{M_x}] & [\mathbf{0}] & [\mathbf{M}^{M_x/S_x}] & [\mathbf{0}] \\ & & [\mathbf{M}^{M_y}] & [\mathbf{0}] & [\mathbf{M}^{M_y/S_y}] \\ & & & [\mathbf{M}^{S_x}] & [\mathbf{0}] \\ \text{sym.} & & & & [\mathbf{M}^{S_y}] \end{bmatrix} \tag{3.2.65}$$

and the sub-matrices can be written as:

$$\begin{aligned}
[\mathbf{M}^B] &= \int_0^a \int_0^b \left[\delta_1^j \frac{\partial \boldsymbol{\phi}_w(x,y)}{\partial x} \frac{\partial \boldsymbol{\phi}_w^{\mathrm{T}}(x,y)}{\partial x} + \delta_7^j \frac{\partial \boldsymbol{\phi}_w(x,y)}{\partial y} \frac{\partial \boldsymbol{\phi}_w^{\mathrm{T}}(x,y)}{\partial y} \right. \\
&+ \left. \delta_{13}^j \boldsymbol{\phi}_w(x,y) \boldsymbol{\phi}_w^{\mathrm{T}}(x,y) \right] \mathrm{d}y \mathrm{d}x \\
[\mathbf{M}^{M_x}] &= \int_0^a \int_0^b \left[\delta_3^j \boldsymbol{\phi}_{u_0}(x,y) \boldsymbol{\phi}_{u_0}^{\mathrm{T}}(x,y) \right] \mathrm{d}y \mathrm{d}x \\
[\mathbf{M}^{M_y}] &= \int_0^a \int_0^b \left[\delta_9^j \boldsymbol{\phi}_{v_0}(x,y) \boldsymbol{\phi}_{v_0}^{\mathrm{T}}(x,y) \right] \mathrm{d}y \mathrm{d}x \\
[\mathbf{M}^{S_x}] &= \int_0^a \int_0^b \left[\delta_2^j \boldsymbol{\phi}_{\varphi_x}(x,y) \boldsymbol{\phi}_{\varphi_x}^{\mathrm{T}}(x,y) \right] \mathrm{d}y \mathrm{d}x \\
[\mathbf{M}^{S_y}] &= \int_0^a \int_0^b \left[\delta_8^j \boldsymbol{\phi}_{\varphi_y}(x,y) \boldsymbol{\phi}_{\varphi_y}^{\mathrm{T}}(x,y) \right] \mathrm{d}y \mathrm{d}x
\end{aligned}$$

$$
\begin{aligned}
[\mathbf{M}^{B/M_x}] &= \frac{1}{2}\int_0^a\int_0^b\left[\delta_5^j\frac{\partial\boldsymbol{\phi}_w(x,y)}{\partial x}\boldsymbol{\phi}_{u_0}^{\mathrm{T}}(x,y)\right]\mathrm{d}y\mathrm{d}x\\
[\mathbf{M}^{B/M_y}] &= \frac{1}{2}\int_0^a\int_0^b\left[\delta_{11}^j\frac{\partial\boldsymbol{\phi}_w(x,y)}{\partial y}\boldsymbol{\phi}_{v_0}^{\mathrm{T}}(x,y)\right]\mathrm{d}y\mathrm{d}x\\
[\mathbf{M}^{B/S_x}] &= \frac{1}{2}\int_0^a\int_0^b\left[\delta_4^j\frac{\partial\boldsymbol{\phi}_w(x,y)}{\partial x}\boldsymbol{\phi}_{\varphi_x}^{\mathrm{T}}(x,y)\right]\mathrm{d}y\mathrm{d}x\\
[\mathbf{M}^{B/S_y}] &= \frac{1}{2}\int_0^a\int_0^b\left[\delta_{10}^j\frac{\partial\boldsymbol{\phi}_w(x,y)}{\partial y}\boldsymbol{\phi}_{\varphi_y}^{\mathrm{T}}(x,y)\right]\mathrm{d}y\mathrm{d}x\\
[\mathbf{M}^{M_x/S_x}] &= \frac{1}{2}\int_0^a\int_0^b\left[\delta_6^j\boldsymbol{\phi}_{u_0}(x,y)\boldsymbol{\phi}_{\varphi_x}^{\mathrm{T}}(x,y)\right]\mathrm{d}y\mathrm{d}x\\
[\mathbf{M}^{M_y/S_y}] &= \frac{1}{2}\int_0^a\int_0^b\left[\delta_{12}^j\boldsymbol{\phi}_{v_0}(x,y)\boldsymbol{\phi}_{\varphi_y}^{\mathrm{T}}(x,y)\right]\mathrm{d}y\mathrm{d}x
\end{aligned}
\tag{3.2.66}
$$

where each of these sub-matrices is a square matrix with dimension $(m\times n)$. The stiffness matrix can be defined as:

$$
[\mathbf{K}] = \begin{bmatrix}
[\mathbf{K}^B] & [\mathbf{K}^{B/M_x}] & [\mathbf{K}^{B/M_y}] & [\mathbf{K}^{B/S_x}] & [\mathbf{K}^{B/S_y}]\\
 & [\mathbf{K}^{M_x}] & [\mathbf{K}^{M_x/M_y}] & [\mathbf{K}^{M_x/S_x}] & [\mathbf{K}^{M_x/S_y}]\\
 & & [\mathbf{K}^{M_y}] & [\mathbf{K}^{M_y/S_x}] & [\mathbf{K}^{M_y/S_y}]\\
 & & & [\mathbf{K}^{S_x}] & [\mathbf{K}^{S_x/S_y}]\\
\text{sym.} & & & & [\mathbf{K}^{S_y}]
\end{bmatrix}
\tag{3.2.67}
$$

and the sub-matrices can be written as:

$$
\begin{aligned}
[\mathbf{K}^B] &= \int_0^a\int_0^b\left[\lambda_1^j\frac{\partial^2\boldsymbol{\phi}_w(x,y)}{\partial x^2}\frac{\partial^2\boldsymbol{\phi}_w^{\mathrm{T}}(x,y)}{\partial x^2}+\lambda_7^j\frac{\partial^2\boldsymbol{\phi}_w(x,y)}{\partial y^2}\frac{\partial^2\boldsymbol{\phi}_w^{\mathrm{T}}(x,y)}{\partial y^2}\right.\\
&+ \left.\lambda_{13}^j\frac{\partial^2\boldsymbol{\phi}_w(x,y)}{\partial x^2}\frac{\partial^2\boldsymbol{\phi}_w^{\mathrm{T}}(x,y)}{\partial y^2}+\lambda_{22}^j\frac{\partial^2\boldsymbol{\phi}_w(x,y)}{\partial x\partial y}\frac{\partial^2\boldsymbol{\phi}_w^{\mathrm{T}}(x,y)}{\partial x\partial y}\right]\mathrm{d}y\mathrm{d}x\\
[\mathbf{K}^{M_x}] &= \int_0^a\int_0^b\left[\lambda_3^j\frac{\partial\boldsymbol{\phi}_{u_0}(x,y)}{\partial x}\frac{\partial\boldsymbol{\phi}_{u_0}^{\mathrm{T}}(x,y)}{\partial x}+\lambda_{25}^j\frac{\partial\boldsymbol{\phi}_{u_0}(x,y)}{\partial y}\frac{\partial\boldsymbol{\phi}_{u_0}^{\mathrm{T}}(x,y)}{\partial y}\right]\mathrm{d}y\mathrm{d}x\\
[\mathbf{K}^{M_y}] &= \int_0^a\int_0^b\left[\lambda_9^j\frac{\partial\boldsymbol{\phi}_{v_0}(x,y)}{\partial y}\frac{\partial\boldsymbol{\phi}_{v_0}^{\mathrm{T}}(x,y)}{\partial y}+\lambda_{26}^j\frac{\partial\boldsymbol{\phi}_{v_0}(x,y)}{\partial x}\frac{\partial\boldsymbol{\phi}_{v_0}^{\mathrm{T}}(x,y)}{\partial x}\right]\mathrm{d}y\mathrm{d}x\\
[\mathbf{K}^{S_x}] &= \int_0^a\int_0^b\left[\lambda_2^j\frac{\partial\boldsymbol{\phi}_{\varphi_x}(x,y)}{\partial x}\frac{\partial\boldsymbol{\phi}_{\varphi_x}^{\mathrm{T}}(x,y)}{\partial x}+\lambda_{23}^j\frac{\partial\boldsymbol{\phi}_{\varphi_x}(x,y)}{\partial y}\frac{\partial\boldsymbol{\phi}_{\varphi_x}^{\mathrm{T}}(x,y)}{\partial y}\right.\\
&+ \left.\lambda_{37}^j\boldsymbol{\phi}_{\varphi_x}(x,y)\boldsymbol{\phi}_{\varphi_x}^{\mathrm{T}}(x,y)\right]\mathrm{d}y\mathrm{d}x
\end{aligned}
$$

$$
\begin{aligned}
[\mathbf{K}^{S_y}] &= \int_0^a \int_0^b \Big[\lambda_8^j \frac{\partial \boldsymbol{\phi}_{\varphi_y}(x,y)}{\partial y} \frac{\partial \boldsymbol{\phi}_{\varphi_y}^{\mathrm{T}}(x,y)}{\partial y} + \lambda_{24}^j \frac{\partial \boldsymbol{\phi}_{\varphi_y}(x,y)}{\partial x} \frac{\partial \boldsymbol{\phi}_{\varphi_y}^{\mathrm{T}}(x,y)}{\partial x} \\
&+ \lambda_{38}^j \boldsymbol{\phi}_{\varphi_y}(x,y) \boldsymbol{\phi}_{\varphi_y}^{\mathrm{T}}(x,y) \Big] \mathrm{d}y \mathrm{d}x \\
[\mathbf{K}^{B/M_x}] &= \frac{1}{2} \int_0^a \int_0^b \Big[\lambda_5^j \frac{\partial^2 \boldsymbol{\phi}_w(x,y)}{\partial x^2} \frac{\partial \boldsymbol{\phi}_{u_0}^{\mathrm{T}}(x,y)}{\partial x} + \lambda_{19}^j \frac{\partial^2 \boldsymbol{\phi}_w(x,y)}{\partial y^2} \frac{\partial \boldsymbol{\phi}_{u_0}^{\mathrm{T}}(x,y)}{\partial x} \\
&+ \lambda_{29}^j \frac{\partial^2 \boldsymbol{\phi}_w(x,y)}{\partial x^2} \frac{\partial \boldsymbol{\phi}_{u_0}^{\mathrm{T}}(x,y)}{\partial x} \Big] \mathrm{d}y \mathrm{d}x \\
[\mathbf{K}^{B/M_y}] &= \frac{1}{2} \int_0^a \int_0^b \Big[\lambda_{11}^j \frac{\partial^2 \boldsymbol{\phi}_w(x,y)}{\partial y^2} \frac{\partial \boldsymbol{\phi}_{v_0}^{\mathrm{T}}(x,y)}{\partial y} + \lambda_{15}^j \frac{\partial^2 \boldsymbol{\phi}_w(x,y)}{\partial x^2} \frac{\partial \boldsymbol{\phi}_{v_0}^{\mathrm{T}}(x,y)}{\partial y} \\
&+ \lambda_{30}^j \frac{\partial^2 \boldsymbol{\phi}_w(x,y)}{\partial x^2} \frac{\partial \boldsymbol{\phi}_{v_0}^{\mathrm{T}}(x,y)}{\partial y} \Big] \mathrm{d}y \mathrm{d}x \\
[\mathbf{K}^{B/S_x}] &= \frac{1}{2} \int_0^a \int_0^b \Big[\lambda_4^j \frac{\partial^2 \boldsymbol{\phi}_w(x,y)}{\partial x^2} \frac{\partial \boldsymbol{\phi}_{\varphi_x}^{\mathrm{T}}(x,y)}{\partial x} + \lambda_{16}^j \frac{\partial^2 \boldsymbol{\phi}_w(x,y)}{\partial y^2} \frac{\partial \boldsymbol{\phi}_{\varphi_x}^{\mathrm{T}}(x,y)}{\partial x} \\
&+ \lambda_{27}^j \frac{\partial^2 \boldsymbol{\phi}_w(x,y)}{\partial x^2} \frac{\partial \boldsymbol{\phi}_{\varphi_x}^{\mathrm{T}}(x,y)}{\partial x} \Big] \mathrm{d}y \mathrm{d}x \\
[\mathbf{K}^{B/S_y}] &= \frac{1}{2} \int_0^a \int_0^b \Big[\lambda_{10}^j \frac{\partial^2 \boldsymbol{\phi}_w(x,y)}{\partial y^2} \frac{\partial \boldsymbol{\phi}_{\varphi_y}^{\mathrm{T}}(x,y)}{\partial y} + \lambda_{14}^j \frac{\partial^2 \boldsymbol{\phi}_w(x,y)}{\partial x^2} \frac{\partial \boldsymbol{\phi}_{\varphi_y}^{\mathrm{T}}(x,y)}{\partial y} \\
&+ \lambda_{28}^j \frac{\partial^2 \boldsymbol{\phi}_w(x,y)}{\partial x^2} \frac{\partial \boldsymbol{\phi}_{\varphi_y}^{\mathrm{T}}(x,y)}{\partial y} \Big] \mathrm{d}y \mathrm{d}x \\
[\mathbf{K}^{M_x/M_y}] &= \frac{1}{2} \int_0^a \int_0^b \Big[\lambda_{21}^j \frac{\partial \boldsymbol{\phi}_{u_0}(x,y)}{\partial x} \frac{\partial \boldsymbol{\phi}_{v_0}^{\mathrm{T}}(x,y)}{\partial y} + \lambda_{36}^j \frac{\partial \boldsymbol{\phi}_{u_0}(x,y)}{\partial y} \frac{\partial \boldsymbol{\phi}_{v_0}^{\mathrm{T}}(x,y)}{\partial x} \Big] \mathrm{d}y \mathrm{d}x \\
[\mathbf{K}^{M_x/S_x}] &= \frac{1}{2} \int_0^a \int_0^b \Big[\lambda_6^j \frac{\partial \boldsymbol{\phi}_{u_0}(x,y)}{\partial x} \frac{\partial \boldsymbol{\phi}_{\varphi_x}^{\mathrm{T}}(x,y)}{\partial x} + \lambda_{32}^j \frac{\partial \boldsymbol{\phi}_{u_0}(x,y)}{\partial y} \frac{\partial \boldsymbol{\phi}_{\varphi_x}^{\mathrm{T}}(x,y)}{\partial y} \Big] \mathrm{d}y \mathrm{d}x \\
[\mathbf{K}^{M_x/S_y}] &= \frac{1}{2} \int_0^a \int_0^b \Big[\lambda_{20}^j \frac{\partial \boldsymbol{\phi}_{u_0}(x,y)}{\partial x} \frac{\partial \boldsymbol{\phi}_{\varphi_y}^{\mathrm{T}}(x,y)}{\partial y} + \lambda_{34}^j \frac{\partial \boldsymbol{\phi}_{u_0}(x,y)}{\partial y} \frac{\partial \boldsymbol{\phi}_{\varphi_y}^{\mathrm{T}}(x,y)}{\partial x} \Big] \mathrm{d}y \mathrm{d}x \\
[\mathbf{K}^{M_y/S_x}] &= \frac{1}{2} \int_0^a \int_0^b \Big[\lambda_{18}^j \frac{\partial \boldsymbol{\phi}_{v_0}(x,y)}{\partial y} \frac{\partial \boldsymbol{\phi}_{\varphi_x}^{\mathrm{T}}(x,y)}{\partial x} + \lambda_{33}^j \frac{\partial \boldsymbol{\phi}_{v_0}(x,y)}{\partial x} \frac{\partial \boldsymbol{\phi}_{\varphi_x}^{\mathrm{T}}(x,y)}{\partial y} \Big] \mathrm{d}y \mathrm{d}x \\
[\mathbf{K}^{M_y/S_y}] &= \frac{1}{2} \int_0^a \int_0^b \Big[\lambda_{12}^j \frac{\partial \boldsymbol{\phi}_{v_0}(x,y)}{\partial y} \frac{\partial \boldsymbol{\phi}_{\varphi_y}^{\mathrm{T}}(x,y)}{\partial y} + \lambda_{35}^j \frac{\partial \boldsymbol{\phi}_{v_0}(x,y)}{\partial x} \frac{\partial \boldsymbol{\phi}_{\varphi_y}^{\mathrm{T}}(x,y)}{\partial x} \Big] \mathrm{d}y \mathrm{d}x \\
[\mathbf{K}^{S_x/S_y}] &= \frac{1}{2} \int_0^a \int_0^b \Big[\lambda_{17}^j \frac{\partial \boldsymbol{\phi}_{\varphi_x}(x,y)}{\partial x} \frac{\partial \boldsymbol{\phi}_{\varphi_y}^{\mathrm{T}}(x,y)}{\partial y} + \lambda_{31}^j \frac{\partial \boldsymbol{\phi}_{\varphi_x}(x,y)}{\partial y} \frac{\partial \boldsymbol{\phi}_{\varphi_y}^{\mathrm{T}}(x,y)}{\partial x} \Big] \mathrm{d}y \mathrm{d}x
\end{aligned}
\tag{3.2.68}
$$

where each of these sub-matrices is a square matrix with dimension $(m \times n)$. For harmonic solicitations of a given angular frequency ω, and considering the damping properties by means of complex material properties as well as the frequency dependence of the mass and stiffness matrices, the system takes the form:

$$(-\omega^2[\mathbf{M}(\omega)] + [\tilde{\mathbf{K}}(\omega)])\{\tilde{\mathbf{X}}\} = \{\tilde{\mathbf{F}}\} \tag{3.2.69}$$

where the tilde denotes the complex variables.

In Equation (3.2.69) the frequency dependence of the stiffness matrix is shown. This is a common feature of the models that are used to simulate structures with viscoelastic treatments once that, as we seen in Chapter 2, the viscoelastic materials are defined by their complex modulus which is frequency dependent. However, in Equation (3.2.69) is also shown that the mass matrix is frequency dependent. This is a particular characteristic of this model and at first sight is a surprising characteristic once that the density of viscoelastic materials isn't frequency dependent. Nevertheless, it is well know that the mass matrix is a function of the integration over the thickness of the velocity field which in turn is the time derivative of the displacement field. Now, as we seen before the displacement field of a generic layer ℓ is written in function of the unknowns of the first layer due to the enforced shear stress continuity at each interface which makes the displacement field a function of the relations between the shear moduli of consecutive layers. Thence, the mass matrix is also written in function of these relations between the shear moduli of consecutive layers and, as we can see in (3.2.66), the mass matrix is a function of δ_i coefficients that establish the displacement and shear stress continuity between layers. Therefore, once that the viscoelastic materials are defined by their complex shear modulus, which as we seen in Chapter 2 is frequency dependent, the mass matrix is also frequency dependent. It's not surprising that the velocity field varies with frequency once that the displacement field of the viscoelastic layer depends on their mechanical properties experiencing a larger displacement when the material is more flexible. To understand this dependence with the frequency, the mass matrix can not be seen exclusively as a property of the system but rather as a measure of the kinetic energy.

The frequency dependence of the stiffness and mass matrices makes this model cumbersome from a processing time point of view once that at each frequency two new matrices need to be calculated. Furthermore, the stiffness matrix, as well as the mass matrix, can't be updated with the right storage modulus and loss factor at each new frequency as was done by Moreira [4] in his work, for example. Instead, the matrices need to be builded at each new frequency once that they depend on relations between the mechanical properties of different layers which can't be simplified. In fact, this is a great disadvantage of this model and is the price o pay for the independence of the number of degrees of freedom with the number of layers.

3.2.6 External Force Vector

Remembering Equation (3.2.62) the virtual work done by the external forces is given by:

$$\int_{t_1}^{t_2} \{\mathbf{F}\}^{\mathrm{T}}\{\delta\mathbf{X}\}\mathrm{d}t \tag{3.2.70}$$

If the generalized force vector is related with the displacement vector $\mathbf{X}(t)$ and their components, then it can be written as:

$$\left\{\tilde{\mathbf{F}}(t)\right\} = \begin{Bmatrix} \tilde{\mathbf{F}}_w \\ \tilde{\mathbf{N}}_x \\ \tilde{\mathbf{N}}_y \\ \tilde{\mathbf{M}}_x \\ \tilde{\mathbf{M}}_y \end{Bmatrix} \tag{3.2.71}$$

where $\tilde{\mathbf{F}}$ is the normal loading, $\tilde{\mathbf{N}}_x$ and $\tilde{\mathbf{N}}_y$ are the generalized in-plane tensions and $\tilde{\mathbf{M}}_x$ and $\tilde{\mathbf{M}}_y$ are the generalized bending moments. In this work, only the transverse load is considered which leads to the following generalized force vector:

$$\left\{\tilde{\mathbf{F}}(t)\right\} = \begin{Bmatrix} \tilde{\mathbf{F}}(t)_w \\ \mathbf{0} \\ \mathbf{0} \\ \mathbf{0} \\ \mathbf{0} \end{Bmatrix} \tag{3.2.72}$$

where the transverse load is given by:

- Pressure Load:

$$\{\tilde{\mathbf{F}}(t)\} = \int_0^a \int_0^b \tilde{P}(x, y)\{\phi_w(x, y)\}\mathrm{d}y\mathrm{d}x \tag{3.2.73}$$

- Punctual Excitation:

$$\{\tilde{\mathbf{F}}(t)\} = \tilde{f}\{\phi_w(x_0, y_0)\} \tag{3.2.74}$$

where $\tilde{P}(x, y)$ is the applied pressure in the plate, $\tilde{f}$ is the point force applied and (x_0, y_0) is the point where this force is applied.

Chapter 4

Mechanical and Vibroacoustic Indicators

4.1 Introduction

The optimal design of viscoelastic structures, just like so many others, requires adequate tools to predict and understand their complex behaviour. The challenge of reducing vibration and noise, that is a matter of interest in the next chapters, is based on the mechanical and vibroacoustic indicators studied in the present chapter, where their mathematical definitions are presented. Therefore, the definitions of frequency response functions of displacement, velocity and acceleration are studied here in order to characterize, in a strictly mechanical point of view, the impact of viscoelastic treatments in system response. In order to quantify the system capability to dissipate energy, is mentioned the concept of modal loss factor that physically represents the ratio between the dissipated energy and the stored one, for a given mode. The noise reduction problem, a research area that is increasingly important, is characterized in this work with some vibroacoustic indicators that are presented by Loredo et al. [10]. They are an efficient tool to predict the vibroacoustic system behaviour and understand the significant changes introduced by viscoelastic treatments.

4.2 Mechanical Indicators

4.2.1 Frequency Response Function - FRF

For the present model and considering a system with viscoelastic treatments applied, the equation of motion can be written as:

$$[\mathbf{M}(\omega)]\{\ddot{\mathbf{X}}(t)\} + [\tilde{\mathbf{K}}(\omega)]\{\mathbf{X}(t)\} = \{\mathbf{F}(t)\} \tag{4.2.1}$$

where $[\mathbf{M}]$ is the mass matrix and $[\tilde{\mathbf{K}}]$ the complex stiffness matrix. The $\{\mathbf{X}(t)\}$ and $\{\mathbf{F}(t)\}$ vectors are the system response and the external force vector, respectively.

For a harmonic excitation, the force vector can be represented by:

$$\{\mathbf{F}(t)\} = \{\mathbf{F}(\omega)\}e^{\mathrm{j}\omega t} \tag{4.2.2}$$

and the system response is another harmonic function, with amplitude $\{\mathbf{X}(\omega)\}$ and the same frequency ω. However, due to the introduced damping the response shows a lag δ:

$$\{\mathbf{X}(t)\} = \{\mathbf{X}(\omega)\}e^{(\mathrm{j}\omega t-\delta)} = \{\tilde{\mathbf{X}}(\omega)\}e^{\mathrm{j}\omega t} \tag{4.2.3}$$

Substituting (4.2.2), (4.2.3) and the respective time derivative in equation of motion (4.2.1), a system of algebraic equations is obtained:

$$\left[[\tilde{\mathbf{K}}(\omega)] - \omega^2[\mathbf{M}(\omega)]\right]\{\tilde{\mathbf{X}}(\omega)\} = \{\mathbf{F}(\omega)\} \tag{4.2.4}$$

The response vector $\{\tilde{\mathbf{X}}(\omega)\}$ can be now calculated by:

$$\{\tilde{\mathbf{X}}(\omega)\} = \left[[\tilde{\mathbf{K}}(\omega)] - \omega^2[\mathbf{M}(\omega)]\right]^{-1}\{\mathbf{F}(\omega)\} \tag{4.2.5}$$

The system response depends upon the mechanical properties and the frequency, and can be rewritten as:

$$\{\tilde{\mathbf{X}}(\omega)\} = [\alpha(\omega)]\{\mathbf{F}(\omega)\} \tag{4.2.6}$$

The frequency response functions of a column k of the receptance matrix $[\alpha(\omega)]$, can be determined by:

$$\alpha_{jk}(\omega) = \frac{\tilde{X}_j(\omega)}{F_k}; F_r = 0, r = 1, ..., n \wedge r \neq k \tag{4.2.7}$$

where $\tilde{X}_j(\omega)$ represents the amplitude and phase of the system response in the degree of freedom j when a excitation F_k is applied in the degree of freedom k.

The system response can also be velocity or acceleration[12]. Replacing the displacement response $\{\tilde{\mathbf{X}}(\omega)\}$ with velocity $\{j\omega\tilde{\mathbf{X}}(\omega)\}$ and acceleration $\{-\omega^2\tilde{\mathbf{X}}(\omega)\}$, two new types of FRF's can be defined:

The mobility FRF is given by:

$$Y_{jk}(\omega) = j\omega\frac{\tilde{X}_j(\omega)}{F_k}; F_r = 0, r = 1, ..., n \wedge r \neq k \tag{4.2.8}$$

which, taken into account Equation (4.2.7), may also be written as:

$$Y_{jk}(\omega) = j\omega(\alpha_{jk}(\omega)) \tag{4.2.9}$$

The accelerance FRF is given by:

$$\mathcal{A}_{jk}(\omega) = -\omega^2\frac{\tilde{X}_j(\omega)}{F_k}; F_r = 0, r = 1, ..., n \wedge r \neq k \tag{4.2.10}$$

which, taken into account Equation (4.2.7), may also be written as:

$$A_{jk}(\omega) = -\omega^2(\alpha_{jk}(\omega)) \tag{4.2.11}$$

4.2.2 Modal Loss Factors

The modal loss factors can be defined as a ratio between the loss and the storage parts of the modal strain energy of the structure and thereby are an excellent mechanical indicator of the treatment's efficiency. The modal strain energy (MSE) approach is a direct method for the prediction of the modal damping ratio and can be defined as:

$$\eta_r = \frac{\{\phi\}_r^{\mathrm{T}}\Im[\tilde{\mathbf{K}}]\{\phi\}_r}{\{\phi\}_r^{\mathrm{T}}\Re[\tilde{\mathbf{K}}]\{\phi\}_r} \tag{4.2.12}$$

where $\{\phi\}_r$ is the normal mode of a generic mode r and is obtained solving the following generalized eigenproblem:

$$\Re[\tilde{\mathbf{K}}]\{\phi\}_r = \omega_r^2[\mathbf{M}]\{\phi\}_r \tag{4.2.13}$$

Physically, the relation (4.2.12) represents the ratio between the dissipated energy, proportional to the imaginary part of the complex stiffness matrix and the stored energy, proportional to the real part of the stiffness matrix. However, as can be seen in Equation (4.2.13), it is assumed that the normal modes obtained from the undamped system are representative of the damped system. This assumption is only true for lightly damped structures once that the coupling between the different modes is small, due to the low damping which is not the case of viscoelastic systems where the structure modification is considerable[1].

Alternatively, in a more realistic approach, the eigensolution taking into account the frequency dependence can be determined independently under an iterative approach where the stiffness matrix is updated - this approach is called iterative modal strain energy (IMSE). The natural frequencies and normal modes are obtained when the convergence is reached. Although the process is iterative in nature, the modal loss factors and natural frequencies are more realistic. In this work, due to the strong damping introduced by viscoelastic treatments the iterative modal strain energy method was implemented, and the algorithm explained by Vasques [1] was used.

IMSE algorithm

Step 1. Eigensolution with $\omega = \omega^0$

$$\Re[\tilde{\mathbf{K}}(\omega^0)]\{\phi\}_r = \omega_r^2[\mathbf{M}(\omega^0)]\{\phi\}_r \tag{4.2.14}$$

Step 2. Loop for each eigenpar (ω_r^0, ϕ_r) with $r = 1, ..., p$

i.Initial value

$$\omega_r^i = \omega_r^0 \tag{4.2.15}$$

ii. Iterative loop for each natural frequency and mode shape

- Eigensolution (ω_s^0, ϕ_s) with $s = 1, ..., r$:

$$\Re[\tilde{\mathbf{K}}(\omega^i)]\{\phi\}_s = (\omega_s^{(i+1)})^2[\mathbf{M}(\omega^i)]\{\phi\}_s \tag{4.2.16}$$

- Iterated natural frequency:

$$\begin{cases} \omega_s^{i+1} : \text{rejected}, & \text{for s<r} \\ \omega_s^{i+1} = \sqrt{(\omega_s^{i+1})^2}, & \text{for s>r} \end{cases} \tag{4.2.17}$$

- Convergence condition test:

$$\Delta_\omega = \frac{|\omega_r^{i+1} - \omega_r^i|}{\omega_r^{i+1}} = \Delta_{max} \tag{4.2.18}$$

iii. Modal loss factor

$$\eta_r = \frac{\{\phi\}_r^{\mathrm{T}} \Im[\tilde{\mathbf{K}}(\omega_r^{i+1})]\{\phi\}_r}{\{\phi\}_r^{\mathrm{T}} \Re[\tilde{\mathbf{K}}(\omega_r^{i+1})]\{\phi\}_r} \tag{4.2.19}$$

4.3 Vibroacoustic Model

4.3.1 Plane Wave Excitation

The vibroacoustic model presented here is based on the model developed by Loredo et al. [10], which considers the plate separated by two semi-infinite fluid media. In Figure 4.1 is shown a representation of the vibroacoustic model.

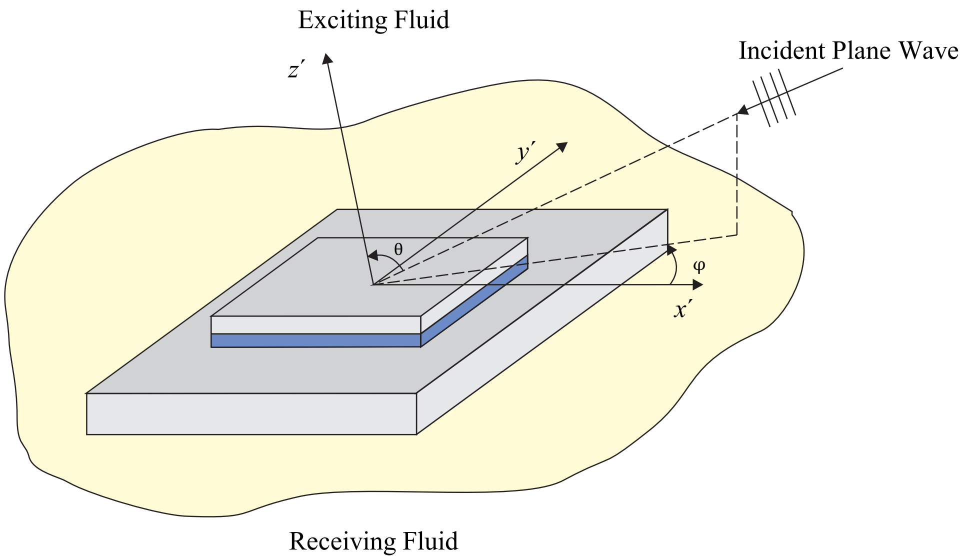

Figure 4.1: Patched plate submitted to a plane wave

The plane wave represented in Figure 4.1 causes forces acting on the plate due to the difference of pressure existing in the two sides. It is assumed light fluid for the two sides of the plate and with this assumption the pressure caused by the radiation impedance of the fluid mediums can be neglected. In Loredo et al. [10] an evaluation of the fluid load importance was made by a comparison with the work developed by Foin et al. [13], where the radiation impedances of the exciting and receiving fluid mediums was taken into account. They showed that, for the studied case, the fluid-structure coupling was weak, neglecting it for all their studies even when the thickness and the density of the considered plates were different. In addition, the radiated pressure in the exciting fluid is generally ignored once that is small compared to the blocked pressure that is the sum of the incident pressure and the reflected one, when the plate is blocked.

Considering these assumptions, the incident pressure field generated by the incident plane wave can be written as:

$$\tilde{P}_{\text{inc}}(x,y) = 2\tilde{p}_{\text{inc}} e^{-\mathrm{j}(k_{1x}(x-\frac{a}{2}))} \times e^{-\mathrm{j}(k_{1y}(y-\frac{b}{2}))} \tag{4.3.1}$$

where $\tilde{p}_{\text{inc}}$ is the amplitude and phase of the incident plane wave. The variables k_{1x} and k_{1y} are the projections of the wave vector $\boldsymbol{k_1}$ and are given by:

$$\begin{aligned} k_{1x} &= k_1 \sin(\theta)\cos(\varphi) \\ k_{1y} &= k_1 \sin(\theta)\sin(\varphi) \end{aligned} \tag{4.3.2}$$

where k_1 is the wave number, that is a relation between the frequency ω and the sound celerity into the exciting fluid c_1, given by:

$$k_1 = \frac{\omega}{c_1} \tag{4.3.3}$$

Remembering Equation (3.2.73) the generalized forces vector due to the incident pressure field $\tilde{P}_{\text{inc}}(x,y)$ can be written as:

$$\{\tilde{\mathbf{F}}_w\} = \int_0^a \int_0^b \tilde{P}_{\text{inc}}(x,y)\{\boldsymbol{\phi_w}(x,y)\}\mathrm{d}y\mathrm{d}x \tag{4.3.4}$$

The computation of this integral is cumbersome once that the pressure field generated by the incident plane wave given in Equation (4.3.1) has exponential terms that are frequency dependents and imaginary. To overcome this issue Loredo et al. [10] propose an alternative way to calculate the generalized forces vector:

$$\{\tilde{\mathbf{F}}_w\} = 2\tilde{p}_{\text{inc}}\{\tilde{\Psi}(\boldsymbol{k_1})\} \tag{4.3.5}$$

where the vector $\{\tilde{\Psi}(\boldsymbol{k_1})\}$ is a $m \times n$ column vector that may be written as:

$$\{\tilde{\Psi}(\boldsymbol{k_1})\} = \begin{Bmatrix} I_x^1(k_{1x})I_y^1(k_{1y}) \\ \vdots \\ I_x^p(k_{1x})I_y^q(k_{1y}) \\ \vdots \\ I_x^m(k_{1x})I_y^n(k_{1y}) \end{Bmatrix} \tag{4.3.6}$$

where $I_x^p(k_{1x})$ and $I_y^q(k_{1y})$, for the adopted basis functions, are given by the following integrals:

$$\begin{aligned} I_x^p(k_{1x}) &= \int_0^a e^{-\mathrm{j}(k_{1x}(x-\frac{a}{2}))} \sin\left(\frac{p\pi x}{a}\right)\mathrm{d}x \\ I_y^q(k_{1y}) &= \int_0^b e^{-\mathrm{j}(k_{1y}(y-\frac{b}{2}))} \sin\left(\frac{q\pi y}{b}\right)\mathrm{d}y \end{aligned} \tag{4.3.7}$$

The vector $\{\tilde{\Psi}(\boldsymbol{k_1})\}$ can be now implemented using the following recurrence:

$$I_x^p(k_{1x}) = \frac{p\pi a[e^{(\mathrm{j}k_{1x}\frac{a}{2})} - (-1)^p e^{(-\mathrm{j}k_{1x}\frac{a}{2})}]}{(p\pi)^2 - (k_{1x}a)^2}$$
$$I_y^q(k_{1y}) = \frac{q\pi b[e^{(\mathrm{j}k_{1y}\frac{b}{2})} - (-1)^q e^{(-\mathrm{j}k_{1y}\frac{b}{2})}]}{(q\pi)^2 - (k_{1y}b)^2} \tag{4.3.8}$$

The use of this trick in the generalized forces vector implementation due to a plane wave excitation make the model less cumbersome which is a great advantage at this point.

4.3.2 Diffuse Field Excitation

The Institute of Noise Control Engineering (INCE-USA) defines an acoustic diffuse field like *"A sound field in which the time average of the mean square sound pressure is everywhere the same and the flow of acoustic energy in all directions is equally probable"*. Mathematically, the concept is simple and a diffuse field excitation of frequency ω can be described by a superposition of many plane waves of random propagation direction. To compute a diffuse field excitation the more classical way consists in doing the mechanical computation for a set of plane waves of different incidences and summing energy types outputs. This computation is non-linear so it needs as many computations than the number of considered plane waves and a discretization of the half-space can help in the computational time[10].

4.3.3 Vibroacoustic Indicators

As was said before, it is assumed light fluid for the two sides of the plate, and with this assumption, the sound power can be calculated from the far-field (hemisphere with infinite radius) sound pressure distribution, in contrast with the near-field (field very close to the sound source) hypothesis, once that the pressure distribution at the surface is not needed. With this assumption the acoustic pressure in the receiving fluid can be calculated at point (r, θ, ϕ) by the simplified Rayleigh's integral as proposed by Loredo et al. [10]:

$$\tilde{P}_2(r, \theta, \varphi) = \frac{-\omega^2 \rho_2 e^{jk_2 r}}{2\pi r} \hat{w}(k_{2x}, k_{2y}) \tag{4.3.9}$$

where ρ_2 is the receiving fluid density and the variables k_{2x} and k_{2y} are the projections of the wave vector $\boldsymbol{k_2}$ and are given by:

$$k_{2x} = k_2 \sin(\theta)\cos(\varphi)$$
$$k_{2y} = k_2 \sin(\theta)\sin(\varphi) \tag{4.3.10}$$

where k_2 is the wave number, that is a relation between the frequency ω and the sound celerity into the receiving fluid c_2, given by:

$$k_2 = \frac{\omega}{c_2} \tag{4.3.11}$$

The variable $\hat{w}(k_{2x}, k_{2y})$ is the double Fourier transform of the plate's displacement and can be written as:

$$\hat{w}(k_{2x}, k_{2y}) = \int_0^a \int_0^b \tilde{w}(x, y) e^{-j(k_{2x}(x-\frac{a}{2}))} \times e^{-j(k_{2y}(y-\frac{b}{2}))} \mathrm{d}y\mathrm{d}x \tag{4.3.12}$$

The transverse displacement $\tilde{w}(x, y)$ in (4.3.12), can be calculated using Equation (3.2.58). Moreover, if we look the similarities between (4.3.12) and (4.3.1) the double Fourier transform of the plate displacement can be calculated like the generalized forces vector due to a plane wave excitation, being defined as:

$$\hat{w}(k_{2x}, k_{2y}) = \{\tilde{\mathbf{A}}\}\{\tilde{\Psi}(\boldsymbol{k_2})\} \tag{4.3.13}$$

where $\{\tilde{\mathbf{A}}\}$ is the coefficient vector of the transverse displacement and $\{\tilde{\Psi}(\boldsymbol{k_2})\}$ is an auxiliary vector like the one defined in (4.3.5), but considering the wave number of the receiving fluid.

The radiated acoustic pressure, and according with the far-field hypothesis, can be calculated by the integration of the radial intensity over a hemisphere of infinite radius:

$$W_{\mathrm{t}} = \frac{\rho_2 \omega^4}{8 c_2 \pi^2} \int_0^{2\pi} \int_0^{\frac{\pi}{2}} |\hat{w}(k_{2x}, k_{2y})|^2 \sin(\theta) \mathrm{d}\theta \mathrm{d}\varphi \tag{4.3.14}$$

Considering that the system is excited by a plane wave, the preceding equation gives the radiated acoustic power for this plane wave which allows to define an oblique incidence transmission coefficient $\tau(\theta, \varphi)$, given by:

$$\tau(\theta, \varphi) = \frac{W_{\mathrm{t}}(\Pi_{\theta,\varphi})}{W_{\mathrm{inc}}(\theta, \varphi)} \tag{4.3.15}$$

where $W_{\mathrm{inc}}(\theta, \varphi)$ is the incident power of this plane wave, that may be written as:

$$W_{\mathrm{inc}}(\theta, \varphi) = \frac{|\tilde{p}_{inc}|^2 \cos(\theta) S}{2 \rho_1 c_1} \tag{4.3.16}$$

where S is the plate area. Defined the incident acoustic power and the radiated acoustic power it is possible to define the acoustic transparency of the plate, by the relation between these two quantities. This relation is known by transmission loss (TL) and can be written as:

$$\mathrm{TL} = 10 \log \left(\frac{W_{\mathrm{inc}}(\theta, \varphi)}{W_{\mathrm{t}}(\Pi_{\theta,\varphi})} \right) \tag{4.3.17}$$

The transmission loss is an important indicator of the treatment effectiveness once that represents the fraction of the incident acoustic power that isn't radiated to the receiving fluid. In addition to the transmission loss, others indicators can be defined like the mean square velocity that is defined as a space and time average of the structure velocity and can be written as:

$$\langle V^2 \rangle = \frac{1}{S} \int_0^a \int_0^b \frac{1}{2} \left| \frac{d\tilde{w}(x, y)}{dt} \right|^2 \mathrm{d}y\mathrm{d}x \tag{4.3.18}$$

The preceding equation can be rewritten, taken into account Equation (3.2.58), as:

$$\langle V^2 \rangle = \frac{\omega^2}{2S} \{\tilde{\mathbf{A}}\}^{\mathrm{T}} \left[\int_0^a \int_0^b \{\boldsymbol{\phi}_w(x, y)\}\{\boldsymbol{\phi}_w(x, y)\}^{*\mathrm{T}} \mathrm{d}y\mathrm{d}x \right] \{\tilde{\mathbf{A}}\}^* \tag{4.3.19}$$

where $*$ represents the complex conjugate operation. As was said, the mean square velocity represents the space and time average of the structure velocity. Taken into account its definition, a new vibroacoustic indicator can be defined as only the time average of the structure velocity and can be defined as:

$$\langle V^2(x,y)\rangle = \frac{\omega^2}{2S}\{\tilde{\mathbf{A}}\}^{\mathrm{T}}\{\boldsymbol{\phi}_w(x,y)\}\{\boldsymbol{\phi}_w(x,y)\}^{*\mathrm{T}}\{\tilde{\mathbf{A}}\}^* \tag{4.3.20}$$

The square velocity is a vibroacoustic indicator that is appropriated to a 2D representation of the time average of structure velocity at a given frequency.

Another indicator that gives an idea of the treatment efficiency is the radiation efficiency and is defined as a non-dimensional ratio between the radiated sound power and the mean square velocity of the plate:

$$\sigma = \frac{W_t}{\rho_2 c_2 S\langle V^2\rangle} \tag{4.3.21}$$

Considering the above definitions, the radiation efficiency expresses the portion of vibration energy transformed into sound. If it is considered a diffuse field, the computation is made with waves of same amplitude and incidence angles (θ_i, φ_i) considering that the half space is divide in n_θ parts for the angle θ and n_φ parts for φ angle.The indicators $\Lambda(\Pi_{\theta_i,\varphi_i})$ (where Λ stands for: the mean square velocity $\langle V^2\rangle$, the incident power W_{inc} and the radiated power W_t) according to the mathematical definition of diffuse field given before, can be summed to obtain the equivalent indicator for a diffuse field excitation:

$$\Lambda_d = \sum_{i=1}^{n_\theta}\sum_{j=1}^{n_\varphi}\Lambda(\Pi_{\theta_i,\varphi_i})\Delta\Omega(\theta_i,\varphi_i) \tag{4.3.22}$$

where $\Delta\Omega(\theta_i,\varphi_i) = \cos(\theta_i)\Delta\theta\Delta\varphi$ is the solid angle corresponding to the plane wave excitation of incidence angle $(\theta_i,\varphi_i)(\Delta\theta = \pi/2r$ and $\Delta\varphi = 2\pi/s)$. The linear system of Equation (3.2.69) must be solved for each orientation (θ_i,φ_i).

Chapter 5

Model Validation and Evaluation

5.1 Introduction

In this chapter, in order to validate and evaluate the mechanical and vibroacoustic model, their main characteristics are studied. The great importance of the maximum order of the basis functions is analysed and a comparison between the degrees of freedom obtained with this model and with other models is performed. The multilayer behaviour is also analysed with a study of the displacement field in a laminate to evaluate the continuity established in the formulation. Finally, in order to validate the vibroacoustic indicators a comparison with the results obtained by Loredo et al. [10] is made and the influence of the incidence angle of a plane wave in the system response is evaluated.

5.2 Basis Dimension and Degrees of Freedom

In the Rayleigh-Ritz method the dimension of the trial functions space is a matter of great importance. As well as the finite elements give the representativeness of the model in the finite element method, the dimension of the basis functions in the Rayleigh-Ritz method determines the structure discretization. With this model, the displacement field is builded with five different unknowns which leads to a model with $(5 \times m \times n)$ degrees of freedom, where m and n are the maximum orders of the trial functions in x and y-direction, respectively. The number of degrees of freedom only depends on these variables and are independents of the number of layers, once that the transverse shear stress continuity was enforced at each interface and the displacements of a generic layer ℓ can be written in function of the displacements of the first layer. On the other hand, a model that considers two new unknowns (two rotations) for each new layer, which is the the case of the displacement field adopted in the layerwise model implemented by Moreira [4], would lead, in the Rayleigh-Ritz method, to a model with $[5 \times m \times n + 2 \times m \times n \times (N-1)]$ degrees of freedom, where N is the total number of layers. For a three layer laminate with m and n order equal to 10, for example, the number of degrees of freedom in the present work is 500, while with other model like that was mentioned above is 700. This is a great difference between models, namely in the number of degrees of freedom which makes the model used in this work less cumbersome. If we consider the finite element method, different calculations are need to estimate the total number of degrees of freedom once that it depends on the mesh but a comparison with an example performed in the software Actran® is made hereafter. To illustrate the difference between the two models mentioned before, the Figure 5.1 represents the number of degrees of freedom function of the number of layers, for the two different models using a Rayleigh-Ritz method and a maximum order of 10 for both directions.

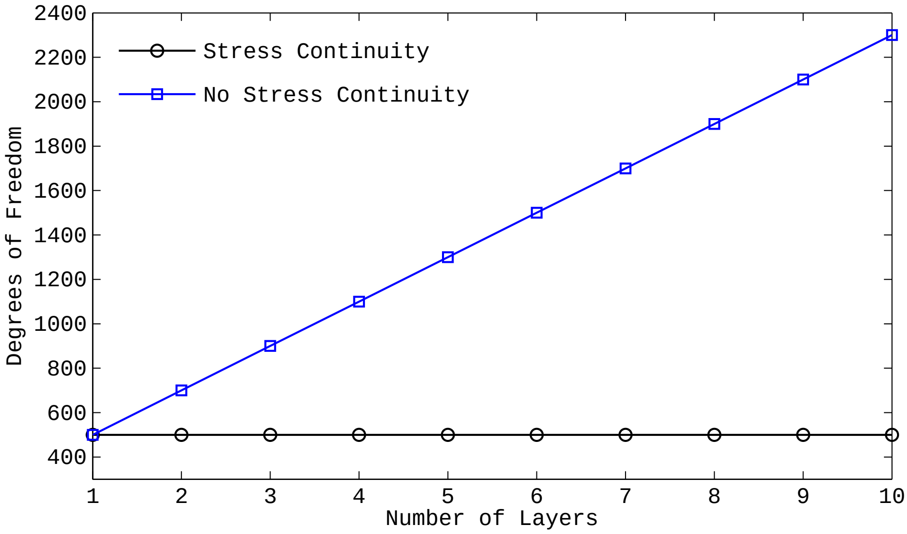

Figure 5.1: Degrees of freedom for different models and number of layers

It is clear now, seeing Figure 5.1 that the model studied in the present work has a great advantage in which concerns to the total number of degrees of freedom.

As was said before, the model discretisation is ensured by the maximum order in x and y-direction of the basis and to study this effect, the magnitude of a frequency response function (receptance) of a simply-supported plate with the properties shown in Table 5.1 is studied. For that, three different cases are analyzed, with $m \times n$ equal to 2×2, 4×4 and 8×8. According to what was said before, this represents a model with 20, 80 and 320 degrees of freedom, respectively. Furthermore, a comparison with the frequency response function given by the software Actran® is performed. In this software, the same plate was studied with the element "HEX08" that is a solid element with 3 degrees of freedom per each node. The use of 1344 elements led to a model with 6525 degrees of freedom. The excitation is a point force applied at (x=0.08m and y=0.07m) from a corner of the plate.

Table 5.1: Geometric and mechanical properties of the plate

a (m)	b (m)	h (mm)	Young's Modulus (Pa)	Density (Kg/m^3)	Poisson's Ratio	Loss Factor
0.48	0.42	3.22	66×10^9	2680	0.33	0.005

Seeing Figure 5.2, is clear the influence of a better structure discretization with the increasing in the order of the basis functions. It can be seen that a model with a maximum order of 2 for x and y-direction is clearly insufficient for a good representation of the frequency response function (receptance), even at low frequencies where only the values of the natural frequencies are correct. Moreover, a 2×2 order for the basis functions can't represent the frequencies above the fourth one. On the other hand, with a 4×4 and 8×8 order, Figure 5.2 show a similar frequency response function only with slight differences as the frequency increases. Recalling what was said before, this means that a similar frequency response is obtained, for this frequency

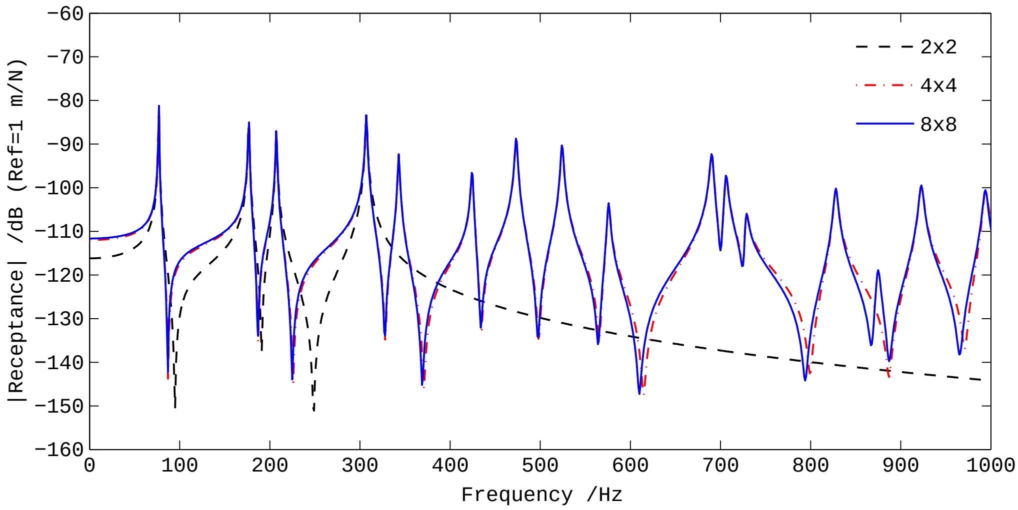

Figure 5.2: Influence of the maximum order of the basis functions

range considered with four times less degrees of freedom (80 vs 320 degrees of freedom).

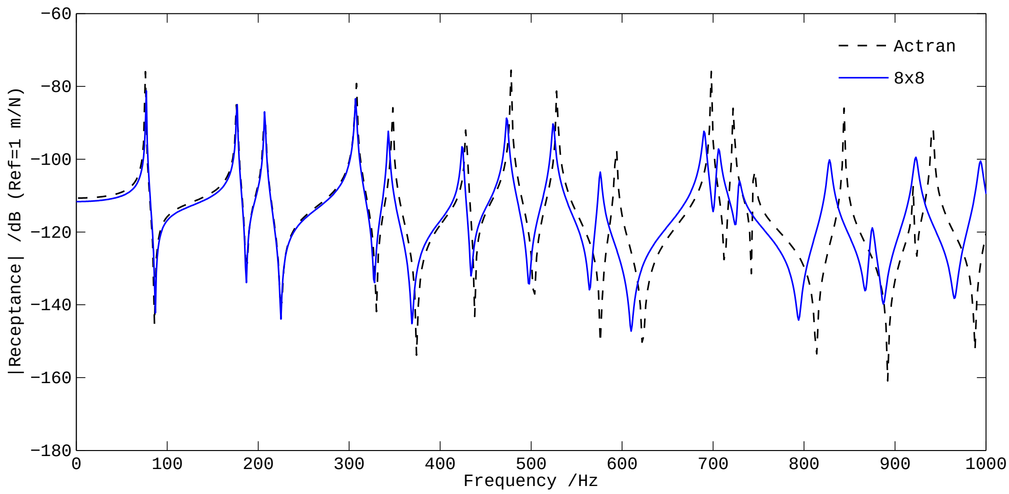

Figure 5.3: Comparison between the present model with 8x8 basis functions and Actran®

The comparison between the present model with a 8x8 order for the basis functions and the frequency response function obtained with the software Actran® in Figure 5.3 show a good agreement between the two models, particulary at low frequencies. As the frequency increases the model studied in this work is more damped and underestimate the natural frequencies relatively to Actran®. Considering that the present model uses a plate theory that considers the effect of the shear stress is acceptable that it tends to underestimate the natural frequencies. It can be said that these results are excellent if we take into account that the two models are completely different, once that in the Actran® a solid finite element is used in contrast with the present work, where is used a plate theory and the Rayleigh-Ritz method. Besides that, the Actran® example was performed with 6525 degrees of freedom against 320 used with the present model, which is overwhelming difference of 6205 degrees of freedom.

5.3 Multilayer Behaviour

5.3.1 Displacement Field

As was said in the presentation of the structural model in Chapter 3, a linear displacement field across the thickness is used, where the displacement continuity is enforced at each interface. At this point, in order to validate the model implementation, namely the displacement continuity, a graphical representation of the displacement in x-direction across the thickness is done. For that, a three layer laminate is studied and its properties are shown in Table 5.2.

Table 5.2: Geometric and mechanical properties of the laminate

Layer	a (m)	b (m)	h (mm)	Young's Modulus (Pa)	Density (Kg/m^3)	Poisson's Ratio
1	0.48	0.42	3	210×10^9	7800	0.3
2	0.48	0.42	2	66×10^9	2680	0.33
3	0.48	0.42	1	210×10^9	7800	0.3

The linear displacement in x-direction for a generic layer ℓ, as was demonstrated before, is given by:

$$u^\ell = u_0^1 + \beta^\ell \left(\frac{\partial w^1}{\partial x}\right) + \delta^\ell_{xx}\varphi^1_x + (z^\ell - z)\left(\frac{\partial w^1}{\partial x} + \alpha^\ell_{xx}\varphi^1_x\right) \tag{5.3.1}$$

This displacement can be now calculated for a static load applied in the structure. For a distributed pressure of 10^5 Pa and considering a simply-supported plate, the displacement field across the thickness, in the center of the plate ($x = 0.24$mm and $y = 0.21$mm), obtained can be seen in Figure 5.4.

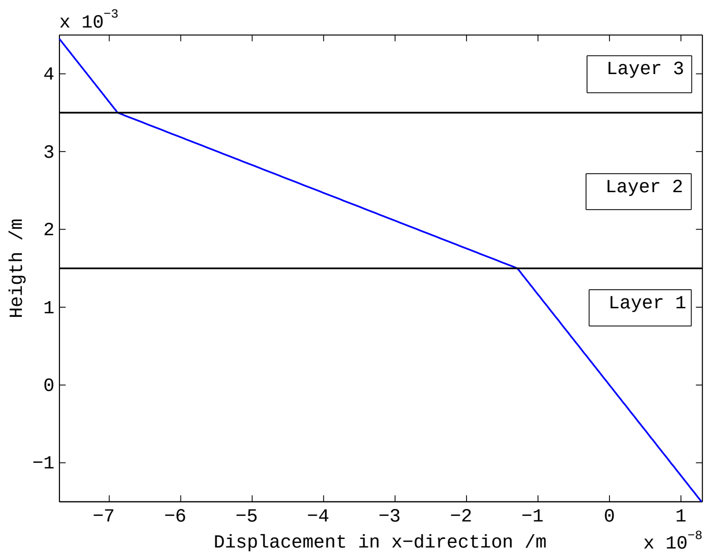

Figure 5.4: Displacement in x-direction for a distributed pressure of 10^5 Pa

It can be seen in Figure 5.4 that the displacement continuity at each interface was ensured as well as the multilayer behaviour despite the displacement of a generic layer ℓ can be written as a function of the displacements of the first layer. In addition, it can be said that the displacement field across the thickness is the expected one, once that the slopes (deformation - $\mathrm{d}u/\mathrm{d}x$) of the first and third layers are equal and smaller than that of the second layer. This reflects the fact that the first and third layers are steel layers and the second one is an aluminum layer with lowest Young's Modulus.

5.4 Vibroacoustic Indicators and Patches Handling

In order to validate the model implementation and obtained results in terms of vibroacoustic indicators, a comparison with the results obtained by Loredo et al. [10] was done. The considered plate is immersed in air and receiving an acoustic excitation of an incident plane wave with unitary amplitude and incidence angles of $\theta = 85°$ and $\varphi = 0°$. The geometric and mechanical properties of the studied plate can be seen in Table 5.3.

Table 5.3: Geometric and mechanical properties of Loredo et al. [10] base plate

a (m)	b (m)	h (mm)	Young's Modulus (Pa)	Density (Kg.m^{-3})	Poisson's Ratio	Loss Factor
0.455	0.376	1	210×10^9	7800	0.3	0.01

In the work performed by Loredo et al. [10] the properties of the exciting and receiving fluid are not given but in this work the properties of the air at 25°C are assumed, once that is the temperature considered for the properties of the viscoelastic layer. The referred properties can be seen in Table 5.4.

Table 5.4: Exciting and receiving fluid properties - Air (T=25°C)

Fluid	Sound Celerity (m.s^{-1})	Density (Kg.m^{-3})
Exciting/Receiving	346.13	1.1839

The vibroacoustic indicators were obtained for three different cases. Firstly, for the base plate alone and then a total and a partial treatment were applied. In the viscoelastic treatments, the constraining layer is also considered to be made with the same steel of the base layer, and thickness is set to 0.5mm. The viscoelastic layer has a thickness of 0.25mm and the material is the 3M ISD112. A constitutive law for the storage modulus and loss factor of this material was shown in Chapter 2, however only discrete values for some frequencies of these properties are given in [10] and there is no certainty that the constitutive law used for all the frequency range is the same. The partial treatment applied covered 40% of the total plate area and was added in the central region with the dimensions of 288×238mm. For the comparison with the work developed by Loredo et al. [10] three different vibroacoustic indicators were studied, which are the mean square velocity, transmission loss and radiation efficiency and the results can be seen in Figures 5.5, 5.6 and 5.7, respectively. The vibroacoustic indicators, as we see before, are frequency dependent and this makes the model cumbersome and slow, specially in this model where the stiffness matrix but also the mass matrix vary with frequency. Therefore, in order to obtain the largest possible number of results in a short period of time the frequency range varies between 0 and 700Hz which is a smaller frequency range than that was used by Loredo et al. [10] but that changes nothing about the targets of this work. Due to the smaller frequency range it was used a maximum order of 6 for the x and y-directions whereas in the work developed by Loredo et al. [10] a maximum order of 13 was used. The results obtained by Loredo et al. [10] can be seen in Appendix C. Analysing the Figures 5.5, 5.6 and 5.7 it can be seen that, in general and for the studied frequency range, a good match is obtained with the results available in Appendix C. Although it has been used a smaller basis functions, the results perfectly match for low frequencies and only in the transmission loss and radiation efficiency indicators, for frequencies near 700Hz is that the results are not representative, due to the smaller basis functions. As we seen before, the increasing of the basis functions can be compared in the finite element method, to the increase in the number of mesh elements. Furthermore, it should be noted that the properties of the fluid are not given in the work developed by Loredo et al. [10] and only discrete values of the storage modulus and loss factor of the viscoelastic material for some frequencies are given in Reference [10].

Analysing the vibroacoustic indicators obtained from a more particular point of view some important aspects should be noted. Firstly, both total and partial treatment makes the plate more efficient in a vibroacoustic viewpoint once that in the resonance frequencies the values of the mean square velocity decreased and the values of transmission loss and radiation efficiency increased. This capability to improve the behaviour of the structure in the resonance zones is achieved either with the total treatment as the partial treatment, yet this fact is most remarkable in the total treatment. However, this result is particularly interesting once that with a smaller structural modification and with less added mass similar results to those of a total treatment can be achieved.

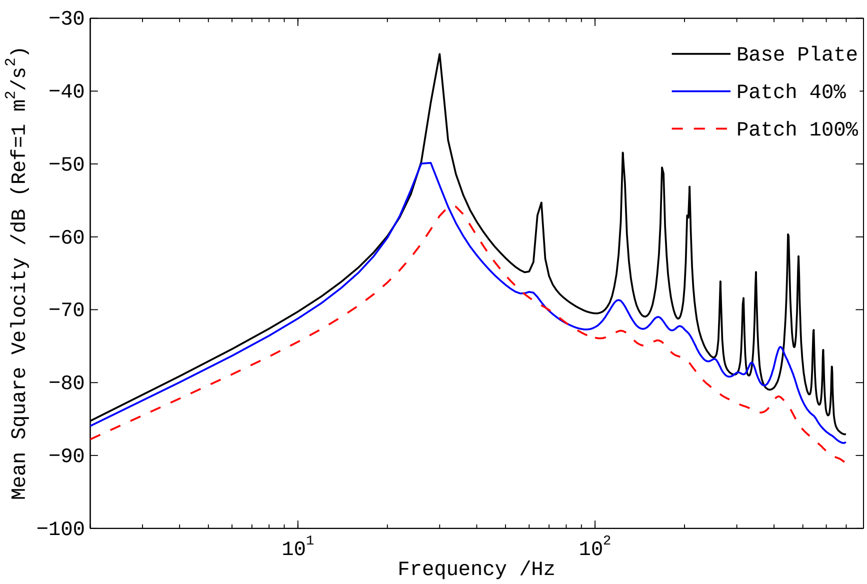

Figure 5.5: Mean square velocity for three different configurations

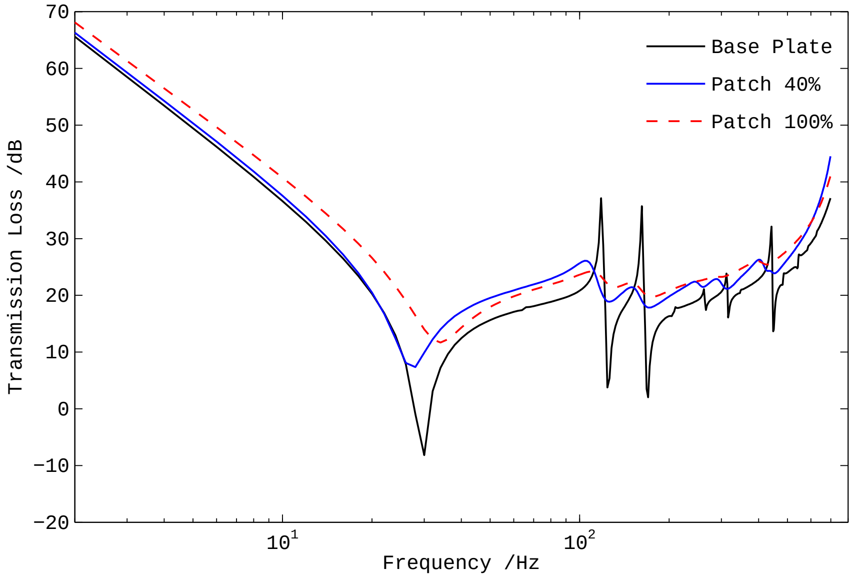

Figure 5.6: Transmission loss for three different configurations

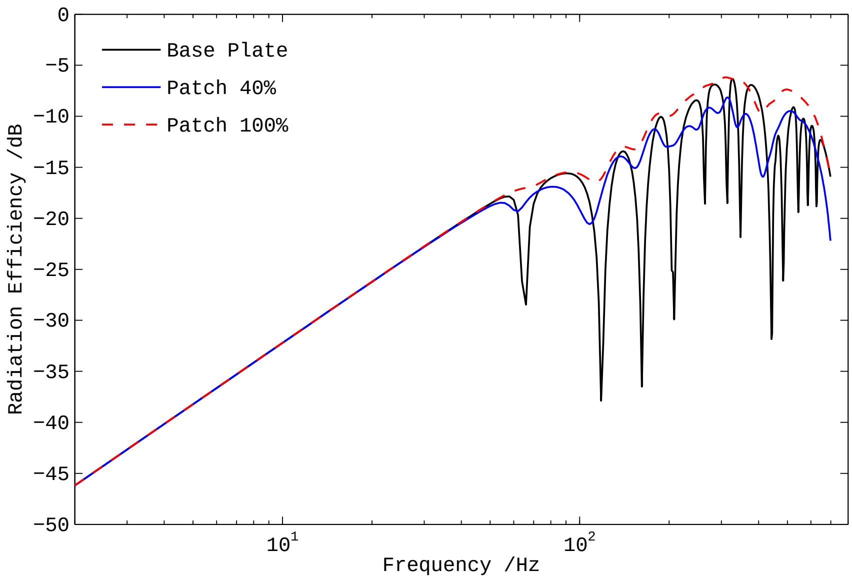

Figure 5.7: Radiation efficiency for three different configurations

At first sight can be weird that the radiation efficiency is better in the damped plates once that expresses the portion of the vibration energy transformed into sound. However the radiation efficiency is defined relatively to a unit of mechanical power and if the damping reduces the energy levels of modes is not strange that the radiation efficiency is better in the damped case once that the vibration energy is lower. Another interesting aspect is verified for the studied case. The use of a partial treatment covering 40% of the total area of the plate shifts the resonance frequencies to left while the total treatment shifts these frequencies to right. In this case, this means that for the partial treatment prevails the added mass effect while for the total treatment prevails the stiffness increase effect.

5.4.1 Influence of the Incidence Angle

The validation of the vibroacoustic indicators was made considering a plane wave with incidence angles $\theta = 85°$ and $\varphi = 0°$, but the incidence angles have influence in the vibroacoustic responde of the plate, as can be seen in Reference [10]. In order to evaluate this influence, the mean square velocity and transmission loss for two different incidence angles are presented in Figure 5.8 and Figure 5.9, respectively. The computations are made with two different angles, one with $\theta = 85°$ and other with $\theta = 0°$. The angle φ is considered 0° for the two cases. The fluid and excitation properties are the same than those which were used in the validation of vibroacoustic model.

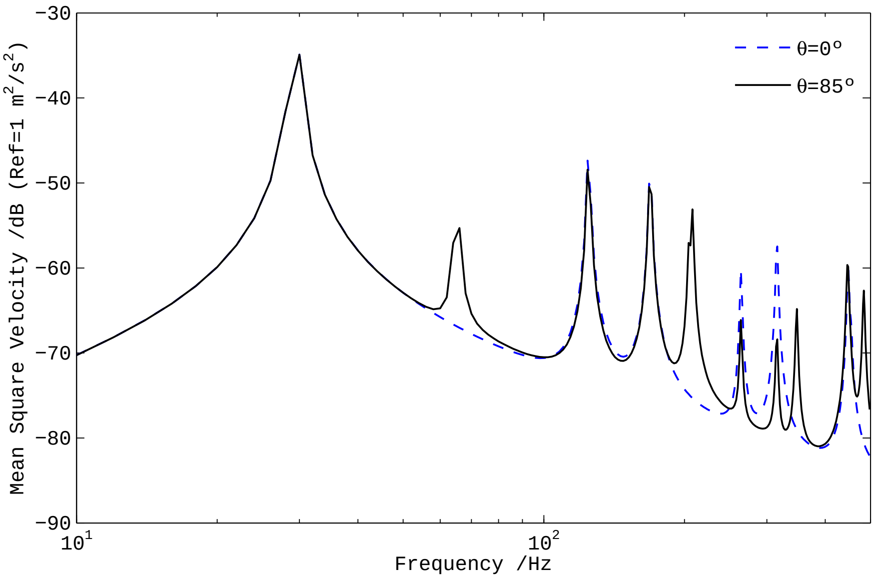

Figure 5.8: Mean square velocity for two different incidence angles

If we see Figure 5.8, it is clear that with an incident angle θ equal to 85° are visible resonances that are not excited with an incident angle of 0°. There are not significant variations in the values of mean square velocity achieved with the different incidence angles in the common resonances, except the resonance that occurs at about 300 Hz, and the great difference between the two considered cases is the number of resonances. With an incident angle θ of 85° we can find 4 more resonances than those that the system has with an incidence angle of 0°, in the considered frequency range. Similarly to what happens when a force is applied on a nodal line of a certain natural mode and that mode is not excited also here for certain incidence angles there are resonances that are not excited. Analysing Figure 5.9 we can see that the transmission

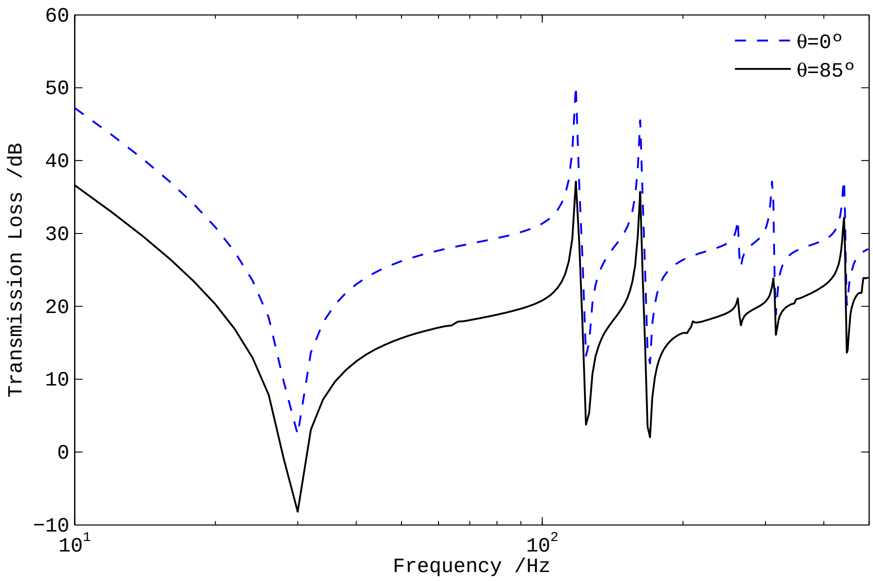

Figure 5.9: Transmission loss for two different incidence angles

loss takes the same form for the two considered incidence angles and there's only a vertical shift in the values of transmission loss where for an incidence angle θ of $0°$ are higher than for an incidence angle of $85°$.

Chapter 6

Analysis of Constrained-Layer Damping Patches

6.1 Introduction

The use of constrained-layer damping patches is an approach to improve the efficiency of viscoelastic treatments because a high damping capacity is achieved with a smaller structural modification and with different configurations a selective damping can be reached. Along this chapter, the main interest is to make the design of constrained-layer damping patches as effective or functional as possible. For this purpose, the analysis of the optimal main key parameters in the design of a damping patch is performed focusing the attention in the damping capability as a benefit and the added mass as a drawback, once that represents the structural modification and the treatment's cost. Therefore, a study of the optimal covered area by a central patch is performed establishing a commitment between damping capability and added mass as well as a study of the optimal constraining layer thickness. Lastly, different configurations and distributions of patches are studied with the purpose of achieve a selective damping and optimise different modes with the same added mass. Naturally, the analysis is also made at an acoustic level and along this chapter different vibroacoustic indicators are shown overlapping different results obtained with different patches' parameters and configurations.

6.2 Analysis of Optimal Covered Area

The results obtained in the previous chapter on the model validation raise an interesting question about the optimal covered area. To answer it an objective needs to be formulated because an optimal solution always depends on the proposed target. In this work, in order to minimise the covered area an objective function that includes the modal loss factors and the added mass with the treatment is adopted. This objective function only considers a mechanical indicator that represents the dissipated energy by the structure but the vibroacoustic behaviour is also a main objective of this work. However, the coupling between the structure and the fluid is negligible and for that reason the mechanical problem is independent of the vibroacoustic model. Therefore, for the vibroacoustic model considered in this work the vibroacoustic response is strongly dependent of vibration levels and, in general, reducing the vibration levels leads reducing the vibroacoustic response. In practice, considering the coupling between fluid and structure, the mechanical and vibroacoustic problems are connected and reduce the vibration levels may not mean that the vibroacoustic response is reduced.

In a similar way to what was done in [14], the objective function can be defined as:

$$J_{\bar{S}}(\bar{m}) = \sum_{i}^{N} \left(\frac{\mathrm{a}_i}{\eta_i} \right) + \mathrm{b}\bar{m} \tag{6.2.1}$$

where $J_{\bar{S}}(\bar{m})$ is the objective function to minimise and $\bar{m}$ is the added mass with the treatment, function of the base plate mass, and can be defined as:

$$\bar{m} = \frac{m_{\mathrm{c}}}{m_{\mathrm{p}}} = \frac{(a_{\mathrm{c}} \times b_{\mathrm{c}} \times h_{\mathrm{vl}} \times \rho_{\mathrm{vl}}) + (a_{\mathrm{c}} \times b_{\mathrm{c}} \times h_{\mathrm{cl}} \times \rho_{\mathrm{cl}})}{(a \times b \times h_{\mathrm{p}} \times \rho_{\mathrm{p}})} \tag{6.2.2}$$

where the subscripts p represent the base plate, c the covered area, vl the viscoelastic layer and cl the constraining layer. In Equation (6.2.1) a_i and b are weighting factors. The value of added mass plays as a penalty variable once that changes the structure characteristics and represents the treatment's cost. The covered area by the treatment function of the base plate area can be written as:

$$\bar{S} = \frac{S_{\mathrm{c}}}{S_{\mathrm{p}}} \tag{6.2.3}$$

where S_{c} is the covered area and S_{p} is the area of the base plate. In order to obtain the optimal covered area the plate studied by Loredo et al. [10] is used. The geometric and mechanical properties of the structure are the same as those from the validation of the vibroacoustic indicators and patches handling (see Table 6.1) as well as the fluid properties from Table 5.4 and the basis functions.

Table 6.1: Geometric and mechanical properties of Loredo et al. [10] base plate and patch treatment

Layer	a (m)	b (m)	h (mm)	Young's Modulus (Pa)	Density (Kg.m^{-3})	ν	Loss Factor
1	0.455	0.376	1	210×10^9	7800	0.3	0.01
2	$(x_2 - x_1)$	$(y_2 - y_1)$	0.25	(Chapter 2)	1140	0.45	(Chapter 2)
3	$(x_2 - x_1)$	$(y_2 - y_1)$	0.5	210×10^9	7800	0.3	0

In this study only the covered area varies, using a rectangular central patch where the relation between length and width is the same on the base plate and the patch. Therefore, for a first analysis was simulated the the covered areas shown in Table 6.2.

In this study, the first three modal loss factors were used in order to minimise the objective function and the results, obtained with the IMSE algorithm explained in Chapter 4, are presented in Table 6.3. The objective function is calculated based on these three modal loss factors and considering the weighting factors $a_i = 1$ and $b = 100$.

The results expressed in Table 6.3 are shown in a graphic form in Figure 6.1. As we can see in Table 6.3 and in Figure 6.1, the optimal covered area for the defined objective function is 40%. Remembering the objective function, this means that the increase in damping capacity with a covered area greater than 40% no longer compensates the added mass and consequently the cost of treatment. It should be noted that this result is valid for the objective function defined here and other results can be obtained for different objectives, not being a covered area of 40% necessarily the best solution. However, as has been said the 40% covered area shows the best damping capacity for the minimum added mass.

In order to a better understanding of the influence of the covered area in the system response is represented in Figure 6.2 a point frequency response function (receptance) of the plate studied here with the covered area of 20%, 40%, 80% and 100%. The excitation is a point force applied at the center of the plate.

Table 6.2: Properties of different patches' distributions

$\bar{S}$	Length (m)		Width (m)		$\bar{m}$
	x_1	x_2	y_1	y_2	
0%	-	-	-	-	0.00%
10%	0.1556	0.2995	0.1286	0.2476	5.37%
20%	0.1258	0.3292	0.1039	0.2721	10.73%
30%	0.1029	0.3521	0.0851	0.2910	16.09%
40%	0.0836	0.3714	0.0691	0.3069	21.46%
50%	0.0667	0.3884	0.0551	0.3210	26.53%
60%	0.0513	0.4037	0.0424	0.3337	32.19%
70%	0.0372	0.4179	0.0307	0.3453	37.56%
80%	0.0241	0.4310	0.0199	0.3562	42.92%
90%	0.0117	0.4436	0.0097	0.3664	48.32%
100%	0	0.455	0	0.376	53.65%

Table 6.3: Modal loss factors for different patches' distributions

$\bar{S}$	Modal Loss Factors			$J_{\bar{S}}(\bar{m})$
	η_1	η_2	η_3	
10%	0.080	0.090	0.060	45.65
20%	0.084	0.142	0.068	44.38
30%	0.130	0.091	0.128	42.59
40%	0.168	0.145	0.136	41.67
50%	0.204	0.175	0.162	43.62
60%	0.228	0.194	0.183	47.20
70%	0.256	0.212	0.2	51.18
80%	0.275	0.232	0.218	55.45
90%	0.290	0.248	0.235	60.05
100%	0.308	0.265	0.25	64.67

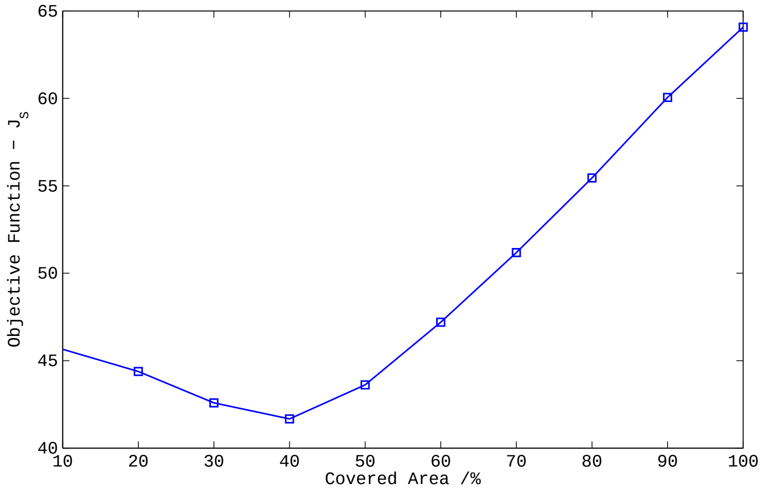

Figure 6.1: Objective function $J_{\bar{S}}$ function of the covered area

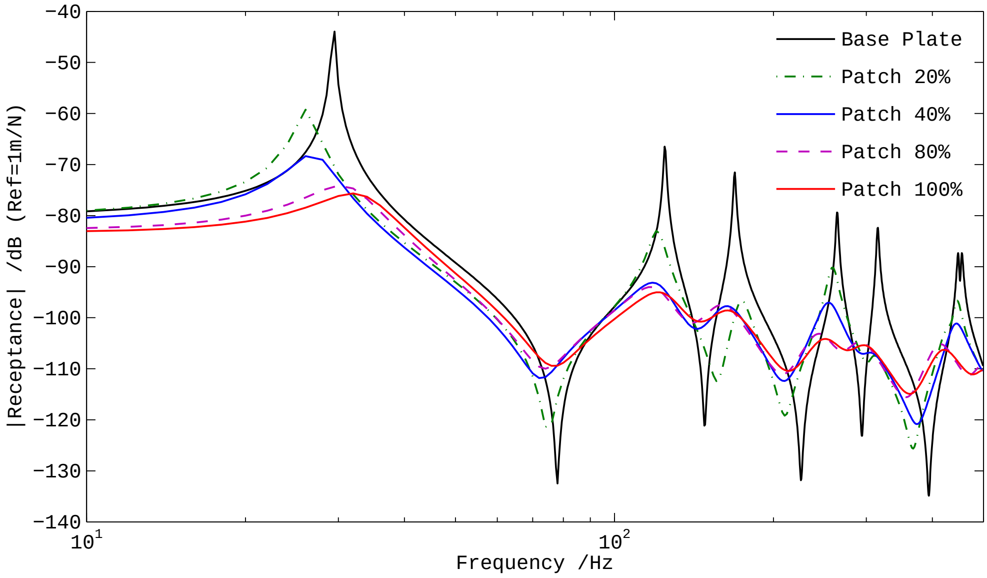

Figure 6.2: Modulus of a point FRF calculated for different patches' configurations

Analysing Figure 6.2 is clear the increase in damping capability with the increase of the covered area. The vibration levels of the different modes are increasingly reduced with the increase of the covered area and this effect is valid for all the frequency range. However, the system response for a covered area of 80% and 100% is significantly the same for all the frequency range and if we see Table 6.2, with a total treatment there is 10% more added mass than a treatment with 80% covered area. In addition, if we see the plate with 40% covered area the system response is not so damped as a treatment with 80% covered area but the vibration levels are strongly reduced in relation to the base plate and the added mass is half of the treatment with 80% covered area. Focusing the analysis in the first resonance frequency it is interesting to note that for low percentages of covered area (20% and 40%) prevails the added mass effect shifting the natural frequencies to the left and for high percentages of covered area (80% and 100%) prevails the effect of the increasing stiffness shifting the natural frequencies to the right. The key factor here is how much we are available to pay for an increase in the damping capacity but this study shows that a treatment with 40% covered area is a good commitment.

With the view to understand the influence of the covered area in vibroacoustic response, the same covered areas as above were studied. The incident plane wave considered is the same as that used on the preceding chapter on the vibroacoustic model validation as well as all the other properties including the fluid properties.

In Figures 6.3, 6.4 and 6.5 are presented, respectively, the mean square velocity, the transmission loss and the radiation efficiency for different covered areas. Analysing the vibroacoustic indicators obtained is clear that with the increase in the covered area the values of the mean square velocity decreased and the values of transmission loss and radiation efficiency increased, in the resonance frequencies. This capability to improve the behaviour of the structure in the resonance frequencies has already been observed in the frequency response function of Figure 6.2 and is now confirmed from a vibroacoustic viewpoint.

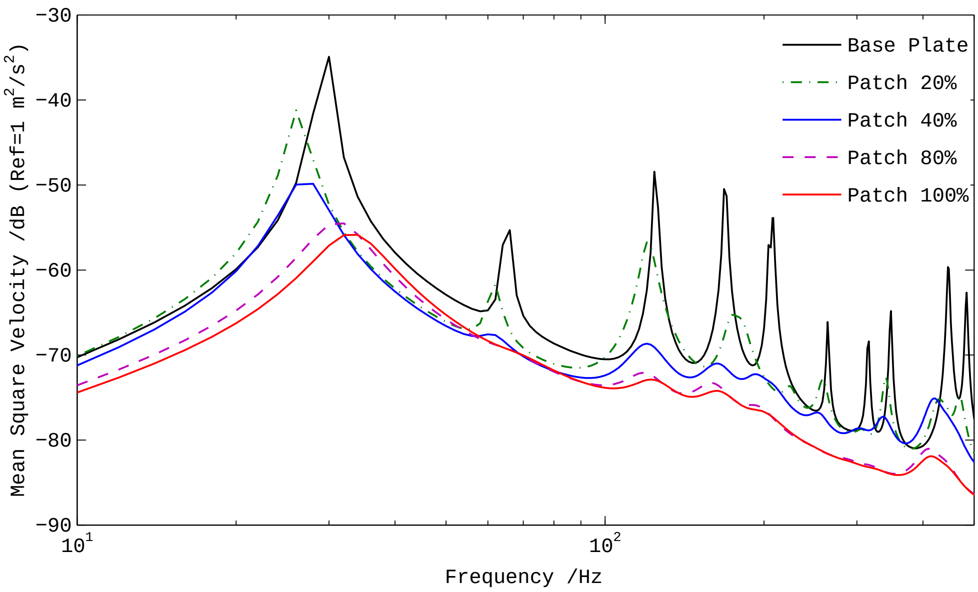

Figure 6.3: Mean square velocity for different patches' configurations

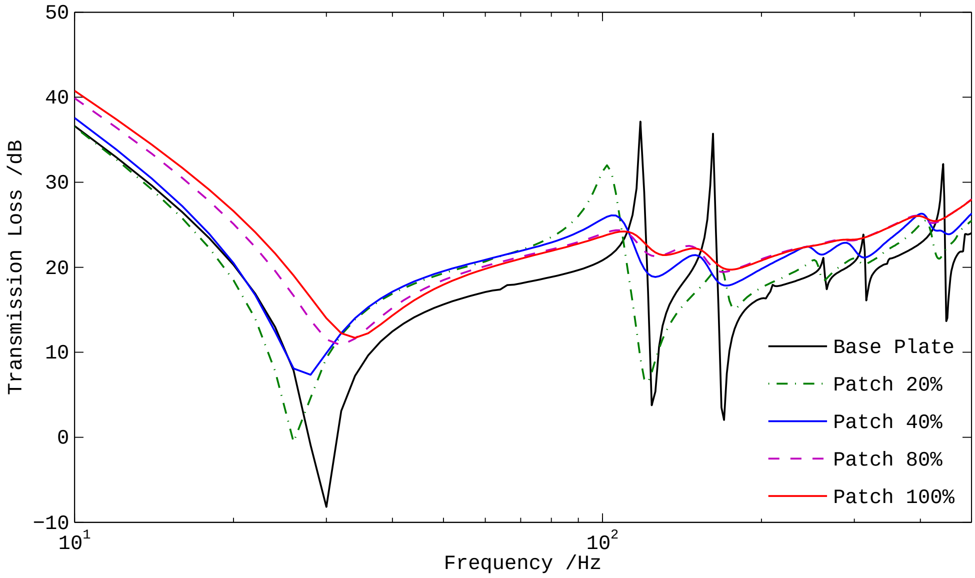

Figure 6.4: Transmission loss for different patches' configurations

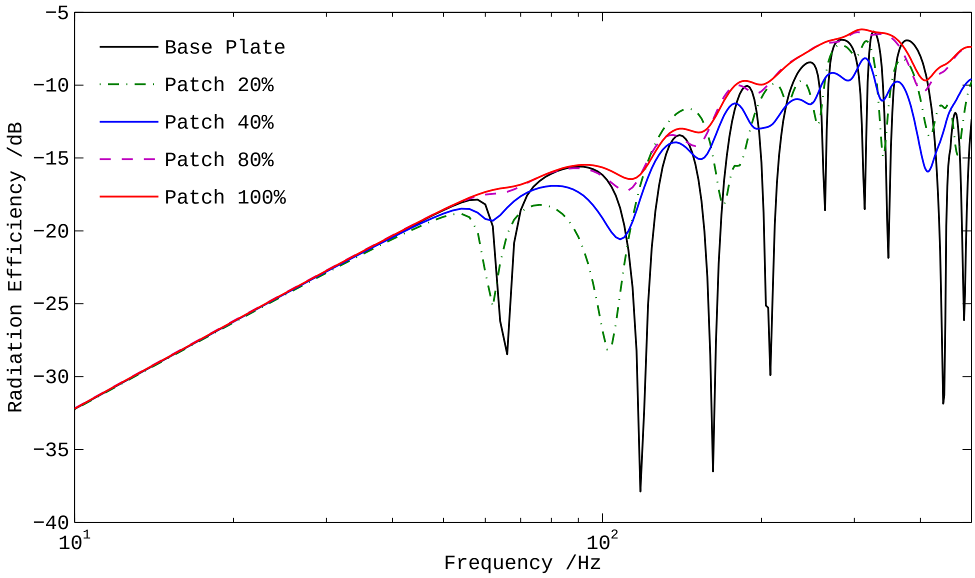

Figure 6.5: Radiation efficiency for different patches' configurations

Once again, and this is valid for the three vibroacoustic indicators, the vibroacoustic behaviour of the structure is significantly the same for the plate with 80% and 100% covered areas. Moreover, in Figure 6.3 is evident the large decrease in the mean square velocity, in the resonance frequencies, obtained with a treatment with 40% of covered area. Similar good results are also obtained for the transmission loss (see Figure 6.4) where the acoustic transparency is greatly reduced with a central patch covering 40% area. Nevertheless, in the range of frequencies between 35 and 60 Hz, the mean square velocity is greater for a plate with a total treatment than for a plate with partial treatments but the differences are negligible and are due to the shift in the value of resonance frequency. A similar result can be seen in the transmission loss (see Figure 6.4) in the same frequency range where the acoustic transparency is slightly greater for a plate with a total treatment in relation to a plate with a partial treatment applied, but the differences are, once again, very small. The radiation efficiency (see Figure 6.5) is a indicator that is not so straightforward like the previous ones and, as was said before, the radiation is improved, in the resonance frequencies, with the increase of treated area. As explained before, this is due to the reduction of the energy levels of the modes with the increase of covered area leading to a higher radiation efficiency. It should be noted that in the definition of radiation efficiency the mean square velocity appears in denominator. The behaviour of radiation efficiency in the non-resonance zones does not follows this reasoning and this indicator takes similar values for the base plate alone and for the plate with a total treatment. However, this not mean that the radiated acoustic power transmitted by both plates is equal but rather that the relationship between radiated acoustic power and mean square velocity is the same. To verify what was said, the radiated acoustic power for the different patches is shown in Figure 6.6. As can be seen, it is confirmed that the increase on the covered area reduces the radiated acoustic power in all the considered frequency range.

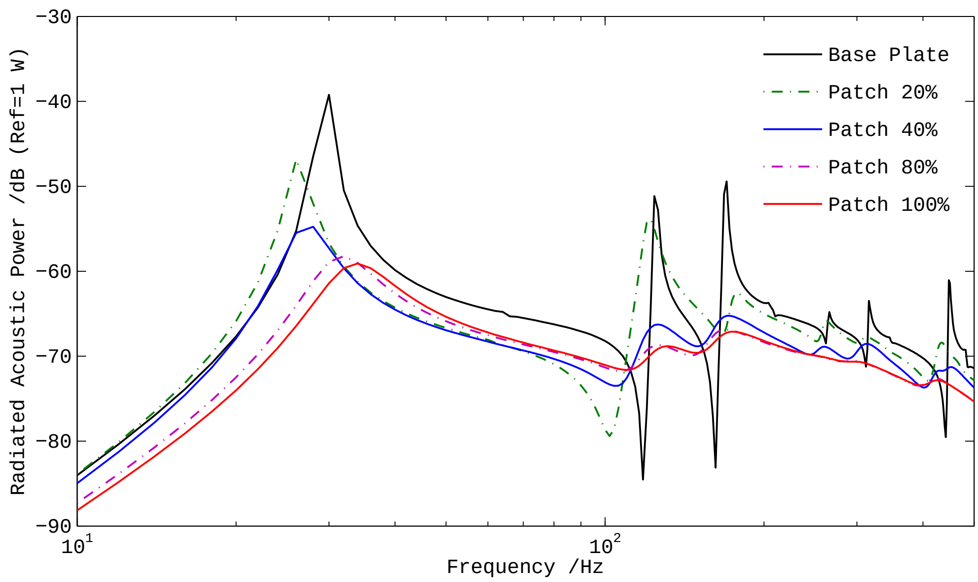

Figure 6.6: Radiated acoustic power for different patches' configurations

6.3 Analysis of Optimal Treatment's Thickness

In the preceding section a minimisation of the covered area was performed keeping constant the treatment's thickness however, the damping performance of these structures also depends on the thickness of the applied treatment. In this section, a similar minimisation of the added mass is made but keeping the covered area and varying the treatment's thickness. Adopting a similar objective function in this analysis:

$$J_{\mathrm{t}}(\bar{m}) = \sum_{i}^{N} \left(\frac{\mathrm{a}_i}{\eta_i} \right) + \mathrm{b}\bar{m} \tag{6.3.1}$$

For this study, the same plate was used with a covered area of 40% and the analysis of optimal treatment's thickness was performed keeping constant the thickness of the viscoelastic layer and varying the thickness of the constraining layer. In fact, small variations on the thickness of the viscoelastic layer do not cause significant variations in added mass not even great improvements in the damping capability, specially for the 2nd and following modes, and this objective function is not suitable for an optimisation of the viscoelastic treatment's thickness. For clarity, a ratio between the thicknesses can be defined as:

$$h_{\mathrm{cld}} = \frac{h_{\mathrm{cl}}}{h_{\mathrm{vl}}} \tag{6.3.2}$$

As was said, the same plate that was studied in the preceding section was used and the thickness of the viscoelastic layer was set constant and equal to 0.25mm. The study was performed for the different thicknesses of the constraining layer defined in Table 6.4.

Table 6.4: Different thicknesses for the constraining layer

Thickness (mm)	h_{cld}	$\bar{m}$
0.125	0.5	6.46%
0.250	1.0	11.46%
0.375	1.5	16.46%
0.500	2.0	21.46%
0.625	2.5	26.46%
0.750	3.0	31.46%

Once again, the first three modal loss factors obtained for the different cases presented in Table 6.4 were considered and the results are shown in Table 6.5.

Analysing Table 6.5 and the results represented in Figure 6.7 there is no clearly defined minimum for the objective function but rather a range, between the thickness ratios 1 and 2 where the values of the objective function are identical. The results obtained here are not so clearly as the obtained in the previous analysis and the desired application will dictate the right selection in the considered range. If in the intended application prevail the damping capability a constraining layer with a thickness twice larger than that of the viscoelastic layer is desirable

Table 6.5: Modal loss factors for different thicknesses of the constraining layer

h_{cld}	Modal Loss Factors			$J_{\mathrm{t}}(\bar{m})$
	η_1	η_2	η_3	
0.5	0.099	0.069	0.069	45.55
1.0	0.128	0.099	0.098	39.58
1.5	0.151	0.123	0.118	39.69
2.0	0.168	0.145	0.136	41.67
2.5	0.189	0.170	0.151	44.26
3.0	0.211	0.198	0.166	47.28

but if the application is unable to bear a higher cost and a small damping capability is not an issue then a constraining layer with the same thickness of the viscoelastic layer is desirable.

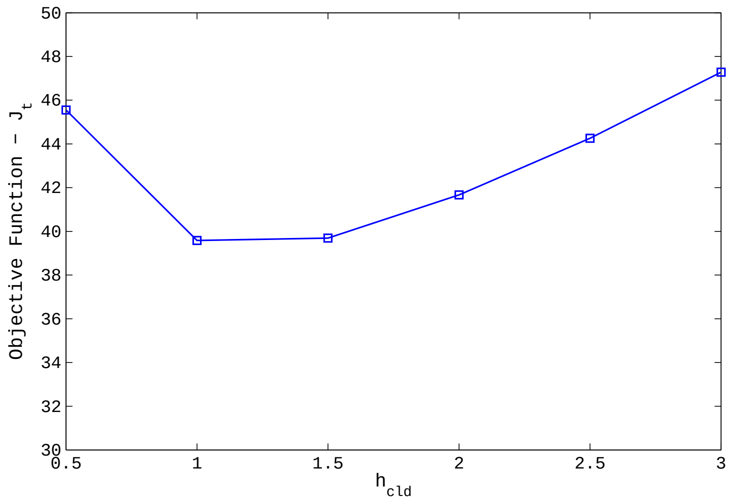

Figure 6.7: Objective function J_{t} function of the constraining layer thickness

In order to a better understanding of the influence of the constraining layer thickness in the system response, is represented in Figure 6.8 a point frequency response function (receptance) of the studied plate with the thickness ratios of 1, 1.5 and 2. The excitation is a point force applied in the center of the plate.

Analysing Figure 6.8, we can see that the differences in the response level, for all the considered frequency range, between the different thickness ratios are small nevertheless, in some resonance frequencies differences of about 5 dB can be viewed. These small differences reflect the results obtained with the objective function in the considered range of thickness ratios. Once again, the key factor is if we are available to pay the cost of a reduction of about 5 dB, or not.

In order to understand the differences between these three thickness ratios on a vibroacoustic level the mean square velocity, transmission loss, radiation efficiency and radiated acoustic power are presented considering the same fluid properties and incidence angle as on the preceding chapter.

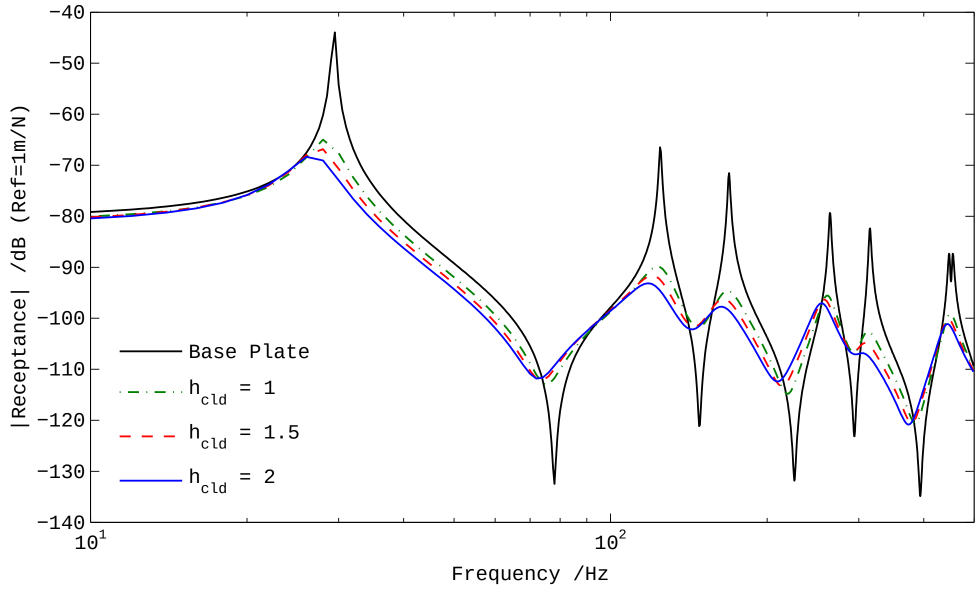

Figure 6.8: Modulus of a point FRF for a plate with different thickness ratios

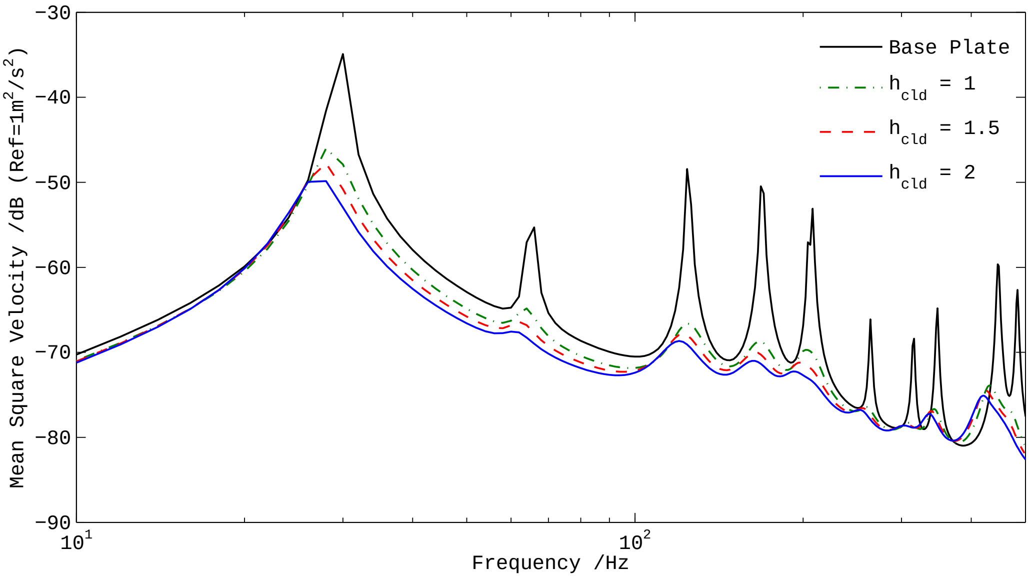

Figure 6.9: Mean square velocity for different patches' configurations

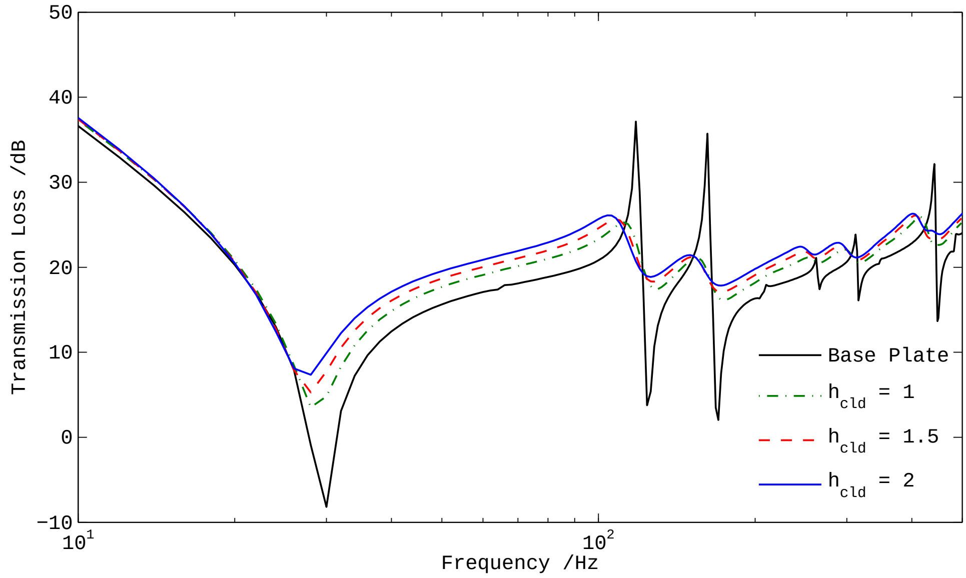

Figure 6.10: Transmission loss for different patches' configurations

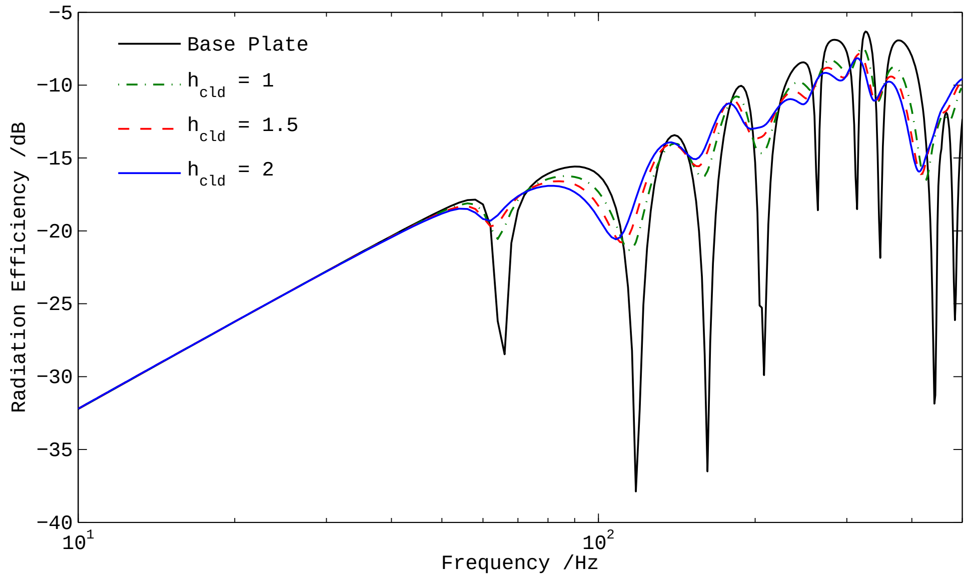

Figure 6.11: Radiation efficiency for different patches' configurations

As expected, the vibroacoustic response of the considered examples follow the same behaviour as the mechanical response. As can be seen in Figure 6.9, the values of the mean square velocity are lower for a thickness ratio of two, which corresponds to the more damped case. For thickness ratios of 1.5 and 1 the modal loss factors are smaller and with less dissipated energy the values of the mean square velocity reach values somewhat higher. Once again, it can be seen the effect of added mass with the shift of resonance frequencies to the left for the larger thickness ratios. Unsurprisingly, the values of transmission loss in Figure 6.10 follow the same behaviour and for a thickness ratio of 2 the transmission loss is higher as well as the the radiation efficiency in the resonance frequencies (Figure 6.11) result of a lower mean square velocity, as explained before. The higher transmission loss for the considered frequency range observed in Figure 6.10 for the plate with a thickness ratio of 2 is explained in Figure 6.12 where is clear the lower values of radiated acoustic power when is considered this treatment's thickness ratio. Once again, the commitment between efficiency and cost is valid for the vibroacoustic indicators and the best choice will depend on the application.

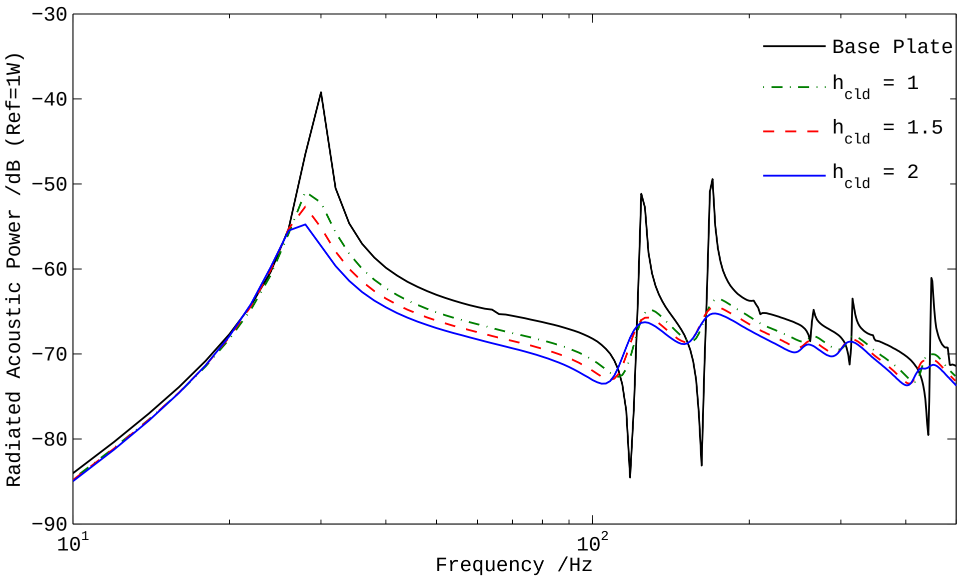

Figure 6.12: Radiated acoustic power for different patches' configurations

6.4 Analysis of Patches' Distribution

Previously, when the analysis of optimal covered area was done, a rectangular central patch was used to make that study and achieve a commitment between damping capability and added mass. However, and considering the great advantage of this model in dealing with the patches' handling, different distributions of covered area can be tested to improve the performance of the structure for a given application. As we know, due to their particular molecular structure, the viscoelastic materials are able to dissipate deformation energy so, the application of viscoelastic damping patches on areas where the shear strain is high can improve the performance of these treatments through a selective damping.

In this section, the main interest is to understand how the performance of viscoelastic damping patches can be improved for a given application focusing the attention in the resonance zones where the system response is higher. To know the areas where the structure reaches the highest displacements at each natural frequency, the natural modes of the first nine natural frequencies of the simply-supported plate used until now in the various analysis are shown in Figure 6.13.

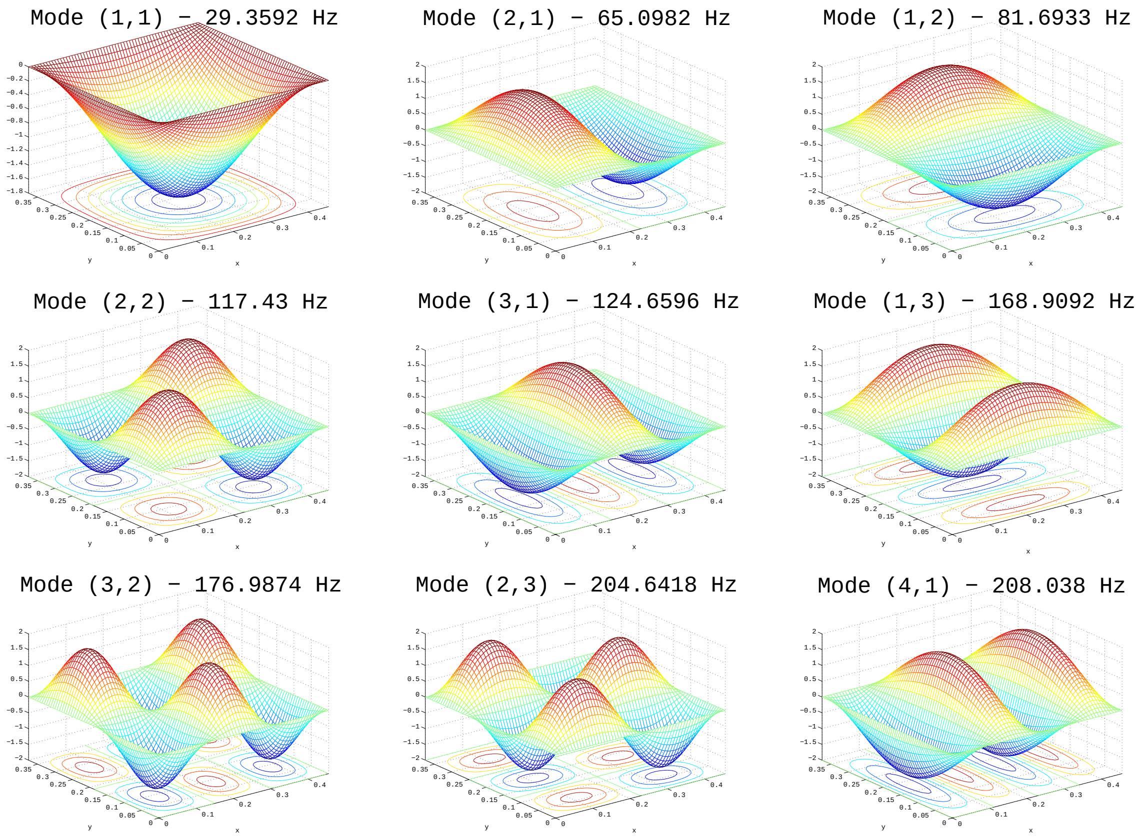

Figure 6.13: Natural modes of the simply-supported plate

As can be seen in Figure 6.13 the nodal lines and the areas where the highest displacements are reached are clearly defined for each mode and to show that a selective damping can be accomplished as a smart strategy in the passive damping using viscoelastic materials we will focus our attention in natural modes (2,1), (1,3) and (2,3). Analysing the natural mode (2,1) we see a nodal line parallel to the y-axis and two rectangular areas in phase opposition. According to what was said, we can try to improve the treatment's efficiency placing two rectangular patches in these two areas. A similar strategy can be adopted for the natural modes (1,3) and (2,3) placing three patches for the passive control of the natural mode (1,3) and six patches for natural mode (2,3). To achieve the proposed target a total covered area of 40% distributed for the different patches will be used as well as a ratio of 2 between the thicknesses of the constraining-layer and viscoelastic layer. The patches' distribution on the plate for the three different cases, natural mode (2,1), (1,3) and (2,3) are shown in Figures 6.14, 6.15 and 6.16, respectively. The geometrical properties of the different patches that define the integration limits for the structural matrices generation can be seen in Table 6.6.

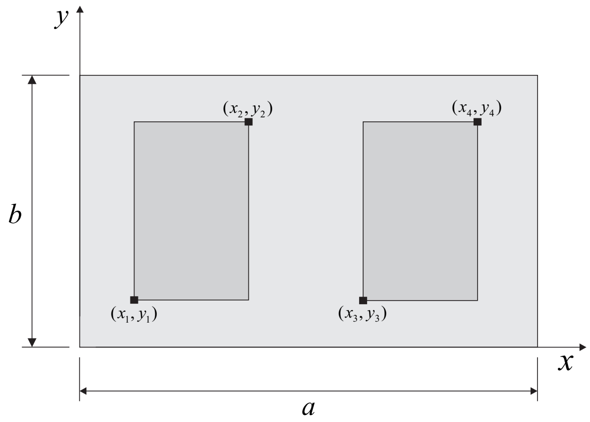

Figure 6.14: Patches' distribution for passive control of natural mode (2,1)

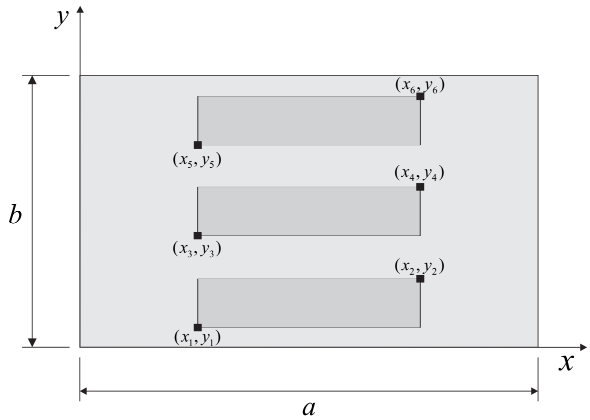

Figure 6.15: Patches' distribution for passive control of natural mode (1,3)

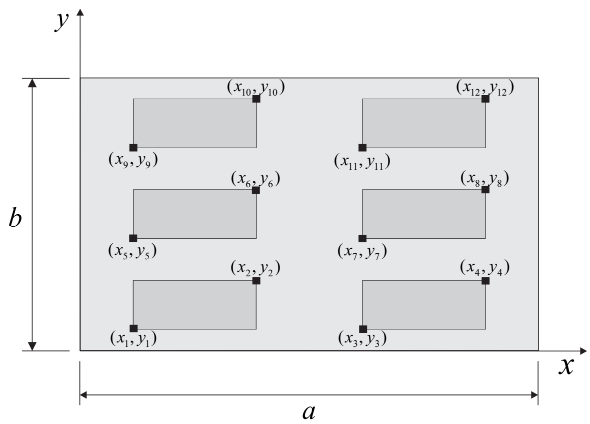

Figure 6.16: Patches' distribution for passive control of natural mode (2,3)

Table 6.6: Geometrical properties of different patches' distributions

Treatment	Length (m)											
	x_1	x_2	x_3	x_4	x_5	x_6	x_7	x_8	x_9	x_{10}	x_{11}	x_{12}
Patches (2,1)	0.0418	0.1857	0.2693	0.4132	-	-	-	-	-	-	-	-
Patches (1,3)	0.0836	0.3714	0.0836	0.3714	0.0836	0.3714	-	-	-	-	-	-
Patches (2,3)	0.0418	0.1857	0.2693	0.4132	0.0418	0.1857	0.2693	0.4132	0.0418	0.1857	0.2693	0.4132

Treatment	Width (m)											
	y_1	y_2	y_3	y_4	y_5	y_6	y_7	y_8	y_9	y_{10}	y_{11}	y_{12}
Patches (2,1)	0.0691	0.3069	0.0691	0.3069	-	-	-	-	-	-	-	-
Patches (1,3)	0.0230	0.1023	0.1484	0.2276	0.2737	0.3530	-	-	-	-	-	-
Patches (2,3)	0.0230	0.1023	0.0230	0.1023	0.1484	0.2276	0.1484	0.2276	0.2737	0.3530	0.2737	0.3530

As previously stated, the main objective with the strategic placement of these patches is improve the treatment's performance for a given application. Once that these three treatments use the same amount of material that the central patch with a covered area of 40% studied before it would be interesting to compare the respective modal loss factors achieved with these three treatments and those which were obtained with the central patch. The results are shown in Table 6.7 and in Figure 6.17 we can see the same results in a graphical form.

Table 6.7: Modal loss factors obtained with different configurations

Treatment	Modal Loss Factor (1,1)	(2,1)	(1,3)	(2,3)
Central Patch	0.1688	0.1449	0.1523	0.1303
Patches (2,1)	0.1575	0.1368	0.1235	0.1129
Patches (1,3)	0.1691	0.1342	0.0865	0.0803
Patches (2,3)	0.1713	0.1189	0.0788	0.0800

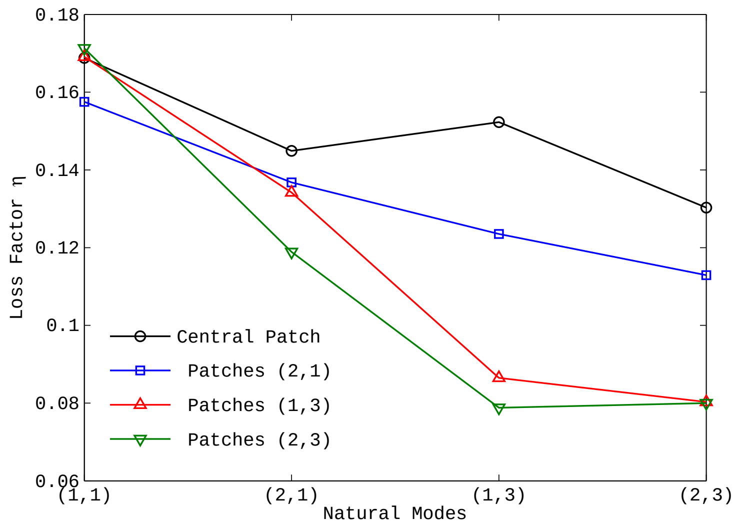

Figure 6.17: Modal loss factors obtained with different configurations

Analysing Figure 6.17 the results are completely opposite to those desired once that the treatments that are designed to improve the performance at a given natural mode did not result in a higher modal loss factor for that modal shape, for any treatment. It is interesting to note that even for the first modal shape the central patch isn't the treatment that brings the higher modal loss factor which in this case is achieved with the treatment that was designed to improve the performance of the natural mode (2,3). For the remaining modal shapes the higher loss factor is achieved with the central patch covering 40% of the total area. For the natural modes (1,3) and (2,3) the differences in the loss factors are even greater and the performance of the designed treatments drops relatively to the treatment with the central patch.

However, we can find an explanation for these results. As stated before, these treatments are able to dissipate a high amount of energy when shear deformation is superimposed to the viscoelastic layer and for a given natural mode is the extensional deformation that is mainly present where the structure reaches the maximum amplitude. Moreover, the areas with high strain can not be the areas where the structure reaches the highest displacements. The application of localized treatments in that areas will only increase the mass in that particular zone and not have any significant effect on increasing the damping capability.

According to that, if we want to improve the performance of viscoelastic damping patches in order to reduce the vibration energy of a given mode, we need to place them in a local where the shear deformation is imposed to the viscoelastic layer. If we see, for example, the natural mode (2,1) in Figure 6.13 we note that the nodal line separates two areas that are vibrating in phase opposition. This means that if we place a patch covering part of these two areas that crosses the nodal line, the vibration of the natural mode (2,1) will impose shear deformation in the viscoelastic layer due to the phase opposition that the two sides of the plate are experiencing and so the treatment's performance is improved. Moreover, with this positioning, the added mass is the same for the two opposite sides of the plate. Following the same reasoning, the treatment of the modal shape (1,3) can be improved placing 2 vertical strips, for example, as well as 3 horizontal and 2 vertical strips for the natural mode (2,3). This new patches's distribution is shown in Figures 6.18, 6.19 and 6.20. The new geometrical properties of the different patches that define the integration limits for the structural matrices generation can be seen in Table 6.8.

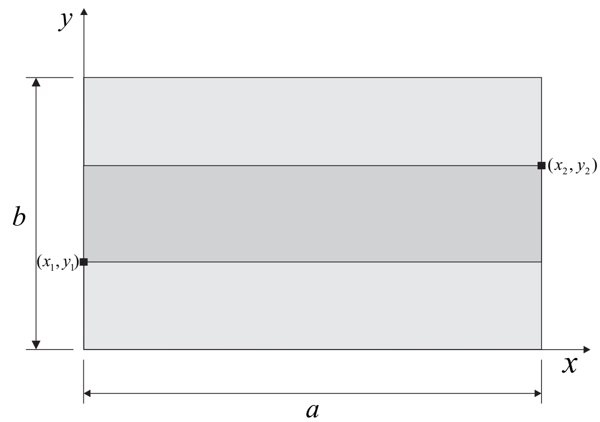

Figure 6.18: New patches' distribution for passive control of natural mode (2,1)

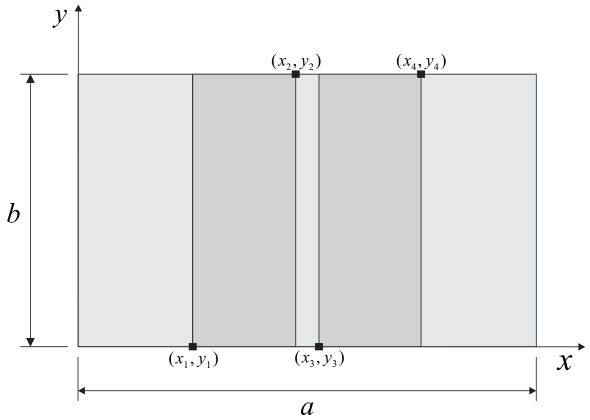

Figure 6.19: New patches' distribution for passive control of natural mode (1,3)

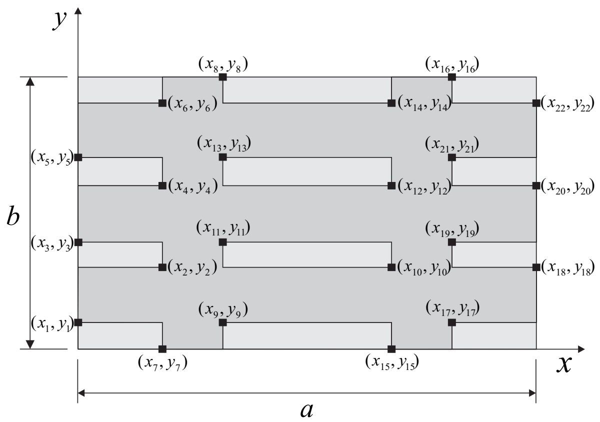

Figure 6.20: New patches' distribution for passive control of natural mode (2,3)

Table 6.8: Geometrical properties of new patches' distributions

Treatment	Length (m)										
	x_1	x_2	x_3	x_4	x_5	x_6	x_7	x_8	x_9	x_{10}	x_{11}
Strip (2,1)	0	0.4550	-	-	-	-	-	-	-	-	-
Strips (1,3)	0.1332	0.2242	0.2309	0.3219	-	-	-	-	-	-	-
Strips (2,3)	0	0.0974	0	0.0974	0	0.0974	0.0974	0.1302	0.1302	0.3249	0.1302
	x_{12}	x_{13}	x_{14}	x_{15}	x_{16}	x_{17}	x_{18}	x_{19}	x_{20}	x_{21}	x_{22}
Strip (2,1)	-	-	-	-	-	-	-	-	-	-	-
Strips (1,3)	-	-	-	-	-	-	-	-	-	-	-
Strips (2,3)	0.3249	0.1302	0.3249	0.3249	0.3577	0.3577	0.4550	0.3577	0.4550	0.3577	0.4550

Treatment	Width (m)										
	y_1	y_2	y_3	y_4	y_5	y_6	y_7	y_8	y_9	y_{10}	y_{11}
Strip (2,1)	0.1128	0.2632	-	-	-	-	-	-	-	-	-
Strips (1,3)	0	0.3760	0	0.3760	-	-	-	-	-	-	-
Strips (2,3)	0.0463	0.0791	0.1716	0.2044	0.2969	0.3297	0	0.3760	0.0463	0.0791	1716
	y_{12}	y_{13}	y_{14}	y_{15}	y_{16}	y_{17}	y_{18}	y_{19}	y_{20}	y_{21}	y_{22}
Strip (2,1)	-	-	-	-	-	-	-	-	-	-	-
Strips (1,3)	-	-	-	-	-	-	-	-	-	-	-
Strips (2,3)	0.2044	0.2969	0.3297	0	0.3760	0.0463	0.0791	0.1716	0.2044	2969	3297

The modal loss factors achieved with these new treatments are shown in Table 6.9 and in Figure 6.21 we can see the same results in a graphical form.

Table 6.9: Modal loss factors obtained with new configurations

Treatment	Modal Loss Factor (1,1)	(2,1)	(1,3)	(2,3)
Central Patch	0.1688	0.1449	0.1523	0.1303
Strip (2,1)	0.1403	0.2060	0.1249	0.1681
Strips (1,3)	0.1655	0.1110	0.3408	0.0969
Strips (2,3)	0.1537	0.1257	0.0582	0.0859

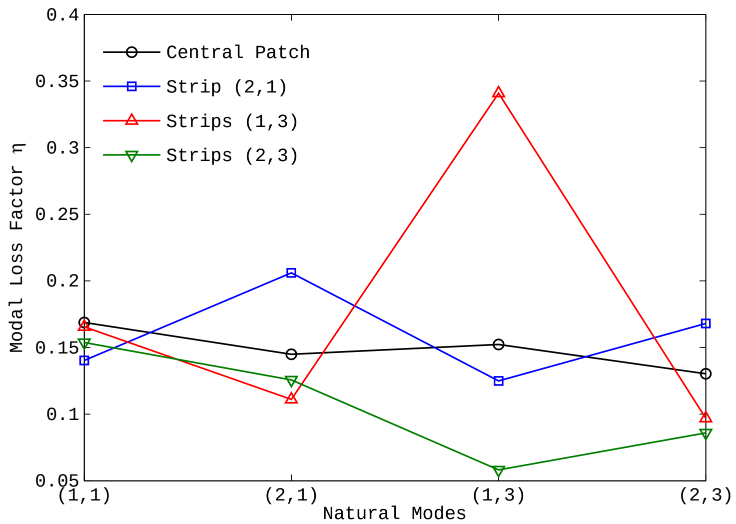

Figure 6.21: Modal loss factors obtained with new configurations

Analysing Figure 6.21 and Table 6.9 the results are now consistent and the loss factor obtained for a given natural mode is now achieved with the respective treatment except for the natural mode (2,3). In fact, the strips designed for the passive control of natural modes (2,1) and (1,3) show a high improvement in the damping capability for the respective natural mode, mainly the treatment designed for the control of mode (1,3) where the respective modal loss factor is more than two times greater than that was achieved with the central patch. These results prove that the phase opposition in the natural modes impose a shear deformation on the viscoelastic layer that are responsible for the greater energy dissipation. However, the greater loss factor obtained for the natural mode (2,3) is not achieved with the cross strips but rather with the horizontal strip which if we analyse is actually a good treatment for this natural mode, for all the reasons that were mentioned. With the cross strips the material is already well distributed throughout the structure and lose effectiveness in controlling a particular natural mode.

In order to evaluate the mechanical response of the plate when these different treatments are applied the frequency response function (receptance) of the studied plate is shown in Figure 6.22. The excitation is a point force applied in the point x=0.1517m and y=0.1880m.

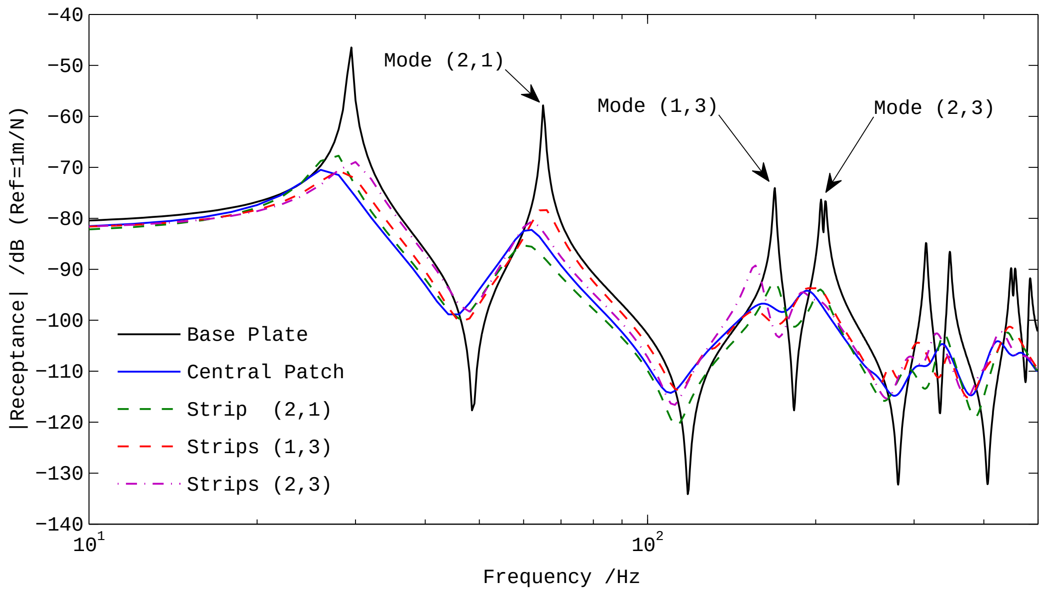

Figure 6.22: Modulus of a point FRF for a plate with different applied treatments

Analysing Figure 6.22 we can see expressed in the system response the obtained results for the modal loss factors. For the natural mode (2,1) we saw in Table 6.9 that the highest loss factor is obtained with the treatment with a horizontal strip (Strip (2,1)) and now we see in Figure 6.22 that the lowest magnitude of receptance for the natural mode (2,1) is achieved with this treatment. The same goes for the natural mode (1,3) where the lowest magnitude of receptance is obtained with the treatment specially designed for this purpose. However, it should be noted that the treatment for wich is obtained the lowest magnitude of receptance for the natural mode (1,3) is the same with that the maximum magnitude of receptance is obtained for the natural mode (2,1) and care should be taken when this kind of treatments are applied. Although the highest loss factor for the natural mode (2,3) is obtained with the treatment with a horizontal strip for the passive control of the natural mode (2,1), as seen before, Figure 6.22 shows us that the system response in terms of magnitude of receptance is basically the same for all the considered treatments in this particular mode. Globally, the differences between these new treatments and the treatment with the central patch are not huge but these results prove that is possible a selective damping if the structure works on a particular range of frequencies.

In order to understand the differences between these new treatments on a vibroacoustic level the mean square velocity, transmission loss, radiation efficiency and radiated acoustic power are presented considering the same fluid properties and incidence angle as on the preceding studies.

In Figure 6.23, we can see the mean square velocity obtained with these new treatments. For the frequency of the natural mode (2,1) the lowest value of mean square velocity is obtained with the treatment where was placed a horizontal strip for the passive control of mode (2,1) and with the central patch covering 40% of the total area. Similarly, with the treatment specifically designed for the natural mode (1,3) is achieved the lowest value of mean square velocity at the frequency of that particular mode. Now, it is interesting to note that is with the treatment - Strips (2,3) - that the lowest value of mean square velocity at the frequency that occurs the natural mode (2,3) is obtained.

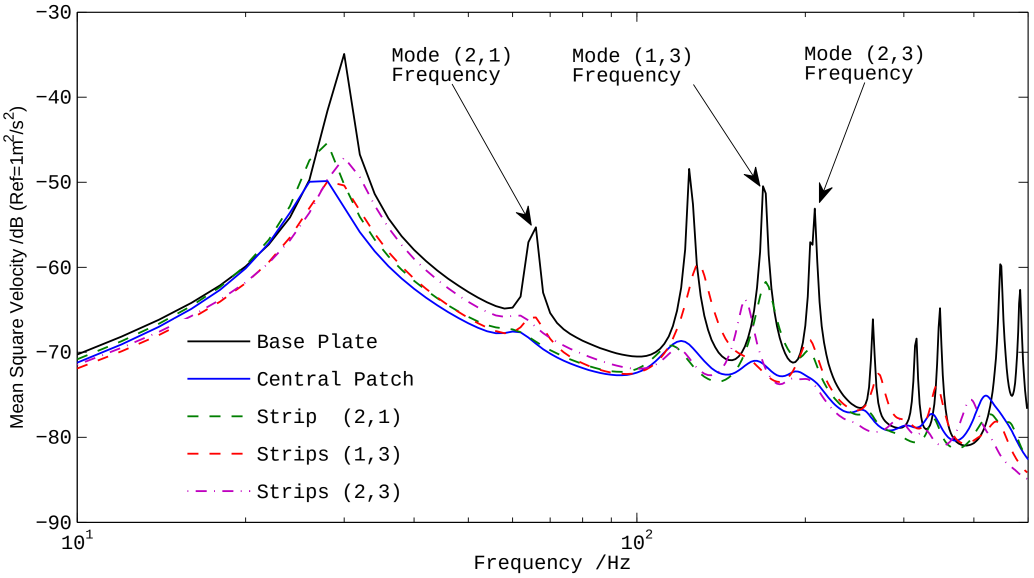

Figure 6.23: Mean square velocity for a plate with different applied treatments

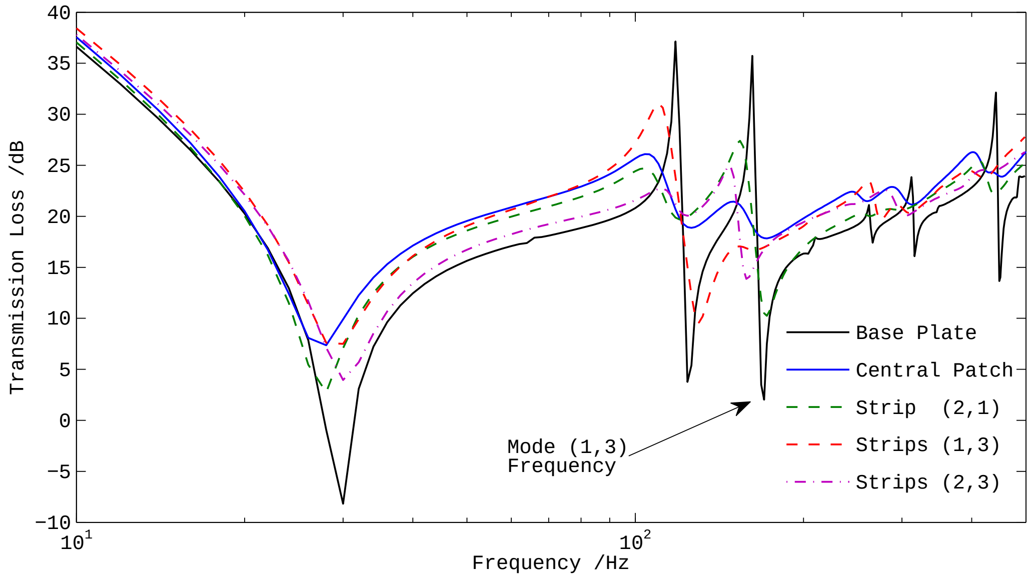

Figure 6.24: Transmission loss for a plate with different applied treatments

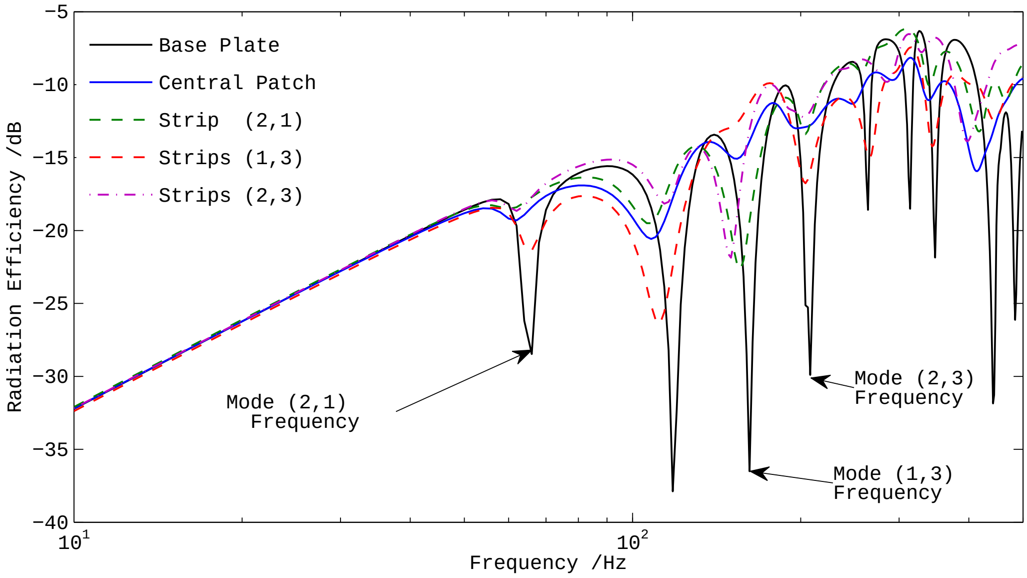

Figure 6.25: Radiation efficiency for a plate with different applied treatments

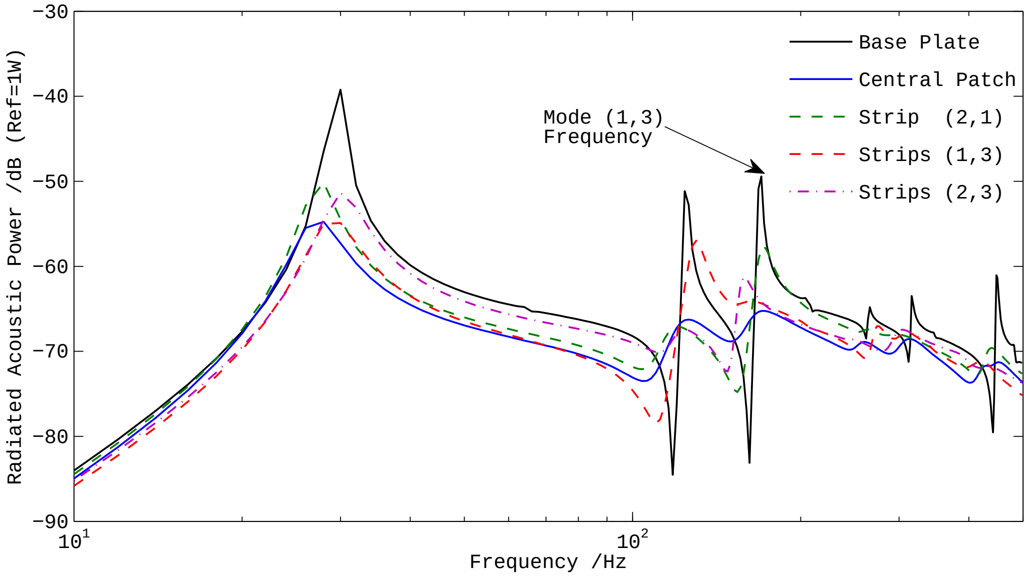

Figure 6.26: Radiated acoustic power for a plate with different applied treatments

This is an interesting result if we remember that was not with this treatment that the highest modal loss factor was achieved. Once again, this good results at some frequencies are achieved with a corresponding higher values for other frequencies and the plate with a central patch is the best commitment for the frequency range considered.

In Figure 6.24 there's only a resonance frequency that coincides with a frequency wherein occurs a natural mode considered in this study, which in case is the mode (1,3). At this frequency, the respective treatment - Strips (1,3) - cancels the resonance that is present at this frequency for the base plate but the treatment with a central patch also achieves the same effect, even canceling the previous resonance. Once again, despite being achieved good localized performances at some frequencies the global behaviour of the plate with the central patch shows to be more balanced. With concerns to the radiation efficiency (see Figure 6.25), at frequencies corresponding to the studied natural modes the highest radiation efficiency is achieved with the respective treatments which makes sense once that the mean square velocity was reduced at these frequencies with the corresponding treatments. Anew, the plate with the central patch shows a better commitment for all the frequency range considered. In Figure 6.26 is presented the radiated acoustic power for the plate with different treatments. There's a resonance frequency that coincides with the frequency of the natural mode (1,3) and the respective treatment - Strips (1,3) - cancels that particular resonance as well as the the central patch covering 40% of the total area with the advantage of also nullify the previous resonance. Again, the plate with the central patch has the best behaviour in terms of radiated acoustic power considering all the frequency range.

Generally, we can say that a selective damping is possible with a right positioning of the viscoelastic patches. It was seen that in a configuration which takes advantage of the imposition of shear stress in the viscoelastic layer for a given mode, the performance of such treatment is high at the frequency of this particular mode. The simple positioning of a viscoelastic patch over an area with high displacement in a certain natural mode does not increase the damping capability and shear stress needs to be imposed to the viscoelastic layer. This is true for the mechanical response of the plate but also on a vibroacoustic level where the performance at some frequencies can be improved in detriment of other.

Chapter 7

Conclusion

7.1 Conclusions and Discussions

It is well-known that the passive damping by viscoelastic patches is an efficient mean for the noise and vibration control of structures.

The model presented in this dissertation provides an interesting and efficient alternative to the widespread finite element method for the simulation of structures where viscoelastic materials are applied for passive control. In the following, we discuss the work that was accomplished in the three different directions of this dissertation (modeling, validation and optimisation), and give recommendations for further developments.

It was seen that the present model has many advantages over the most widely used models to study that structures, such as the "composite" models or layerwise models that were described in chapter 1. In that chapter we are enlightened about the difficulties in dealing with viscoelastic patches using "composite" models during the pre-processing stage which makes the design of any structure an endeavor job and precludes every optimal analysis timely. In addition to requiring a high intervention by the user, these models also require a large number of degrees of freedom which makes them cumbersome, with high computer memory requirements.

In chapter 2, the viscoelastic materials were presented from a practical viewpoint giving basic concepts of these materials and how to take advantage of its better properties. The temperature and frequency dependence of these materials were studied and although the temperature dependence has not been considered on the developed mechanical model is shown that is in the transition zone that the loss factor peak is achieved and consequently the best damping capability. The frequency dependence is also addressed considering its implementation on the mechanical model which introduce serious difficulties in a complex model as the present one.

In chapter 3 the proposed mechanical model for the study of plates with viscoelastic damping patches is presented and clarified. Presenting itself as an efficient alternative to the finite element method this model uses a shear stress continuity between layers, in addition to the displacements continuity, with the purpose of exposing the displacements of each layer from the displacements of the first layer. Although this assumption does not represent what really happens in the laminate it allows a significant reduction of the number of degrees of freedom and the computational memory required. But the most noteworthy advantage of this model is the extremely easy patches's handling due to the Rayleigh-Ritz method that allows the application of a superposition principle to the patches and so apply as many treatments as we want working at an energetic level and only changing the integration limits which is extremely easy to implement. Thus, this model presents an overwhelming advantage relatively to the finite element method and can be considered as a powerful tool to modeling not only viscoelastic damping patches but also the local stiffening of a specific area on the plate with an elastic material, for example. However there is a price to pay for this great advantage, and as is shown in chapter 3, the mass matrix is frequency dependent due to the adopted shear stress continuity between layers that imposes to the velocity field a dependence on the viscoelastic properties. Hence, the mass matrix needs to be seen as a measure of the kinetic energy of the laminate which in this model depends on the material properties of the layers. This and the fact that we can not split the mass and stiffness matrix into elastic and viscoelastic matrices, due to their complex construction, makes this model slow in the matrices generation once that forces the store of one mass matrix and one stiffness matrix for each frequency.

In chapter 4 the mechanical and vibroacoustic indicators used in this work were presented. Besides the mathematical formulation of frequency response function and the presentation of an algorithm for an iterated calculation of the modal loss factors the main interest here goes to the vibroacoustic model specially developed for an easy computation using the basis functions used in the Rayleigh-Ritz method. It is worth to mention that this model is based on a far-field hypothesis neglecting the impedance of the fluid. This one-way model that ignores the fluid/structure coupling can be used for light fluids like air but is unrealistic for heavy fluids like water, for example.

Chapter 5 provides numerical results for the model validation and evaluation of the main characteristics of this mechanical model. A numerical comparison in terms of degrees of freedom increasing the number of layers was performed and show that this model keeps the same number of degrees of freedom for a plate with one or N layers. The influence of the basis functions maximum order in the structure discretisation is studied and is possible to see that an increase in the functions order gives a better representation of the system response although the difference between a maximum order of 4 and 8 for the two directions is not large in a range of frequency between 0 and 1000 Hz. A comparison, in terms of frequency response function, was also made with a solution obtained with the commercial software Actran®, using a solid element, and the model was validated, recording only a few differences with the increase of frequency. The present model shows a more damped response and tends to underestimate the natural frequencies which is acceptable for a model that contemplates the effect of the shear stress. Besides that, this results were obtained using 6525 degrees of freedom in Actran® against 320 used with the present model, which demonstrates the potential of this model. The multi-layer behaviour was also proven with a representation of the displacement in x-direction for a three layer laminate which express that each layer has their own behaviour despite the fact that its displacements can be written in terms of first layer displacements. The vibroacoustic indicators were validated using an example performed with the present model in the literature and although was used a low order for the basis functions they were validated until 700Hz. For a better understanding of the influence of the incidence angle on the vibroacoustic indicators was represented the mean square velocity and transmission loss for two different incidence angles and we can see that the number of resonance frequencies in the mean square velocity depends on the incidence angle. For the transmission loss there's no differences in the number of resonance frequencies, considering an incidence angle of 85° and other with 0°, and only a vertical shift occurs with a higher transmission loss for a plane wave with an incidence angle of 0°.

Finally, in chapter 6 was performed an analysis of constrained-layer damping patches with a clearly defined objective, achieve the best damping capability with the lower added mass for an inexpensive treatment and for a small structural modification. The optimisation was made in terms of modal loss factors with the perspective to achieve a damped mechanical response but also a well designed plate in vibroacoustic terms. First, an optimal analysis of the covered area by a central patch was performed with and using a minimisation function a covered area of 40% was obtained as the better commitment between damping capability and added mass. At a vibroacoustic level a covered area also shows a good level of efficiency with the decrease of mean square velocity, the increase in the transmission loss, the increase in the radiation efficiency due to the decrease in the mean square velocity and the decrease of the radiated acoustic power. These values for a 40% covered area didn't reach the values of a plate with a total treatment but shows a better commitment between cost and efficiency. Then the same philosophy was used for an analysis of the optimal treatment's thickness varying the constraining layer thickness for a 40% covered area and we see that the best commitment between added mass and damping capability is achieved for a range of thickness ratios (constraining layer/viscoelastic layer) between 1 and 2 with very close values in this range for the minimisation function. A thickness ratio of 2 shows better damping capability but a ratio of 1 adds less mass and at a vibroacoustic level, the thickness ratio of 2 shows also a better behaviour. However the differences for this thicknesses range are small and we need to evaluate if a more expensive treatment worths. Lastly on this chapter was performed an analysis of the patches' distribution to achieve a selective damping and develop a strategy for the passive control of a certain normal mode. The natural frequencies for a simply supported plate were calculated and it appears that with the simple positioning of the viscoelastic patches on the areas with higher displacements for a given natural mode the damping capability isn't increased, in comparison with that which is obtained with a central patch covering 40% of the total area. In fact, it was seen that these materials have an efficient behaviour when shear stress is superimposed to the viscoelastic layer and the higher shear stresses may not be present where the higher displacements are reached. So, is shown that a strategic placement of the viscoelastic patches to take advantage of the phase opposition of a certain natural mode can be very efficient once that shear stress can be superimposed to the viscoelastic layer. With this approach is exposed an effective method for selective damping. At a vibroacoustic level it is shown that at the frequencies that a certain natural mode occurs the respective treatment has better indicators. However, it also verifies that the central patch has a better performance for all the considered frequency range where for some frequencies the selective treatments can be inefficient.

It is hoped that this work provides a contribution to the literature regarding the study of this powerful model for the study of viscoelastic damping patches where a Rayleigh-Ritz method is used and a superposition principle is applied to the structure. This subject is still on an earlier stage of development and there's a recent interest for the study that still need further developments hoping that this work provides o good understanding of the fundamental principles.

7.2 Development Suggestions

Several other studies can be done from the present work and some suggestions are done for further development:

- Improve the developed Matlab® code for a lower processing time;
- Better comparison, using convergence analysis, with the finite element method;
- Realise the influence of the boundary conditions on the studies developed in this work;
- Proper validation and study of a orthotropic plate and study its mechanical and vibroacoustic behaviour;
- Study the vibroacoustic response to a diffuse field excitation;
- Calculation of the shear strain energy of the plate in order to improve patches' positioning;

Appendix A

Energy Coefficients

A.1 Definition of Coefficients δ_i

$$\delta_1^j = \sum_{\ell=1}^{N^j} \int_{-\frac{h^\ell}{2}}^{\frac{h^\ell}{2}} \rho^\ell \left((\beta^\ell)^2 + (z^\ell - z)^2 \right) \mathrm{d}(z^\ell - z) = \sum_{\ell=1}^{N^j} \rho^\ell \left(h^\ell (\beta^\ell)^2 + \frac{(h^\ell)^3}{12} \right)$$

$$\delta_2^j = \sum_{\ell=1}^{N^j} \int_{-\frac{h^\ell}{2}}^{\frac{h^\ell}{2}} \rho^\ell \left((\delta_{xx}^\ell)^2 + (z^\ell - z)^2 (\alpha_{xx}^\ell)^2 \right) \mathrm{d}(z^\ell - z) = \sum_{\ell=1}^{N^j} \rho^\ell \left(h^\ell (\delta_{xx}^\ell)^2 + \frac{(h^\ell)^3}{12} (\alpha_{xx}^\ell)^2 \right)$$

$$\delta_3^j = \sum_{\ell=1}^{N^j} \int_{-\frac{h^\ell}{2}}^{\frac{h^\ell}{2}} \rho^\ell \mathrm{d}(z^\ell - z) = \sum_{\ell=1}^{N^j} \rho^\ell h^\ell$$

$$\delta_4^j = \sum_{\ell=1}^{N^j} \int_{-\frac{h^\ell}{2}}^{\frac{h^\ell}{2}} 2\rho^\ell \left(\beta^\ell \delta_{xx}^\ell + \alpha_{xx}^\ell (z^\ell - z)^2 \right) \mathrm{d}(z^\ell - z) = \sum_{\ell=1}^{N^j} 2\rho^\ell \left(h^\ell \beta^\ell \delta_{xx}^\ell + \frac{(h^\ell)^3}{12} \alpha_{xx}^\ell \right)$$

$$\delta_5^j = \sum_{\ell=1}^{N^j} \int_{-\frac{h^\ell}{2}}^{\frac{h^\ell}{2}} 2\rho^\ell \beta^\ell \mathrm{d}(z^\ell - z) = \sum_{\ell=1}^{N^j} 2\rho^\ell h^\ell \beta^\ell$$

$$\delta_6^j = \sum_{\ell=1}^{N^j} \int_{-\frac{h^\ell}{2}}^{\frac{h^\ell}{2}} 2\rho^\ell \delta_{xx}^\ell \mathrm{d}(z^\ell - z) = \sum_{\ell=1}^{N^j} 2\rho^\ell h^\ell \delta_{xx}^\ell$$

$$\delta_7^j = \sum_{\ell=1}^{N^j} \int_{-\frac{h^\ell}{2}}^{\frac{h^\ell}{2}} \rho^\ell \left((\beta^\ell)^2 + (z^\ell - z)^2 \right) \mathrm{d}(z^\ell - z) = \sum_{\ell=1}^{N^j} \rho^\ell \left(h^\ell (\beta^\ell)^2 + \frac{(h^\ell)^3}{12} \right)$$

$$\delta_8^j = \sum_{\ell=1}^{N^j} \int_{-\frac{h^\ell}{2}}^{\frac{h^\ell}{2}} \rho^\ell \left((\delta_{yy}^\ell)^2 + (z^\ell - z)^2 (\alpha_{yy}^\ell)^2 \right) \mathrm{d}(z^\ell - z) = \sum_{\ell=1}^{N^j} \rho^\ell \left(h^\ell (\delta_{yy}^\ell)^2 + \frac{(h^\ell)^3}{12} (\alpha_{yy}^\ell)^2 \right)$$

$$\delta_9^j = \sum_{\ell=1}^{N^j} \int_{-\frac{h^\ell}{2}}^{\frac{h^\ell}{2}} \rho^\ell \mathrm{d}(z^\ell - z) = \sum_{\ell=1}^{N^j} \rho^\ell h^\ell$$

$$\delta_{10}^j = \sum_{\ell=1}^{N^j} \int_{-\frac{h^\ell}{2}}^{\frac{h^\ell}{2}} 2\rho^\ell \left(\beta^\ell \delta_{yy}^\ell + \alpha_{yy}^\ell (z^\ell - z)^2 \right) \mathrm{d}(z^\ell - z) = \sum_{\ell=1}^{N^j} 2\rho^\ell \left(h^\ell \beta^\ell \delta_{yy}^\ell + \frac{(h^\ell)^3}{12} \alpha_{yy}^\ell \right)$$

$$
\begin{aligned}
\delta^j_{11} &= \sum_{\ell=1}^{N^j}\int_{-\frac{h^\ell}{2}}^{\frac{h^\ell}{2}} 2\rho^\ell\beta^\ell \mathrm{d}(z^\ell-z) = \sum_{\ell=1}^{N^j} 2\rho^\ell h^\ell\beta^\ell \\
\delta^j_{12} &= \sum_{\ell=1}^{N^j}\int_{-\frac{h^\ell}{2}}^{\frac{h^\ell}{2}} 2\rho^\ell\delta^\ell_{yy} \mathrm{d}(z^\ell-z) = \sum_{\ell=1}^{N^j} 2\rho^\ell h^\ell\delta^\ell_{yy} \\
\delta^j_{13} &= \sum_{\ell=1}^{N^j}\int_{-\frac{h^\ell}{2}}^{\frac{h^\ell}{2}} \rho^\ell \mathrm{d}(z^\ell-z) = \sum_{\ell=1}^{N^j} \rho^\ell h^\ell
\end{aligned}
\tag{A.1.1}
$$

A.2 Definition of Coefficients λ_i

Previous Note:

For simplicity, all the terms that are function of $(z^\ell - z)$ are not written in the definition of coefficients λ_i, because:

$$\int_{-\frac{h^\ell}{2}}^{\frac{h^\ell}{2}} (z^\ell-z)\mathrm{d}(z^\ell-z) = 0$$

$$
\begin{aligned}
\lambda^j_1 &= \sum_{\ell=1}^{N^j}\int_{-\frac{h^\ell}{2}}^{\frac{h^\ell}{2}} C^\ell_{1111}\left((\beta^\ell)^2+(z^\ell-z)^2\right)\mathrm{d}(z^\ell-z) = \sum_{\ell=1}^{N^j} C^\ell_{1111}\left(h^\ell(\beta^\ell)^2+\frac{(h^\ell)^3}{12}\right) \\
\lambda^j_2 &= \sum_{\ell=1}^{N^j}\int_{-\frac{h^\ell}{2}}^{\frac{h^\ell}{2}} C^\ell_{1111}\left((\delta^\ell_{xx})^2+(\alpha^\ell_{xx})^2(z^\ell-z)^2\right)\mathrm{d}(z^\ell-z) = \sum_{\ell=1}^{N^j} C^\ell_{1111}\left(h^\ell(\delta^\ell_{xx})^2+\frac{(h^\ell)^3}{12}(\alpha^\ell_{xx})^2\right) \\
\lambda^j_3 &= \sum_{\ell=1}^{N^j}\int_{-\frac{h^\ell}{2}}^{\frac{h^\ell}{2}} C^\ell_{1111}\mathrm{d}(z^\ell-z) = \sum_{\ell=1}^{N^j} C^\ell_{1111}h^\ell \\
\lambda^j_4 &= \sum_{\ell=1}^{N^j}\int_{-\frac{h^\ell}{2}}^{\frac{h^\ell}{2}} C^\ell_{1111}\left(2\beta^\ell\delta^\ell_{xx}+2\alpha^\ell_{xx}(z^\ell-z)^2\right)\mathrm{d}(z^\ell-z) = \sum_{\ell=1}^{N^j} 2C^\ell_{1111}\left(h^\ell\beta^\ell\delta^\ell_{xx}+\frac{(h^\ell)^3}{12}\alpha^\ell_{xx}\right) \\
\lambda^j_5 &= \sum_{\ell=1}^{N^j}\int_{-\frac{h^\ell}{2}}^{\frac{h^\ell}{2}} C^\ell_{1111}\left(2\beta^\ell\right)\mathrm{d}(z^\ell-z) = \sum_{\ell=1}^{N^j} 2C^\ell_{1111}\left(h^\ell\beta^\ell\right) \\
\lambda^j_6 &= \sum_{\ell=1}^{N^j}\int_{-\frac{h^\ell}{2}}^{\frac{h^\ell}{2}} C^\ell_{1111}\left(2\delta^\ell_{xx}\right)\mathrm{d}(z^\ell-z) = \sum_{\ell=1}^{N^j} 2C^\ell_{1111}\left(h^\ell\delta^\ell_{xx}\right) \\
\lambda^j_7 &= \sum_{\ell=1}^{N^j}\int_{-\frac{h^\ell}{2}}^{\frac{h^\ell}{2}} C^\ell_{2222}\left((\beta^\ell)^2+(z^\ell-z)^2\right)\mathrm{d}(z^\ell-z) = \sum_{\ell=1}^{N^j} C^\ell_{2222}\left(h^\ell(\beta^\ell)^2+\frac{(h^\ell)^3}{12}\right) \\
\lambda^j_8 &= \sum_{\ell=1}^{N^j}\int_{-\frac{h^\ell}{2}}^{\frac{h^\ell}{2}} C^\ell_{2222}\left((\delta^\ell_{yy})^2+(\alpha^\ell_{yy})^2(z^\ell-z)^2\right)\mathrm{d}(z^\ell-z) = \sum_{\ell=1}^{N^j} C^\ell_{2222}\left(h^\ell(\delta^\ell_{yy})^2+\frac{(h^\ell)^3}{12}(\alpha^\ell_{yy})^2\right)
\end{aligned}
$$

$$
\begin{aligned}
\lambda_9^j &= \sum_{\ell=1}^{N} \int_{-\frac{h^\ell}{2}}^{\frac{h^\ell}{2}} C_{2222}^\ell \mathrm{d}(z^\ell - z) = \sum_{\ell=1}^{N^j} C_{2222}^\ell h^\ell \\
\lambda_{10}^j &= \sum_{\ell=1}^{N^j} \int_{-\frac{h^\ell}{2}}^{\frac{h^\ell}{2}} C_{2222}^\ell \left(2\beta^\ell \delta_{yy}^\ell + 2\alpha_{yy}^\ell (z^\ell - z)^2\right) \mathrm{d}(z^\ell - z) = \sum_{\ell=1}^{N^j} 2C_{2222}^\ell \left(h^\ell \beta^\ell \delta_{yy}^\ell + \frac{(h^\ell)^3}{12}\alpha_{yy}^\ell\right) \\
\lambda_{11}^j &= \sum_{\ell=1}^{N^j} \int_{-\frac{h^\ell}{2}}^{\frac{h^\ell}{2}} C_{2222}^\ell \left(2\beta^\ell\right) \mathrm{d}(z^\ell - z) = \sum_{\ell=1}^{N^j} 2C_{2222}^\ell \left(h^\ell \beta^\ell\right) \\
\lambda_{12}^j &= \sum_{\ell=1}^{N^j} \int_{-\frac{h^\ell}{2}}^{\frac{h^\ell}{2}} C_{2222}^\ell \left(2\delta_{yy}^\ell\right) \mathrm{d}(z^\ell - z) = \sum_{\ell=1}^{N^j} 2C_{2222}^\ell \left(h^\ell \delta_{yy}^\ell\right) \\
\lambda_{13}^j &= \sum_{\ell=1}^{N^j} \int_{-\frac{h^\ell}{2}}^{\frac{h^\ell}{2}} 2C_{1122}^\ell \left((\beta^\ell)^2 + (z^\ell - z)^2\right) \mathrm{d}(z^\ell - z) = \sum_{\ell=1}^{N^j} 2C_{1122}^\ell \left(h^\ell (\beta^\ell)^2 + \frac{(h^\ell)^3}{12}\right) \\
\lambda_{14}^j &= \sum_{\ell=1}^{N^j} \int_{-\frac{h^\ell}{2}}^{\frac{h^\ell}{2}} 2C_{1122}^\ell \left(\beta^\ell)\delta_{yy}^\ell + \alpha_{yy}^\ell (z^\ell - z)^2\right) \mathrm{d}(z^\ell - z) = \sum_{\ell=1}^{N^j} 2C_{1122}^\ell \left(h^\ell \beta^\ell \delta_{yy}^\ell + \frac{(h^\ell)^3}{12}\alpha_{yy}^\ell\right) \\
\lambda_{15}^j &= \sum_{\ell=1}^{N^j} \int_{-\frac{h^\ell}{2}}^{\frac{h^\ell}{2}} 2C_{1122}^\ell \left(\beta^\ell\right) \mathrm{d}(z^\ell - z) = \sum_{\ell=1}^{N^j} 2C_{1122}^\ell \left(h^\ell \beta^\ell\right) \\
\lambda_{16}^j &= \sum_{\ell=1}^{N^j} \int_{-\frac{h^\ell}{2}}^{\frac{h^\ell}{2}} 2C_{1122}^\ell \left(\beta^\ell)\delta_{xx}^\ell + \alpha_{xx}^\ell (z^\ell - z)^2\right) \mathrm{d}(z^\ell - z) = \sum_{\ell=1}^{N^j} 2C_{1122}^\ell \left(h^\ell \beta^\ell \delta_{xx}^\ell + \frac{(h^\ell)^3}{12}\alpha_{xx}^\ell\right) \\
\lambda_{17}^j &= \sum_{\ell=1}^{N^j} \int_{-\frac{h^\ell}{2}}^{\frac{h^\ell}{2}} 2C_{1122}^\ell \left(\delta_{xx}^\ell \delta_{yy}^\ell + \alpha_{xx}^\ell \alpha_{yy}^\ell (z^\ell - z)^2\right) \mathrm{d}(z^\ell - z) = \sum_{\ell=1}^{N^j} 2C_{1122}^\ell \left(h^\ell \delta_{xx}^\ell \delta_{yy}^\ell + \frac{(h^\ell)^3}{12}\alpha_{xx}^\ell \alpha_{yy}^\ell\right) \\
\lambda_{18}^j &= \sum_{\ell=1}^{N^j} \int_{-\frac{h^\ell}{2}}^{\frac{h^\ell}{2}} 2C_{1122}^\ell \left(\delta_{xx}^\ell\right) \mathrm{d}(z^\ell - z) = \sum_{\ell=1}^{N^j} 2C_{1122}^\ell \left(h^\ell \delta_{xx}^\ell\right) \\
\lambda_{19}^j &= \sum_{\ell=1}^{N^j} \int_{-\frac{h^\ell}{2}}^{\frac{h^\ell}{2}} 2C_{1122}^\ell \left(\beta^\ell\right) \mathrm{d}(z^\ell - z) = \sum_{\ell=1}^{N^j} 2C_{1122}^\ell \left(h^\ell \beta^\ell\right) \\
\lambda_{20}^j &= \sum_{\ell=1}^{N^j} \int_{-\frac{h^\ell}{2}}^{\frac{h^\ell}{2}} 2C_{1122}^\ell \left(\delta_{yy}^\ell\right) \mathrm{d}(z^\ell - z) = \sum_{\ell=1}^{N^j} 2C_{1122}^\ell \left(h^\ell \delta_{yy}^\ell\right) \\
\lambda_{21}^j &= \sum_{\ell=1}^{N^j} \int_{-\frac{h^\ell}{2}}^{\frac{h^\ell}{2}} 2C_{1122}^\ell \mathrm{d}(z^\ell - z) = \sum_{\ell=1}^{N^j} 2C_{1122}^\ell \left(h^\ell\right) \\
\lambda_{22}^j &= \sum_{\ell=1}^{N^j} \int_{-\frac{h^\ell}{2}}^{\frac{h^\ell}{2}} C_{1212}^\ell \left(4(\beta^\ell)^2 + 4(z^\ell - z)^2\right) \mathrm{d}(z^\ell - z) = \sum_{\ell=1}^{N^j} C_{1212}^\ell \left(4h^\ell (\beta^\ell)^2 + 4\frac{(h^\ell)^3}{12}\right) \\
\lambda_{23}^j &= \sum_{\ell=1}^{N^j} \int_{-\frac{h^\ell}{2}}^{\frac{h^\ell}{2}} C_{1212}^\ell \left((\delta_{xx}^\ell)^2 + (\alpha_{xx}^\ell)^2 (z^\ell - z)^2\right) \mathrm{d}(z^\ell - z) = \sum_{\ell=1}^{N^j} C_{1212}^\ell \left(h^\ell (\delta_{xx}^\ell)^2 + \frac{(h^\ell)^3}{12}(\alpha_{xx}^\ell)^2\right)
\end{aligned}
$$

$$
\begin{aligned}
\lambda^j_{24} &= \sum_{\ell=1}^{N^j} \int_{-\frac{h^\ell}{2}}^{\frac{h^\ell}{2}} C^\ell_{1212} \left((\delta^\ell_{yy})^2 + (\alpha^\ell_{yy})^2 (z^\ell - z)^2\right) \mathrm{d}(z^\ell - z) = \sum_{\ell=1}^{N^j} C^\ell_{1212} \left(h^\ell (\delta^\ell_{yy})^2 + \frac{(h^\ell)^3}{12} (\alpha^\ell_{yy})^2\right) \\
\lambda_{25} &= \sum_{\ell=1}^{N^j} \int_{-\frac{h^\ell}{2}}^{\frac{h^\ell}{2}} C^\ell_{1212} \mathrm{d}(z^\ell - z) = \sum_{\ell=1}^{N^j} C^\ell_{1212} \left(h^\ell\right) \\
\lambda^j_{26} &= \sum_{\ell=1}^{N^j} \int_{-\frac{h^\ell}{2}}^{\frac{h^\ell}{2}} C^\ell_{1212} \mathrm{d}(z^\ell - z) = \sum_{\ell=1}^{N} C^\ell_{1212} \left(h^\ell\right) \qquad \text{(A.2.1)} \\
\lambda^j_{27} &= \sum_{\ell=1}^{N^j} \int_{-\frac{h^\ell}{2}}^{\frac{h^\ell}{2}} 2C^\ell_{1212} \left(2\beta^\ell \delta^\ell_{xx} + 2\alpha^\ell_{xx} (z^\ell - z)^2\right) \mathrm{d}(z^\ell - z) = \sum_{\ell=1}^{N^j} 2C^\ell_{1212} \left(2h^\ell \beta^\ell \delta^\ell_{xx} + 2\frac{(h^\ell)^3}{12} \alpha^\ell_{xx}\right) \\
\lambda^j_{28} &= \sum_{\ell=1}^{N^j} \int_{-\frac{h^\ell}{2}}^{\frac{h^\ell}{2}} 2C^\ell_{1212} \left(2\beta^\ell \delta^\ell_{yy} + 2\alpha^\ell_{yy} (z^\ell - z)^2\right) \mathrm{d}(z^\ell - z) = \sum_{\ell=1}^{N^j} 2C^\ell_{1212} \left(2h^\ell \beta^\ell \delta^\ell_{yy} + 2\frac{(h^\ell)^3}{12} \alpha^\ell_{yy}\right) \\
\lambda^j_{29} &= \sum_{\ell=1}^{N^j} \int_{-\frac{h^\ell}{2}}^{\frac{h^\ell}{2}} 2C^\ell_{1212} \left(2\beta^\ell\right) \mathrm{d}(z^\ell - z) = \sum_{\ell=1}^{N^j} 2C^\ell_{1212} \left(2h^\ell \beta^\ell\right) \\
\lambda^j_{30} &= \sum_{\ell=1}^{N^j} \int_{-\frac{h^\ell}{2}}^{\frac{h^\ell}{2}} 2C^\ell_{1212} \left(2\beta^\ell\right) \mathrm{d}(z^\ell - z) = \sum_{\ell=1}^{N^j} 2C^\ell_{1212} \left(2h^\ell \beta^\ell\right) \\
\lambda^j_{31} &= \sum_{\ell=1}^{N^j} \int_{-\frac{h^\ell}{2}}^{\frac{h^\ell}{2}} 2C^\ell_{1212} \left((\delta^\ell_{xx}\delta^\ell_{yy}) + (\alpha^\ell_{xx}\alpha^\ell_{yy})(z^\ell - z)^2\right) \mathrm{d}(z^\ell - z) = \sum_{\ell=1}^{N^j} 2C^\ell_{1212} \left(h^\ell \delta^\ell_{xx}\delta^\ell_{yy} + \frac{(h^\ell)^3}{12} \alpha^\ell_{xx}\alpha^\ell_{yy}\right) \\
\lambda^j_{32} &= \sum_{\ell=1}^{N^j} \int_{-\frac{h^\ell}{2}}^{\frac{h^\ell}{2}} 2C^\ell_{1212} \left(\delta^\ell_{xx}\right) \mathrm{d}(z^\ell - z) = \sum_{\ell=1}^{N^j} 2C^\ell_{1212} \left(h^\ell \delta^\ell_{xx}\right) \\
\lambda^j_{33} &= \sum_{\ell=1}^{N^j} \int_{-\frac{h^\ell}{2}}^{\frac{h^\ell}{2}} 2C^\ell_{1212} \left(\delta^\ell_{xx}\right) \mathrm{d}(z^\ell - z) = \sum_{\ell=1}^{N^j} 2C^\ell_{1212} \left(h^\ell \delta^\ell_{xx}\right) \\
\lambda^j_{34} &= \sum_{\ell=1}^{N^j} \int_{-\frac{h^\ell}{2}}^{\frac{h^\ell}{2}} 2C^\ell_{1212} \left(\delta^\ell_{yy}\right) \mathrm{d}(z^\ell - z) = \sum_{\ell=1}^{N^j} 2C^\ell_{1212} \left(h^\ell \delta^\ell_{yy}\right) \\
\lambda^j_{35} &= \sum_{\ell=1}^{N^j} \int_{-\frac{h^\ell}{2}}^{\frac{h^\ell}{2}} 2C^\ell_{1212} \left(\delta^\ell_{yy}\right) \mathrm{d}(z^\ell - z) = \sum_{\ell=1}^{N^j} 2C^\ell_{1212} \left(h^\ell \delta^\ell_{yy}\right) \\
\lambda_{36} &= \sum_{\ell=1}^{N^j} \int_{-\frac{h^\ell}{2}}^{\frac{h^\ell}{2}} 2C^\ell_{1212} \mathrm{d}(z^\ell - z) = \sum_{\ell=1}^{N^j} 2C^\ell_{1212} \left(h^\ell\right) \\
\lambda^j_{37} &= \sum_{\ell=1}^{N^j} \int_{-\frac{h^\ell}{2}}^{\frac{h^\ell}{2}} C^\ell_{1313} \left(\alpha^\ell_{xx}\right)^2 \mathrm{d}(z^\ell - z) = \sum_{\ell=1}^{N^j} C^\ell_{1313} \left(h^\ell (\alpha^\ell_{xx})^2\right) \\
\lambda^j_{38} &= \sum_{\ell=1}^{N^j} \int_{-\frac{h^\ell}{2}}^{\frac{h^\ell}{2}} C^\ell_{2323} \left(\alpha^\ell_{yy}\right)^2 \mathrm{d}(z^\ell - z) = \sum_{\ell=1}^{N^j} C^\ell_{2323} \left(h^\ell (\alpha^\ell_{yy})^2\right)
\end{aligned}
$$

(A.2.2)

Appendix B

Vibroacoustic Indicators - Loredo et al. [10]

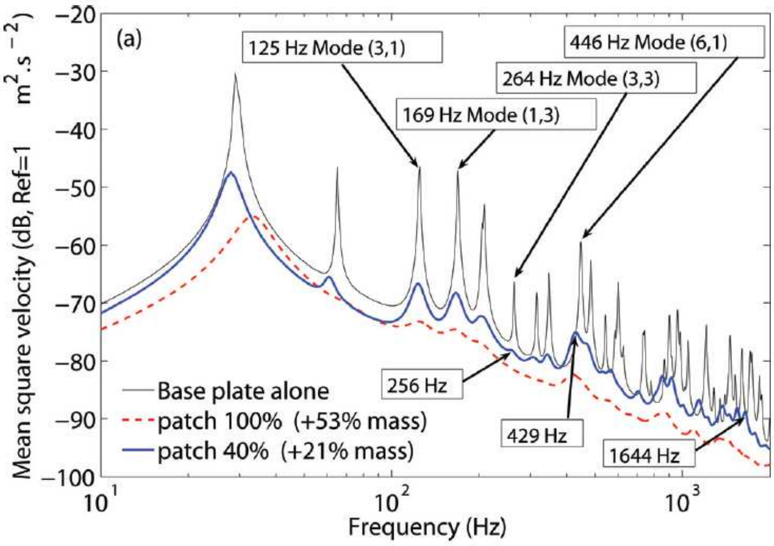

Figure B.1: Mean square velocity for three different configurations [10]

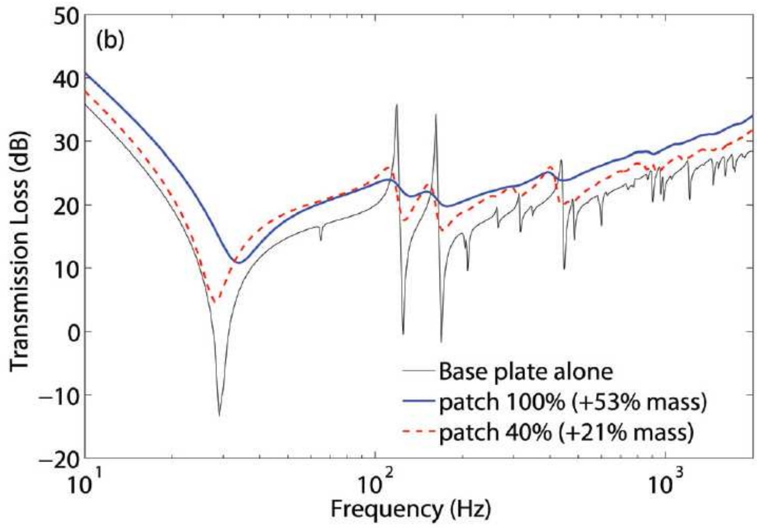

Figure B.2: Transmission loss for three different configurations [10]

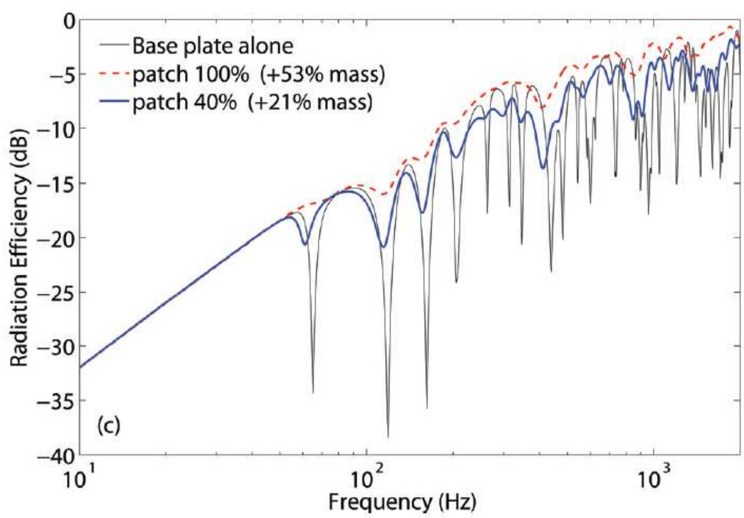

Figure B.3: Radiation efficiency for three different configurations [10]

References

[1] C. M. A. Vasques. *Vibration Control of Adaptive Structures.* PhD thesis, Faculdade de Engenharia da Universidade do Porto, 2008.

[2] M. D. Rao. Recent applications of viscoelastic damping for noise control in automobiles and commercial airplanes. *Journal of Sound and Vibration*, 262:457–474, 2003.

[3] F. Fahy and P. Gardonio. *Sound and Structural Vibration: Radiation, Transmission and Response.* 2nd edition, 2007.

[4] R. A. S. Moreira. *Modelação e análise de tratamentos viscoeláticos multi-camada para controlo passivo de vibrações.* PhD thesis, Faculdade de Engenharia da Universidade do Porto, 2004.

[5] L. Hazard. *Design of viscoelastic damping for vibration control: modelling, experiments and optimisation.* PhD thesis, Faculté des Sciences Appliquées, Université Libre de Bruxelles, 2006.

[6] J. L. Guyader and C. Lesueur. Acoustic transmission through orthotropic multilayered plates, part i:plate vibration modes. *Journal of Sound and Vibration*, 58:51–68, 1978.

[7] A. Castel, A. Loredo, Ali El Hafidi, and Martin B. Complex power distribution analysis in plates covered with passive constrained layer damping patches. *Journal of Sound and Vibration*, 331:2485–2498, 2012.

[8] Roland L. Woodcock. Free vibration of advanced anisotropic multilayered composites with arbitrary boundary conditions. *Journal of Sound and Vibration*, 312:769–788, 2008.

[9] Roland L. Woodcock, R. B. Bhat, and I. G. Stiharu. Effect of ply orientation on the in-plane vibration of single-layer composite plates. *Journal of Sound and Vibration*, 312: 94–108, 2008.

[10] A. Loredo, A. Plessy, Ali El Hafidi, and N. Hamzaoui. Numerical vibroacoustic analysis of plates with constrained-layer damping patches. *Journal of Acoustical Society of America*, 129:1905–1918, 2011.

[11] A. Loredo and A. Castel. A multilayer anisotropic plate model with warping functions for the study of vibrations reformulated from Woodcock's work. *Journal of Sound and Vibration*, 332:102–125, 2013.

[12] J. He and Zhi-Fang Fu. *Modal Analysis.* 1st edition, 2001.

[13] O. Foin, J. Nicolas, and Atalla N. An efficient tool for predicting the structural acoustic and vibration response of sandwich plates in light or heavy fluid. *Journal of Applied Acoustics*, 57:213–242, 1999.

[14] Yi-Cheng Chena and Shyh-Chin Huangb. An optimal placement of CLD treatment for vibration suppression of plates. *Journal of Mechanical Sciences*, 44:1801–1821, 2002.